

**Quality mapping of potato tuber storage facility using real-time location system, wireless communication and machine vision for improved traceability**

**by**

**Colton Al Campbell**

**Submitted in partial fulfilment of the requirements**

**for the degree of Master of Science**

**at**

**Dalhousie University**

**Halifax, Nova Scotia**

**December 2024**

**© Copyright by Colton Al Campbell 2024**

**Table of Contents:**

List of Tables: ..... iv

List of Figures: ..... v

Abstract: ..... vi

List of Abbreviations and symbols Used: ..... vii

Acknowledgements: ..... viii

1. Introduction: ..... 1

2. Literature Review: ..... 4

    2.1. Precision agriculture ..... 4

    2.2. IoT in Agriculture ..... 5

    2.3. Traceability Systems ..... 6

    2.4. Real-Time Localization Systems ..... 7

        2.4.1. Sensing Paradigms and Ranging in RTLS ..... 7

        2.4.2. Ranging and Hardware ..... 9

        2.4.3. Multipath and NLOS Mitigation ..... 10

    2.5. Long Range Data Transmission ..... 11

    2.6. Ultra-Wideband (UWB) ..... 12

        2.6.1. UWB Modalities ..... 13

        2.6.2. Advantages of UWB ..... 14

        2.6.3. Challenges with UWB TOA ..... 15

        2.6.4. UWB Hybrid Systems ..... 16

    2.7. Algorithms for Positioning and Prediction in RTLS ..... 16

        2.7.1. Least Squares Algorithm (LS) ..... 17

        2.7.2. The Kalman Filter ..... 17

        2.7.3. Support Vector Regressor (SVR) ..... 18

    2.8. UWB Existing Systems in Literature and Industry ..... 19

3. Development of Potato Bin-Piler Localization System using UWB in Lab and Field Environments ..... 24

    3.1. Overview ..... 24

    3.2. Materials ..... 24

    3.3. Experimental Design and Setup ..... 25

        3.3.1. Experiment 1: Obstacle-Free Small Volume Environment in Lab ..... 27

        3.3.2. Experiment 2: Uniform Anchor Height Large Volume Environment at Lab ..... 29

3.3.3.	Experiments 3 and 4: Small and Large Pile Anchor Locations in Lab.....	30
3.3.4.	Experiment 5: Bin-piler Large Volume Environment in Field.....	31
3.3.5.	Experiments 6 and 7: Harvest Operations Small and Large Pile in Field .....	33
3.4.	System Design and Evaluation Methods .....	34
3.5.	Results and Discussion .....	37
3.5.1.	Controlled Grid LS Experimental Generalized Results and Discussion .....	37
3.5.2.	Controlled Grid LS Algorithm and SVR Localization Experimental Results and Discussion.....	60
3.5.3.	Harvest Operations Small and Large Pile in Field Results and Discussion .....	63
3.6.	Summary .....	67
4.	Mapping of Potato Quality Data by Synchronizing with Localization Information .....	69
4.1.	Overview.....	69
4.2.	Materials .....	69
4.2.1.	Belt Speed Monitoring.....	69
4.2.2.	Conveyor Extension and Retraction Monitoring .....	71
4.3.	System Design, Experimental Design and Setup.....	71
4.3.1.	GLSS Experiment .....	71
4.3.2.	Quality Map Generation and Server Upload .....	74
4.4.	Results and Discussion .....	75
4.5.	Summary .....	82
5.	Conclusion.....	83
5.1.	Steps Forward .....	83
	References.....	86

**List of Tables:**

Table 2.1: Real-Time Localization Systems .....	21
Table 3.1: Anchor Positions of the Different Localization Experiments.....	26
Table 3.2: Controlled Grid Least Squares Algorithm Localization Experimental Results.....	57
Table 3.3: Controlled Grid Localization Experimental Results.....	63
Table 4.1: GLSS Experimental Results .....	77

**List of Figures:**

Figure 1.1: Project Overview ..... 4

Figure 2.1: Pulse Position Modulation ..... 14

Figure 3.1: Tag Enclosure and Power Bank ..... 25

Figure 3.2: (a) Room 47 Top View..... 27

Figure 3.3: Experiment 1 Layout ..... 28

Figure 3.4: Experiment 1 Setup ..... 29

Figure 3.5: Experiments 2-4 Layouts..... 30

Figure 3.6: Experiment 5 Setup ..... 31

Figure 3.7: Bin 3906 Experiment 5 Setup ..... 33

Figure 3.8: Experiment 7 Anchor 1 ..... 34

Figure 3.9: Tag Software Flowchart ..... 35

Figure 4.1: Belt Speed Monitoring Software Flowchart..... 70

Figure 4.2: Location of Synchronization Sensors on Bin-piler ..... 73

Figure 4.3: Synchronization Experiment Actual Travel Time Diagram..... 73

Figure 4.4: Grading Station Software Flowchart..... 75

Figure 4.5: GLSS Box and Whisker Plots ..... 76

Figure 4.6: Quality Map Interactive 3D Plot ..... 79

Figure 4.7: Quality Map Interactive 3D Plot with Features..... 80

Figure 4.8: Grading and Quality Results Output File ..... 81

**Abstract:**

This thesis proposes a novel post-harvest potato tuber storage traceability system designed to enhance quality monitoring and management. The system leverages a real-time localization system (RTLS), wireless communication and machine vision to identify and map the quality characteristics of potato tubers. RTLS experiments, conducted in both controlled laboratory settings and field environments, utilized a 3D grid structure with up to 60 actual tag locations, each generating 100 predicted positions. To further enhance accuracy, a Kalman filter was employed in conjunction with LS and a Support Vector Regressor, achieving a total Root Mean Square error (RMSE) as low as 0.183 meters in obstacle-free environments. Field tests were conducted during active harvest operations at a commercial potato farm, demonstrating the system's robustness under real-world conditions.

Additionally, a Grading Localization Synchronization System (GLSS) was implemented to predict tuber travel times during bin filling operations: thus, synchronizing localization with machine vision grading. The experiment was repeated for 30 trials, capturing both actual tuber travel times, and predicted times for nine combinations of bin-piler extension and conveyor belt speed. The system integrated real-time monitoring of bin-piler extension and belt speed, achieving synchronization RMSE values as low as 0.356 seconds with a Linear Regression model, compared to 0.585 seconds without. By creating a detailed 3D quality map of the storage facility, integrating tuber quality data with their spatial and temporal placement, and uploading this information to a remote server, the system enables centralized monitoring and analysis. This integrated approach significantly enhances traceability, reduces post-harvest losses, and improves the overall quality management of stored potato tubers.

## **List of Abbreviations and symbols Used:**

AOA: Angle of Arrival

BLE: Bluetooth Low Energy

DS-TWR: Double Sided Two-Way Ranging

FAOSTAT: Food and Agriculture Organization of the United Nations Statistical Database

FCC: Federal Communication Commission

GLSS: Grading Localization Synchronization System

GPS: Global Positioning System

IR-UWB: Impulse Radio Ultra-Wideband

LED: Light Emitting Diode

PWM: Pulse Width Modulated

RFID: Radio Frequency Identification

RMSE: Root Mean Square Error

RPM: Repetitions Per Minute

RSSI: Received Signal Strength Indicator

RTLS: Real-Time Localization System

$R^2$ : Coefficient of Determination

SS: Signal Strength

TDoA: Time Difference of Arrival

TOA: Time of Arrival

TOF: Time of Flight

TWR: Two Way Ranging

UART: Universal Asynchronous Receiver Transmitter

UWB: Ultra-Wideband

WSN: Wireless Sensor Network

## **Acknowledgements:**

First, I would be nothing without my family. My wife, Reem, my forever and always partner; you are my everything. My mom and dad, Misti and Jeff—because of whom, I haven't known a second in this life without love and support; I owe you everything. My brother, Cody, I see your well-earned success, am inspired, am proud, and always cheer you on. To my new family, my in-laws—how you do without any semblance of privilege yourselves, and yet, provide immense privilege to me; It's an honor to count myself, if I may, among the Abukmeils of Gaza—peace and love. Lastly, to our newest family, my son, Adam:

“... If you can fill the unforgiving minute

With sixty seconds' worth of distance run,

Yours is the Earth and everything that's in it,

And—which is more—you'll be a Man, my son!” – If by Rudyard Kipling (1895)

I also, of course, extend my sincerest gratitude to my supervisor, Dr. Ahmad Al-Mallahi, for the opportunity, continual support, and guidance. His intellect, wisdom, vision, and integrity set an example for me from which I shall eternally profit. A heartfelt thank you as well to my committee members, Doctors Vincent Sieben and Yves Leclerc. Time and energy are expensive, especially for those who extend such as yourselves. It is an honor to count you two among my committee—I thank you. Next, I'd like to thank all the members of the Applied Intelligent Engineering Systems (AIES) Research Group, whom I am blessed to call both colleagues and, which is more, friends: Ighodaro Emwinghare, Sama Huseynova, Imran Hassan, Humphrey Maambo, Ali Shirzadifar and last, though certainly not least, Mozammel Bin Motalab. Thank you as well to Ashvir Singh, Aniket Mandal, and Mohamed Hbaieb, AIES interns, for their valuable contributions to this research.

## **1. Introduction:**

Potatoes (*Solanum tuberosum*) are a nutrient-rich root vegetable, containing carbohydrates, minerals, vitamins, and essential amino acids (Caliskhan et al., 2023). Since the dawn of civilization, humans have actively sought to extend the shelf life of potatoes. For example, about 2000 years ago the Quechua people, residing in modern-day Peru, transformed their potatoes into the long-lasting chuno, a flour variant (Rastovski & Van, 1981; D'Altroy, 1987). Shifting northward, the temperate climate in Europe and North America limited farmers to only one potato harvest per annum, necessitating the development of tuber storage technologies to bridge the gap between constant demand and seasonal production (Pinhero et al., 2009). Early techniques involved covering the tubers with a layer of straw, or later earth, to protect them from cold temperatures. Building off this foundation, contemporary storage facilities allow for strict control of temperature and humidity, further delaying decomposition (Guenthner, 1995). High-quality storage of potatoes is essential to provide high-grade product throughout the entire year (Singh & Kaur, 2016), which is doubly necessary when feeding sophisticated and mechanized potato processing plants (Gottschalk, 2011). For farmers, storing potatoes adds value and reduces risk, while for consumers, storage provides additional choices and increased satisfaction (Booth & Shaw, 1981). Accordingly, storage and post-harvest technologies are crucial for the entire potato production process (Akello et al., 2022).

Global potato production has been steadily rising in recent decades. In the early 1960s, production was less than 30 million tons, increasing to more than 165 million tons by 2007 (Miah, 2009). Currently, the potato is grown in more than 150 countries (Caliskhan et al., 2023), with a total production approximately 374, 777, 763 tonnes in 2022 (FAOSTAT, 2024). In 2020, Canadian growers produced 4.26 million tonnes of potatoes, generating \$1.4 billion (CAD) in farm cash

receipts and \$2 billion in export revenue (AAFC, 2022). Despite this success, the potato industry faces challenges due to high loss rates (Hafner et al., 2013; WWF, 2014). Across the entire value chain, about 53-55% of initial fresh potato production is lost (Willersinn et al., 2015), primarily due to biotic factors like sprouting and disease, as well as abiotic stresses such as low-temperature sweetening and mechanical damage (Pinhero et al., 2009). Losses can similarly arise from dry core, deformities, slugs and wire worms (Keiser et al., 2007). This loss of stock can be minimized through proper crop management, and by maintaining storage facilities with optimal conditions (Booth & Shaw, 1981; Gottschalk & Ezhekiel, 2006; Rastovski & Van , 1981). Additionally, accurate distribution of tubers to processing plants based on their specific quality attributes, such as size, shape, and sugar content, can reduce waste by ensuring that only suitable batches are directed to appropriate end-use processes (Naumann et al., 2020). Correspondingly, reducing post-harvest losses are one of the best approaches to improving potato farmers' livelihoods (Kumar & Kalita, 2017), and thus, current trends in the potato industry are driven by the need to reduce losses while maintaining quality (Olsen, 2014). Research on both technology and infrastructure improvement, like investing in innovative storage technologies, are critical to achieving this goal (Gottschalk, 2011).

Nowadays, potatoes are stored in one of two different arrangements, loosely in a heap, or in basket containers that get stacked over each other (Rastovski & Van, 1981). These techniques are known as bulk and boxed storage, respectively. In agriculture, there is a growing trend toward using boxed storage containers, which, when paired with specialized equipment like Radio Frequency Identification (RFID) tags, enhance traceability (Ruiz-Garcia & Lunadei, 2011). Boxed storage has become increasingly important due to its high flexibility, transportability, gentle handling, and ability to partition varieties into smaller groups (Gottschalk, 2011). Bulk storage is, however, more

suitable for large quantities of potatoes (Vaduva, 2021), as it is commonly used in large buildings that can hold several million kilograms of potatoes, and is less expensive (Pinhero et al., 2009). Also, importantly, potatoes can be transported into and out of more quickly, making bulk the more common choice of the processing industry (Schorling, 2001). For these reasons, piling potatoes in large heaps is the most common procedure for on-farm storage (Paul and Ezekiel, 2004), particularly in Canada and the United States (Pinhero et al., 2009), where potato farms tend to be of larger scale than Europe. This all being said, it is best to combine the efficiency and simplicity of bulk storage with the traceability benefits of boxed storage to optimize potato storage practices.

The principal objective of this research project is, therefore, to design and implement a potato tuber bulk storage traceability system (Figure 1.1). This system will utilize ultra-wideband (UWB) electromagnetic waves to locate and track the position of potato offloading conveyor (known as bin-piler) to map potato quality information within the storage as it gets filled by potatoes. The traceability system synchronizes its bin-piler localization information with a machine vision system mounted at a conveyor located between the potato loading truck and storage unit to create different potato quality maps. The originality of this system is two-fold. First, this research is the first to track a bin-pilers position in storage using UWB. Second, this is the only system which synchronizes real time localization with a machine vision grading station. Once tubers are imaged beneath the grading station, their drop-off time is approximated by monitoring conveyor belt speed and measuring path length of the offloading conveyor. The asynchronous localization data is then time-matched to the closest, predicted drop-off times of the imaged tubers. The following literature review will outline some more concepts necessary for understanding this research project, and then summarize and evaluate similar, pre-existing research.

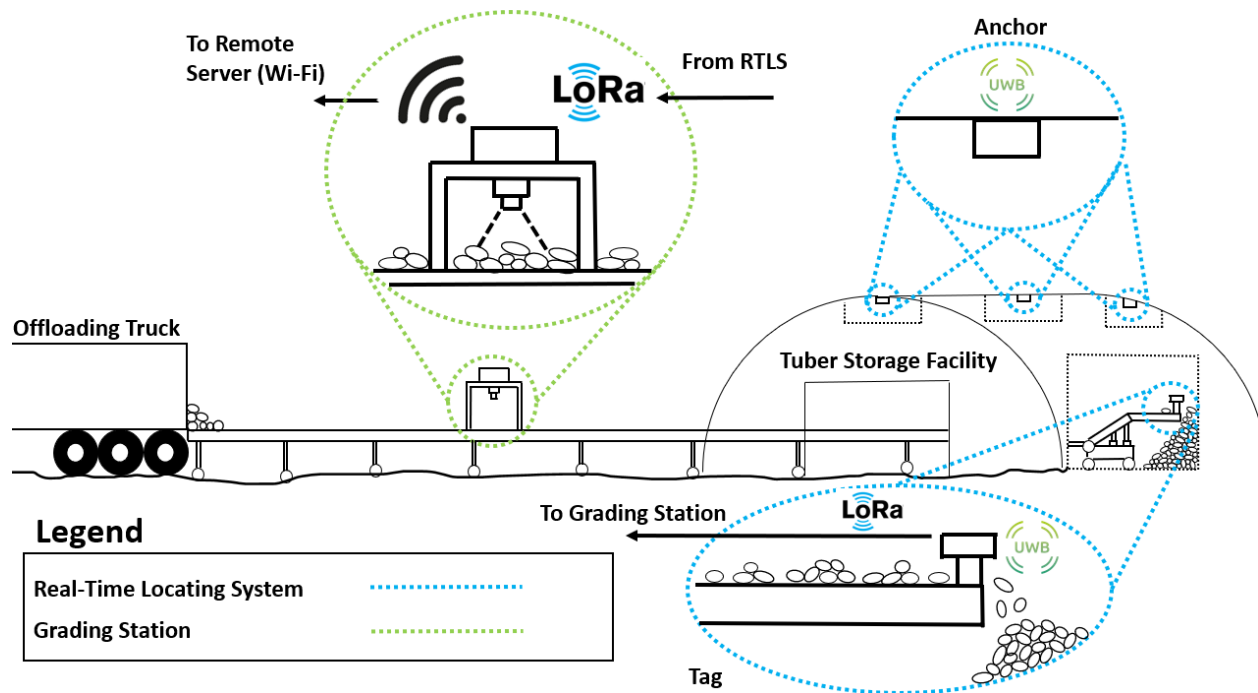


Figure 1.1: Project Overview

## 2. Literature Review:

### 2.1. Precision agriculture

Advancements in information, instrumentation, and communication technology revolutionized the agricultural industry in the second half of the 20th century, paving the way for what is now known as precision agriculture. As we progress further into the 21st century, the meaning of precision agriculture continues to expand, encompassing emerging technologies, techniques, and ever-deepening scientific knowledge (Al-Mallahi, 2024). These technologies include remote sensing data acquisition, variable rate agrochemical sprayers, yield monitoring, long-range wireless communication, and decision support systems (DSS) (Badhai et al., 2022). Regarding potatoes, growers can utilize sophisticated DSS technologies to receive weather information, potato variety, plant maturity as inputs, and output advice on which fungicide to apply, and at what dosage (Haverkort and Kempenaar, 2016). Through precision agriculture, farmers are empowered to decrease costs, enhance yield quality, increase crop production, minimize environmental impact,

reduce production inputs, decrease costs, and improve farm income (Bongiovanni and Lowenberg-Deboer, 2004; Paustian and Theuvsen, 2017).

## **2.2. IoT in Agriculture**

The Internet of Things (IoT) refers to a network of interconnected physical objects, such as devices, instruments, vehicles, and buildings, embedded with sensors, electronics, and software that enable them to collect, share, and exchange data over existing networks (Gokhale et al., 2018). By integrating the physical world with computer-based systems, IoT enhances efficiency, automation, and accuracy across various industries (Velasquez et al., 2017). The growing ecosystem of IoT incorporates a range of technologies, including wireless sensor networks (WSNs), RFID, near-field communications (NFC), barcodes, intelligent sensing systems, and cloud computing (Gokhale et al., 2018; González-Amarillo et al., 2018).

In agriculture, IoT systems provide innovative solutions to promote good agricultural practices and the effective use of land, while orchestrating real-time data collection and monitoring. One example is the traceability of fresh, edible products, where the process must be efficient and rapid to prevent spoilage (González-Amarillo et al., 2018). The design and implementation of IoT-based traceability systems enable better monitoring and management of agricultural produce from the field to the consumer, ensuring product quality and safety (Velasquez et al., 2017). Correspondently, one of the primary application areas of IoT in business processes is logistics, particularly in the traceability of outdoor assets in supply chains, such as transport vehicles or freight containers (Velasquez et al., 2017). As IoT technologies become more prevalent, their integration with traceability systems holds the potential to revolutionize supply chain transparency, offering end-to-end visibility and control.

### **2.3. Traceability Systems**

Traceability systems, using technologies like Quick Response codes (QR), IMUs and machine vision, provide stakeholders with quantitative and qualitative information about products, their processing, distribution, and origins (Trautman et al., 2008). These systems rely on continuous data exchange to track the history, location, and condition of products throughout production and distribution. Early traceability systems involved workers manually recording information in-field and transferring all data into logbooks or computers. However, this procedure suffers from inaccuracy, data loss, and significant time consumption (Basir et al., 2024; Demestichas et al., 2020). Tracking and identification of products has proven to increase asset value and net profits, while simultaneously improving consumer security, customer trust, and – in agriculture – food safety, which is subject to increasingly stringent controls and enforcement (Demestichas et al., 2020; Gottschalk, 2011). In potato production, traceability also allows for monitoring the effects of agricultural practices on tuber quality during storage, such as the impact of high nitrogen fertility, which increases yield but can decrease storage quality (Booth & Shaw, 1981). Moreover, most of the disorders arising in storages, such as blight or fusarium rot, are a consequence of field-growing conditions (Phillips, 1957; Xue & Yang, 2021). Traceability systems, and tracking from field to storage, can therefore help understand and manage these disorders.

Information such as the geographic location of the harvester and the truck transporting the harvest, the storage destination of the truck, and the environmental conditions of the storage over a long period of time can be used to assess the production process, detect source of faults in production, and improve customer satisfaction. For bulk storage, systems such as Ritetrace (Ritetrace, Greentronics, Elmira, Canada) gather yield, time, and GPS data at the harvester, relay this information to storage by transport truck-mounted RF transmitters, and determine when and where these tuber loads are placed within storage bins (Greentronics, 2021) based on dead reckoning – a

method that combines gyroscopes, accelerometers, and shaft-rotation sensors to track bin-piler movement. However, since dead reckoning tracks dynamics over time, location estimates rely on the accuracy of previous predictions, which means that localization error inevitably grows with time (Tsai, 1998). Thus, to maintain accuracy, it is common to combine dead reckoning sensors with absolute, time-independent location prediction systems (Liu et al., 2010; Dewhurst et al., 2016; Elbes et al., 2012), such as RTLS (Racz-Szabo et al., 2020).

#### **2.4. Real-Time Localization Systems**

Also known as Real-Time Localization Systems, or Indoor Positioning Systems (IPS), RTLS are electronic devices used to position and track objects of interest in real time, typically in indoor environments where global navigation satellite systems (GNSS) like GPS are either inaccurate or unusable (Racz-Szabo et al., 2020; Niu et al., 2023; Mendoza-Silva et al., 2019). RTLS have increasingly gained importance across industries, including agriculture, where they are essential in managing large-scale operations like animal husbandry, where fewer workers are responsible for more livestock (Will et al., 2017). However, the application of RTLS in cropping systems remains largely unexplored, presenting a potential avenue for future research and innovation.

##### **2.4.1. Sensing Paradigms and Ranging in RTLS**

There are various sensing paradigms used in RTLS to determine the location of objects. These systems can be broadly classified based on the type of signal measurement: time-of-arrival (TOA), angle-of-arrival (AOA), and signal strength (SS) (Mendoza-Silva et al., 2019). TOA measures the time it takes for a signal to travel from one transceiver to another – otherwise known as ranging - while AOA measures the angle at which the signal arrives at the receiver. Similar to TOA systems, SS can be used to determine distance, where the internodal distance is ascertained through the attenuation of signals across space, per the inverse square law. This relationship models how the power of the transmitted signal decreases proportionally to the square of the distance, allowing for

ranging by quantifying the energy loss over the propagation medium. Each technique, however, has its own limitations. For instance, AOA is less effective for indoor environments where signals scatter due to obstacles, complicating angle estimation (Gezici et al., 2005), which is further exacerbated as the accuracy of AOA degrades with distance (Grambozov et al., 2015). In contrast, SS-based localization suffers from inconsistent accuracy due to variations in the transmission medium (Gezici et al., 2005) such as multipath fading and shadowing, where signal path loss models are site-specific and fail to extrapolate generally. When one employs TOA, their approach must include some manner of accounting for, or overcoming, imperfect system clocks; every nanosecond of time of flight (TOF) measurement error may be translated to 30 cm of ranging error (Rathje & Landsiedel, 2024). There are two relevant kinds of clock errors: drift and offset. Clock Drift refers to the gradual deviation in a clock's frequency over time due to environmental factors, aging, and other influences. Clock drift accumulates over time, causing relative discrepancies in timing, which lead to inaccuracies in distance measurements if not corrected. Clock Offset is the initial difference or discrepancy between the clocks of two devices at the beginning of a measurement. Clock offset occurs because no two clocks are perfectly synchronized, and this offset affects the accuracy of TOA measurements unless accounted for in the ranging method (Laird, 2012).

The most popular TOA ranging technique is measuring the TOF and using the approximate speed of light to ascertain the distance. Methods for dealing with clock errors include hard-wired clock synchronization, where a common clock signal is shared directly among transceivers as well as synchronizing clocks using the preamble of the wireless signal, where parts of the transmitted signal are specifically allotted to timing information, allowing receivers to adjust for clock drift. Also, two-way ranging (TWR) can be employed, which calculates the time delay of round-trip

signals between UWB anchors and UWB tags, effectively bypassing the need for absolute synchronization by relying on relative timing measurements (Gezici, 2008; Jiang & Leung, 2007). Single-sided TWR involves a single exchange of messages between two devices, where the initiating device sends a signal and calculates the distance based on the round-trip time of the signal. However, this method can introduce inaccuracies due to clock offset and processing delays at the receiving end. Double-sided Two-Way Ranging (DS-TWR), on the other hand, requires two complete exchanges between the devices, allowing each device to measure the TOF and account for clock discrepancies. By averaging the timing from these exchanges, DS-TWR significantly reduces errors associated with clock drift and processing delays, thus providing more accurate and reliable distance measurements, especially in dynamic or cluttered environments (Rathje & Landsiedel, 2024).

The combination of distances between a tag (a mobile device attached to an object or person) and multiple fixed anchor nodes which have static, known positions can then be used to determine location. These mathematical algorithms, utilizing both distance and geometry are known as localization algorithms. Examples include Trilateration, Triangulation, Time-Difference-of-Arrival (TDoA), centroid-based techniques, Least Squares Algorithm (LS) and Landmark Positioning.

#### **2.4.2. Ranging and Hardware**

Shifting to the hardware, one of the most common methods to determine the arrival time of a received signal is through either a matched filter or a bank of correlation receivers. In the matched filter approach, the estimate of the arrival time is based on identifying the instant when the filter output reaches its peak, whereas in the correlation receiver approach, the arrival time is estimated by finding the time shift of the template signal that maximizes the correlation with the received

signal (Gezici et al., 2005). Both methods are mathematically equivalent - the choice between them often depends on design complexity and implementation costs. The matched filter approach requires a single filter but must be closely approximate to the time-reversed waveform of the received signal, while correlation receivers may require a large number of parallel computations to achieve the same result. These methods, however, face challenges in more complex environments, such as those with multipath propagation, multiple access interference (MAI), and non-line-of-sight (NLOS) conditions, which can distort the signal and make accurate location estimation more difficult (Gezici et al., 2005). In narrowband systems, the multipath effect causes multiple replicas of the transmitted signal to overlap, shifting the peak of the correlation and potentially leading to inaccuracies in TOA estimation.

### **2.4.3. Multipath and NLOS Mitigation**

Multipath refers to the phenomenon where transmitted signals reach the receiver via multiple paths due to reflections, diffractions and scattering from obstacles. To address the challenges of multipath interference in TOA estimation, high-resolution time delay estimation techniques have been developed. These techniques, while more complex than traditional correlation-based algorithms, are particularly effective in UWB systems due to their large bandwidth, and hyper-low duty cycle – approximately 0.1% - which allows multipath components to be more easily resolved. However, despite this advantage, multiple correlation peaks still arise, requiring specialized algorithms to accurately detect the first arriving signal path (Gezici et al., 2005; Scholtz and Win, 1997; Sodeyama et al., 2010).

When the direct line-of-sight (LOS) between two nodes is blocked, only reflected UWB pulses scattering from the surrounding reach the receiving node, resulting in a delay of the first pulse and introducing NLOS. This error creates a positive bias in the time delay, causing inaccuracies in

location estimation, especially when using techniques like the LS, which assume zero-mean Gaussian measurement errors. In cases where no information about NLOS errors is available, non-parametric techniques, such as pattern recognition, can be employed to match new TOA measurements with a reference set collected from known locations. Additionally, statistical methods can be used to differentiate between LOS and NLOS conditions by analyzing the variance in TOA measurements, with NLOS cases typically showing much larger variances (Marano et al., 2010). This variance can then be used in conjunction with LOS reconstruction algorithms to reduce the location estimation error.

### **2.5. Long Range Data Transmission**

Long range transmission and little power availability are crucial obstacles in agricultural deployments, particularly in reference to remote sensing. LoRa can help to overcome these challenges (Swain et al., 2021). LoRa is a low-power and robust wireless networking technology which applies spread spectrum techniques, allowing for high receiver sensitivity and long-distance transmission (Li et al., 2019). In fact, LoRa has the link budget of 155-170 dB, the highest of any standardized communication technology (Shamaas, 2022). This allows LoRa transceivers to communicate at distances larger than 10 km. Accordingly, the need for repeaters is reduced, greatly simplifying system design. Another advantage to LoRa is orthogonality, meaning, multiple transceivers can occupy the same band simultaneously without mutual interference. LoRa uses the chirp spread spectrum modulation technique in the license-free 915 MHz band.

LoRa wide area networks (LoRaWAN) allow for a scalable bandwidth of 125 kHz, 250 kHz or 500 kHz (Reynders and Pollin, 2016). According to Kufakunesu et al. (2020), this, among other mechanisms, form LoRa's Adaptive Data Rate (ADR), which helps extend battery life by adjusting the data rate according to the link budget quality between the end device and gateway. When the

connection is stable and the end device is close to a gateway, ADR reduces the spreading factor and increases the data rate, thereby decreasing transmission time and conserving energy. Conversely, for devices further from the gateway, a higher spreading factor is employed to ensure reliable communication by increasing the link budget, even though it consumes more airtime and power (Kufakunesu et al., 2020).

According to Singh et al., 2020, LoRaWAN uses a star-of-stars topology, where central gateways relay messages between client devices and a central network server. This structure allows for efficient communication, even in networks with many connected devices, by using multiple gateways to cover large areas. Accordingly, WSN networks are often constructed using LoRa, with examples in agriculture.

## **2.6. Ultra-Wideband (UWB)**

Given the challenges of indoor positioning, UWB technology has emerged as one of the most promising solutions for achieving accurate real time localization. UWB is an umbrella concept coming to signify various synonymous and complementary terms such as: carrier-free, baseband, high time resolution impulses and non-sinusoidal orthogonal function (Barrett, 2000). Correspondently, different summary definitions have been proposed, for instance, UWB are signals that have a large relative (fractional) or absolute bandwidth (Win et al., 2009). Relative bandwidth ( $BW_{Rel}$ ) refers to the ratio between absolute bandwidth ( $BW_{Ab}$ ) and carrier frequency ( $f_c$ ) Eq. 2.1. Absolute bandwidth, or what is more generally called, bandwidth, is the range of the frequency spectrum wherein the signal power exceeds 50% its peak level. In other words, absolute bandwidth is the difference between the upper ( $f_H$ ) and lower ( $f_L$ ) cutoff frequencies, which themselves, are the frequencies above and below which the power drops -3dB (half-power) from its peak level.

$$BW_{\text{Rel}} = \frac{BW_{\text{Ab}}}{f_c} = \frac{f_H - f_L}{2(f_H + f_L)} \quad (2.1)$$

The FCC provides further quantifies this definition, elaborating that UWB signals have a relative bandwidth larger than 0.2, or occupying greater than 500 MHz of absolute bandwidth (Nikookar and Prasad, 2009). Simultaneously, they mandate that commercial use of UWB devices be restricted to the frequency band from 3.1GHz to 10.6GHz, with a quite restrictive Equivalent Isotropically Radiated Power (EIRP) of -41.3dBm/MHz (Pirch and Leong, 2020). The restrictive regulations on emission power do, however, make sense when one considers that high power systems transmitting in broad frequency ranges will induce significant cross talk unto nearby wireless communication systems.

### **2.6.1. UWB Modalities**

UWB technology encompasses several different modalities, each designed for specific applications and performance characteristics. One of the most common types is Impulse Radio Ultra-Wideband (IR-UWB, or UWB-IR), the variant most germane for localization, although there is also Multi-band Orthogonal Frequency Division Multiplexing (MB-OFDM), and Chirp Spread Spectrum (CSS-UWB), both being more appropriate for data communication. IR-UWB systems are characterized by short duration Gaussian pulse waveforms, typically 3<sup>rd</sup> or 7<sup>th</sup> derivative, and importantly, in the order of nanoseconds (Sahinoglu et al., 2008). The 3<sup>rd</sup> and 7<sup>th</sup> derivatives strike a balance between performance and implementation complexity. While higher-order derivatives provide narrower pulses and better spectral properties, they are more challenging to generate and process reliably (Phan et al., 2007). Short pulses enable high time resolution ranging, which is the key to accurate positioning; and can be further improved by increasing the signal-to-noise ratio, making them ideal for high-definition localization tasks (Dardari et al., 2009).

Modulation is the process of changing certain characteristics of a signal, such as its frequency, phase, or amplitude, to encode information for transmission. In simpler terms, it's like adjusting the way a signal is shaped or timed so that it can carry messages over a communication channel: like open air, or a cable. IR-UWB employs one of several modulation techniques, including Pulse Position Modulation (PPM) (Figure 2.1), Binary Phase Shift Keying (BPSK), and On-Off Keying (OOK) (Molisch, 2009). In PPM, information is encoded by varying the timing of the pulse, or the chip interval ( $T_c$ ) within the period of the frame ( $T_f$ ).

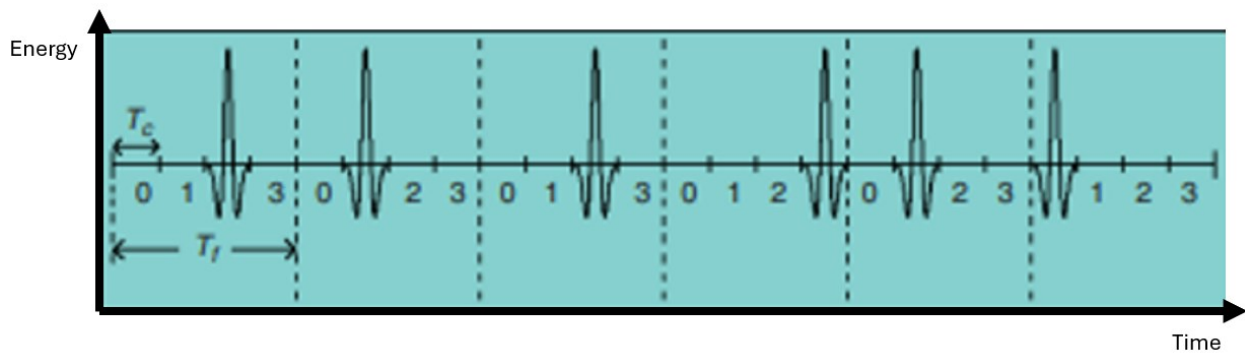


Figure 2.1: Pulse Position Modulation (Gezici et al., 2005)

### 2.6.2. Advantages of UWB

Localization technologies can generally be divided into two categories based on the type of infrastructure they utilize. The first category leverages existing wireless infrastructure, such as Wi-Fi networks or Bluetooth-based systems, making them relatively cost-effective and easier to deploy (Liu et al., 2007). In contrast, the second category consists of systems that require dedicated infrastructure, such as UWB or RFID networks (Alarifi et al., 2016). These systems are designed specifically for precise tracking and offer superior performance but their implementation involves higher costs (Liu et al., 2007). UWB's short pulses require low transmission power, and minimizes interference with wireless technologies like Wi-Fi and Bluetooth (Mendoza-Silva et al., 2019). Moreover, UWB's large bandwidth improves reliability by allowing signals to contain different

frequency components, which increases the likelihood that at least some will penetrate or bypass obstacles, enhancing its performance in cluttered environments (Gezici et al., 2005). In narrowband systems, the multipath effect causes multiple replicas of the transmitted signal to overlap, shifting the peak of the correlation and potentially leading to inaccuracies in TOA estimation. Correspondently, narrowband technologies like Wi-Fi and Bluetooth Low Energy (BLE) signals can be disrupted by obstacles such as walls, furniture, and other devices using similar frequency bands. This interference induces erratic fluctuations in SS, making precise localization difficult to achieve (Sung et al., 2023). To counter these issues, some systems utilize hybrid solutions that combine multiple types of sensors to increase accuracy, though this approach raises hardware costs, processing time and complexity (Sung et al., 2023). As RTLS continues to evolve, UWB stands out as the preferred technology for precise indoor localization, offering a more reliable, higher performance solution than traditional methods: like GPS, Wi-fi and RFID.

### **2.6.3. Challenges with UWB TOA**

UWB TOA systems are relatively low-cost compared to AOA-based techniques, which require more complex hardware: like antenna arrays, and RF phase shifters (Gezici et al., 2005). It is important to note, however, that UWB TOA systems are particularly sensitive to clock synchronization issues, such as clock drift and jitter, which are especially crucial due to the nanosecond time resolution of their Gaussian pulses (Gezici et al., 2005; Zhao et al., 2020). Also, the set of delay positions, or received signal replicates, is often longer than chip duration, necessitating the search through numerous chips to determine the correct TOA. This makes conventional correlation-based serial search approaches impractical and calls for faster TOA estimation schemes. To overcome these challenges, framerate or symbol-rate sampling techniques are preferred to ensure high-performance TOA estimation at lower complexity and power consumption. To address clock synchronization issues, TDoA offers an alternative by measuring

the relative arrival times of signals at different receivers, allowing for position calculation even without synchronization between a tag and reference nodes (Liu et al., 2007). These time-based approaches are further enhanced by UWB, which is capable to minimize multipath interference that typically affects other positioning technologies (Alarifi et al., 2016).

#### **2.6.4. UWB Hybrid Systems**

Hybrid UWB systems, which combine SS measurements with time-based techniques, have been developed to enhance localization accuracy further. While SS measurements are relatively easy to obtain, they are not as precise on their own, especially in cellular networks where SS depends on distance from base stations. However, when used in conjunction with TOA or TDoA, SS can improve the overall accuracy of UWB systems, particularly in short-range applications (Gezici et al., 2005). The ability of UWB to resolve multipath issues by leveraging its inter-pulse periods and wide bandwidth is a key reason for its growing popularity in hybrid positioning systems (Mendoza-Silva et al., 2019). Additionally, modulation techniques such as pulse position modulation (PPM) further reduce multipath interference, ensuring that UWB systems can operate reliably in cluttered environments (Alarifi et al., 2016). The carrier-less transmission of UWB and baseband signal processing also make it a cost-effective solution, as the hardware required is simpler and more affordable than that of narrowband systems (Yavari & Nickerson, 2014).

#### **2.7. Algorithms for Positioning and Prediction in RTLS**

In RTLS, algorithms for positioning and prediction are essential to transform raw signal data into actionable information about the location and movement of objects or people. Without algorithmic processing, the data received from anchors or sensors remains merely a collection of signal strengths, times of arrival, or other measurements, which are insufficient by themselves to determine precise positions. By using algorithms, RTLS systems can interpret these raw signals, compensate for inaccuracies introduced by noise, interference, and environmental obstacles, and

produce accurate, reliable location estimates. Additionally, predictive algorithms are necessary for tracking movement trends and forecasting future positions, which is particularly valuable in dynamic environments. Thus, algorithms serve as the bridge between raw signal acquisition and useful information.

### **2.7.1. Least Squares Algorithm (LS)**

LS is widely used in RTLS to determine the position of a target based on distance measurements from multiple fixed anchors. According to Pelka (2015), A straightforward implementation involves solving a system of linear equations, commonly referred to as the closed-form solution. This approach works by linearizing the position equations through algebraic manipulation, which transforms the system into matrix form. The position is then computed by directly solving the system using linear algebra, without iterative refinement. This technique is computationally efficient and often sufficient when precise distance measurements are available.

In contrast, more complex environments or nonlinear systems often require an iterative LS approach, where the algorithm minimizes the sum of the squared differences between the observed distances (TOA or TDoA measurements) and the predicted distances from the estimated position. This approach works by refining the position estimate over successive iterations, progressively reducing errors introduced by factors such as multipath propagation or NLOS conditions (Gezici et al., 2005). The iterative approach is crucial in environments where high accuracy is required, especially for UWB systems with complex signal propagation characteristics.

### **2.7.2. The Kalman Filter**

The Kalman filter is an algorithm used for estimating the state of a dynamic system from a series of incomplete and noisy measurements (Sung et al., 2023). It operates through two main phases: prediction and update. In the prediction phase, the filter uses a defined system model—often

assuming a constant velocity model in positioning applications—to predict the next state based on the current estimate. In the update phase, the Kalman gain is calculated to weight the predicted state and the new measurements, thereby updating the state estimates (Sung et al., 2023). The Kalman gain determines whether the system prediction model or the measurement model is more reliable for predicting the subsequent states. Key parameters influencing the filter’s performance include the initial estimation error, which reflects the filter’s initial confidence in the state estimates, the measurement error, which represents the expected level of noise in the input measurements, and the process noise, which accounts for unmodeled system dynamics or random variations (Welch & Bishop, 2001). In the context of RTLS, particularly those utilizing UWB technology, the Kalman filter enhances positioning accuracy by helping to filter out noise (Zhang et al., 2016), yielding up to 15% improvement (Abreu et al., 2014). This is crucial in environments where signal interference, multipath and NLOS effects can degrade measurement reliability (Yavari and Nickerson, 2014).

### **2.7.3. Support Vector Regressor (SVR)**

The SVR is a supervised machine learning technique used to estimate the optimal hyperplane for minimizes prediction errors. A key feature of SVR is the use of kernels, which transform the input data into higher-dimensional spaces to capture relationships that may not be apparent in the original feature space. Commonly used kernels include the linear kernel, which assumes a direct linear relationship between features and targets,; the radial basis function (RBF) kernel, which is well-suited for modeling non-linear relationships (Rohmah et al., 2021). In addition to its use in regression tasks, Support Vector Machines (SVMs) are also employed in classification tasks, where they are particularly effective in distinguishing between different data classes, such as LOS and NLOS conditions (Sung et al., 2023). In the context of UWB-based RTLS, SVRs are applied to improve the accuracy of range estimation, especially in challenging NLOS environments. By

using SVM techniques, researchers have developed models capable of mitigating ranging errors under NLOS conditions, outperforming traditional parametric methods. Furthermore, SVMs can be used for localization purposes by employing both offline and SS measurements – measured using received signal strength indicator (RSSI) - to classify and predict location data, making them a powerful tool in UWB-based RTLS for ensuring higher accuracy and robustness in varying signal conditions (Sung et al., 2023).

### **2.8. UWB Existing Systems in Literature and Industry**

UWB technology is rapidly being integrated into a wide range of applications, from industrial positioning systems to consumer devices. One well-known commercial application of UWB is the Ubisense system, where users carry tags that transmit signals to fixed sensors, which then determine the user's location using the TOA method (Alarifi et al., 2016). The potential for UWB in the consumer market has also gained attention, with products like the Samsung Galaxy Note 20 Ultra and Apple iPhones incorporating UWB chips for precise device-to-device communication and spatial awareness (Molisch, 2009). UWB is known for its low-power consumption, signal invariance, and high accuracy (Niu et al., 2023).

The development of various RTLS has been documented in the body of academic literature. Among which, location dimensionality is variable according to application and hardware complexity. Zhang et al. (2022) developed a system for determining the 2D location of tags, which overcomes positioning error due to clock drift/offset, using their wireless clock synchronization scheme. Others locate objects according to all three spatial dimensions. Mikoda et al. (2020) completed a 3D RTLS to test positioning accuracy for manufacturing systems.

RTLS system can either locate static objects, or objects with no-zero velocities. Huang et al. (2017) developed an RTLS, utilizing UWB and RFID, which determines the static position of objects.

Alternatively, many systems track objects as they move through space. Halawa et al. (2020) deployed an UWB-based RTLS in order to track the movement of forklifts throughout a 180m x 60m warehouse with an accuracy of 0.1-0.3m. The corresponding data was used to optimize warehouse safety, and operational efficiency. In addition, this paper demonstrates that RTLS can be deployed in large volume facilities, while maintaining accurate position data.

Some applications of RTLS networks require position data of a high temporal resolution. Also tracking the movement of forklifts within a warehouse, Li et al. (2016) developed a system with an update rate of 3.3Hz. Within the agricultural context, an UWB-based RTLS was used to track dairy cow movement within an open stall barn (Porto et al, 2014). This system provided location data at 1Hz within a 55.6m x 20.7m barn, and with an average error of 0.515m. This data was used to monitor and analyze cow resting and feeding habits. Most importantly, the literature demonstrates that RTLS systems can produce accurate location data. For example, Zhou et al. (2012) developed an ultra low-power RTLS yielding an average position error of only 10cm. The system by Zhang et al. (2022), produced even more accurate results, achieving average accuracies of 6.5cm and 7.2cm for 6 and 4 anchor node deployments. For a compendium of all systems analyzed as part of this literature review, see Table 1.1. Summarily, this literature review reinforced the originality of this system. First, this system is the only one which locates crop inventory within a pile. Second, this is the only system which integrates an RTLS tracking system with that of a quality inspection station. For a compendium of all systems analyzed as part of this literature review, see Table 1. Summarily, this literature review reinforced the originality of this system. First, this system is the only one which locates crop inventory within a pile. Second, this is the only system which integrates the use of an RTLS, with that of a quality inspection station and RFID traceability system.

Table 2.1: Real-Time Localization Systems

Cited Work	Mapping Area (m)	Technology	Number of Anchors	Accuracy (m)	Localization Algorithm	Ranging Method	Static or Dynamic Tags	Temporal Resolution (s)	Dimensionality	Real-time
Huang et al., 2017	N/D	UWB	4	0.183	Trilateration	TOA	Static	0.5	2D	✓
		RFID	4	0.387	Landmark	RSSI	Static	0.5	2D	✓
Schantz, 2007	930m <sup>2</sup>	Near-field Electromagnetic Ranging	N/D	1	N/D	POA & SS	Dynamic	0.1	2D	✓
Mikoda et al., 2020	9.5 x 5	UWB	4	0.377	TDoA & AOA	TOA	Static	N/D	3D	✓
Zhang et al., 2022	9.88 x 11.02	UWB	4	0.065	TDoA	TOA	Static	0.15	2D	✓
		UWB	4	0.072	TDoA	TOA	Static	0.15	2D	✓
		UWB	6	0.192	TDoA	TOA	Dynamic	0.15	2D	✓
Monta et al., 2016	12.5 x 6.36	UWB	3	0.48	Trilateration	RSS	Static	N/D	2D	x
		UWB	3	0.21	Trilateration	TOA	Static	N/D	2D	x
Choi et al., 2010	40 x 20	Chirp Spread Spectrum	9	1.0-7.0	TDoA	TWR	Static	N/D	2D	✓
Li et al., 2016	43.3 x 33.1	UWB	86	1.005-2.02	N/D	N/D	Dynamic	0.3	3D	✓
Halawa et al., 2020	180 x 60	UWB	N/D	0.1-0.3	N/D	TOF	Dynamic	2	3D	✓

Li et al., 2019	10 x 13	UWB	4	0.11	Triangle Centroid Optimization	TOA & DS-TWR	Static	N/D	2D	X
Zhou et al., 2012	6 x 6	UWB	4	0.1	TDoA	TOA	Static	N/D	2D	X
Porto et al., 2014	55.6 x 20.7	UWB	4	0.515	AOA & TDoA	TOA	Dynamic	1	3D	✓
Contigiani et al., 2016	10 x 10	UWB	4	0.15	TDoA	TOA	both	N/D	2D	✓
Delamare et al., 2020	4.03 x 5.10 x 1.45	UWB	4	0.01	TDoA	TWR	Static	N/D	2D	✓
		UWB	4	0.01	TDoA	TWR	Static	N/D	3D	✓
		UWB	4	0.21	TDoA	TWR	Dynamic	N/D	2D	✓
		UWB	4	0.24	TDoA	TWR	Dynamic	N/D	3D	✓
		UWB	5	0.16	TDoA	TWR	Dynamic	N/D	2D	✓
		UWB	5	0.18	TDoA	TWR	Dynamic	N/D	3D	✓
		UWB	6	0.17	TDoA	TWR	Dynamic	N/D	2D	✓
		UWB	6	0.2	TDoA	TWR	Dynamic	N/D	3D	✓
Jiménez-Ruiz & Granja, 2017	14 x 14	UWB (Ubisense)	6	1.1	AOA & TDoA	TOF	Dynamic	0.05	3D	✓
		UWB (Bespoon)	6	0.71	N/D	N/D	Dynamic	0.4	N/D	✓
		UWB (Decawave)	6	0.49	TWR & TDoA	TWR & TOF	Dynamic	0.286	2D & 3D	✓
Will et al., 2017	19.5 x 37	UWB	12	2	Trilateration	TOA	Static	1	2D	✓

Niu et al., 2023	8.74 x 5.45	UWB	4	0.1731	LS	DS-TWR	Static	N/D	2D	✓
Sung et al., 2023	11 x 11	UWB	3	0.25	TDoA	TWR	Dynamic	N/D	2D	✓
Meunier et al., 2018	41 x 117	UWB	18	0.16-0.19	N/D	N/D	Static and Dynamic	1.1-1.2	2D	✓

**N/D – Not Disclosed**

### **3. Development of Potato Bin-Piler Localization System using UWB in Lab and Field Environments**

#### **3.1. Overview**

The first step in mapping the quality information of the potato tubers transported into a storage unit is to be able to determine the location at which the bin-piler would drop them as it forms potato piles. By mounting a tag at the tip of the bin-piler and anchors on the walls of the storage unit, the bin-piler tip can be traced across storage. This positioning, in conjunction with data from the grading station's imaging and quality assessments, supports the creation of a synchronized quality map for stored tubers. Based on different experimental setups, the objectives in this chapter are to:

- 1) verify the ability of a set of anchors to determine the location of a tag in indoor environment,
- 2) find the optimum algorithm to accurately calculate the location of the tag based on signal data,
- 3) compare the performance of the set of anchors under different environments in lab and field so that the effects of distance, building structure, and obstacles can be verified and included in the design of the system.

#### **3.2. Materials**

The UWB transceivers used in this research project are ESP32 UWB boards (Makerfab, Shenzhen China). These devices use a microcontroller (ESP-WROOM-32, Espressif, Shanghai China) to control a UWB module (DW1000, Qorvo, Greensboro, North Carolina, United States). The UWB module is interfaced with an ESP32 microcontroller using the Serial Peripheral Interface (SPI) in a master-slave configuration, where the ESP32 acts as the master and the module functions as the slave. The module includes an IR-UWB chip the DW1000. The tag as well as the anchors include one UWB board as its primary component. However, the tag has an extra component which is a LoRa antenna (RYLR896, REYAX, Taipei, Taiwan) added to serve as a wireless communication

port to transmit all data collected from the anchors by the tag for further processing. In the tag (Figure 3.1), the communication between the board and antenna is via UART, with key commands configuring the address, baud rate, radio frequency, and network ID.

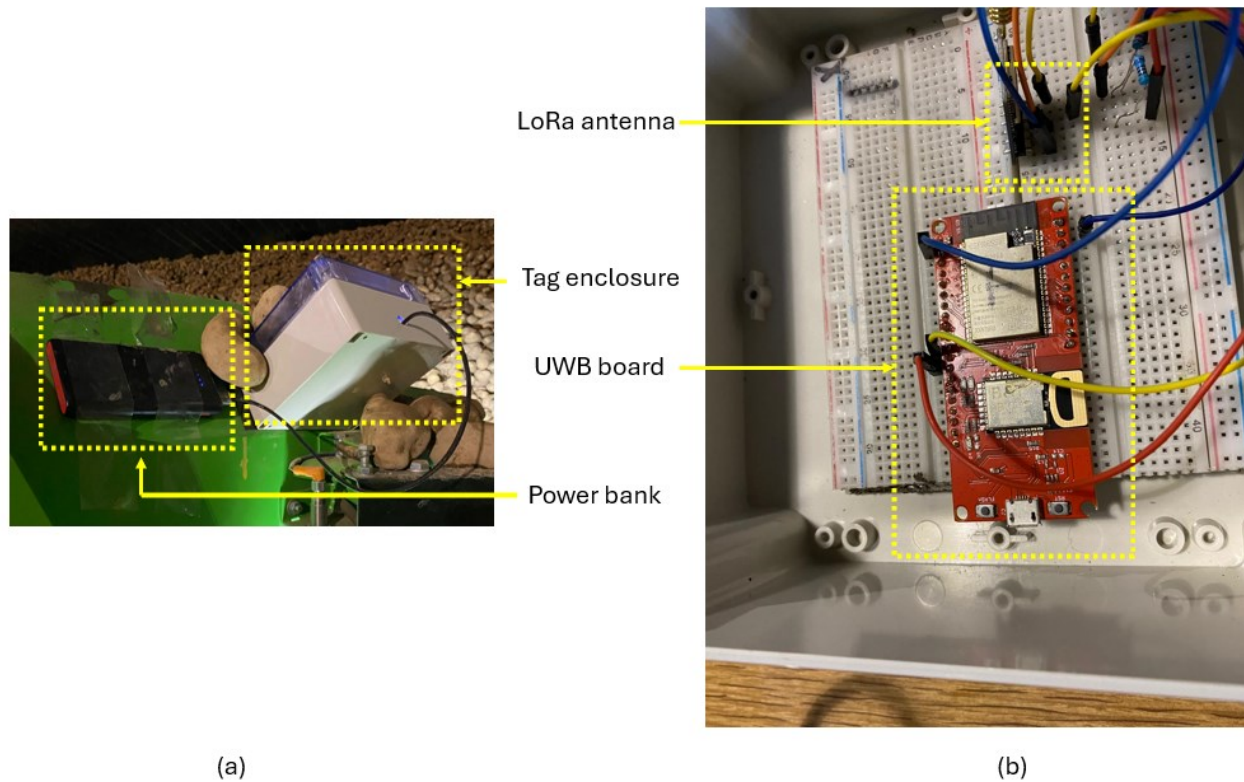


Figure 3.1: Tag Enclosure and Power Bank (a) Enclosure of a tag mounted upon bin-piler crest (b) Components of tag – a UWB board connected and a vertically oriented LoRa antenna

### 3.3. Experimental Design and Setup

A series of experimental setups were prepared in which parameters such as location, volume, coordinates of the anchors, and presence of objects introducing wireless noise were varied. Every experiment consisted of choosing a 3D space, around which 4 anchors were placed. The space was divided into a 3D grid, and the discrete locations for placing the tag were selected, corresponding to the whole numbered coordinates within the grid. At each location 100 predicted positions were generated. Table 3.1 lists the experiments and the location of the anchors.

Table 3.1: Anchor Positions of the Different Localization Experiments

Experiment Name	Experiment Number	Location	Anchor ID	Position (m)		
				X	Y	Z
Obstacle-free small volume environment	1	Room 47	1	0.00	0.00	0.18
			2	6.00	0.00	1.86
			3	0.00	6.00	0.58
			4	6.00	6.00	2.27
Uniform anchor height large volume	2	Room 47	1	-4.94	0.00	3.47
			2	14.64	0.00	3.47
			3	-4.94	13.94	3.47
			4	14.64	13.94	3.47
Small pile anchor locations	3	Room 47	1	0.00	3.70	4.00
			2	3.80	16.79	0.52
			3	11.32	28.34	2.24
			4	10.82	27.64	4.37
Large pile anchor locations	4	Room 47	1	0.00	11.44	3.92
			2	3.80	16.79	0.52
			3	11.32	28.34	2.24
			4	10.82	27.64	4.37
Bin-piler large volume environment	5	Bin 3906	1	0.52	-0.16	3.47
			2	11.00	0.00	0.52
			3	0.52	7.08	3.47
			4	11.00	7.08	0.54
Harvest operations small pile	6	Bin 3906	1	0.00	3.70	4.00
			2	10.82	27.64	0.52
			3	11.32	28.34	2.24
			4	0.00	16.79	4.37
Harvest operations large pile	7	Bin 3906	1	0.00	11.44	4.00
			2	10.82	27.64	0.52
			3	11.32	28.34	2.24
			4	0.00	16.79	4.37

The lab and field experiments were conducted in Room 47 of the Banting Building at Dalhousie Agricultural Campus (Bible Hill, Nova Scotia, Canada) (Figure 3.2a), and Bin 3906 in the main potato storage building of McCain’s Farm of the Future (Florenceville, New Brunswick, Canada) (Figure 3.2b).

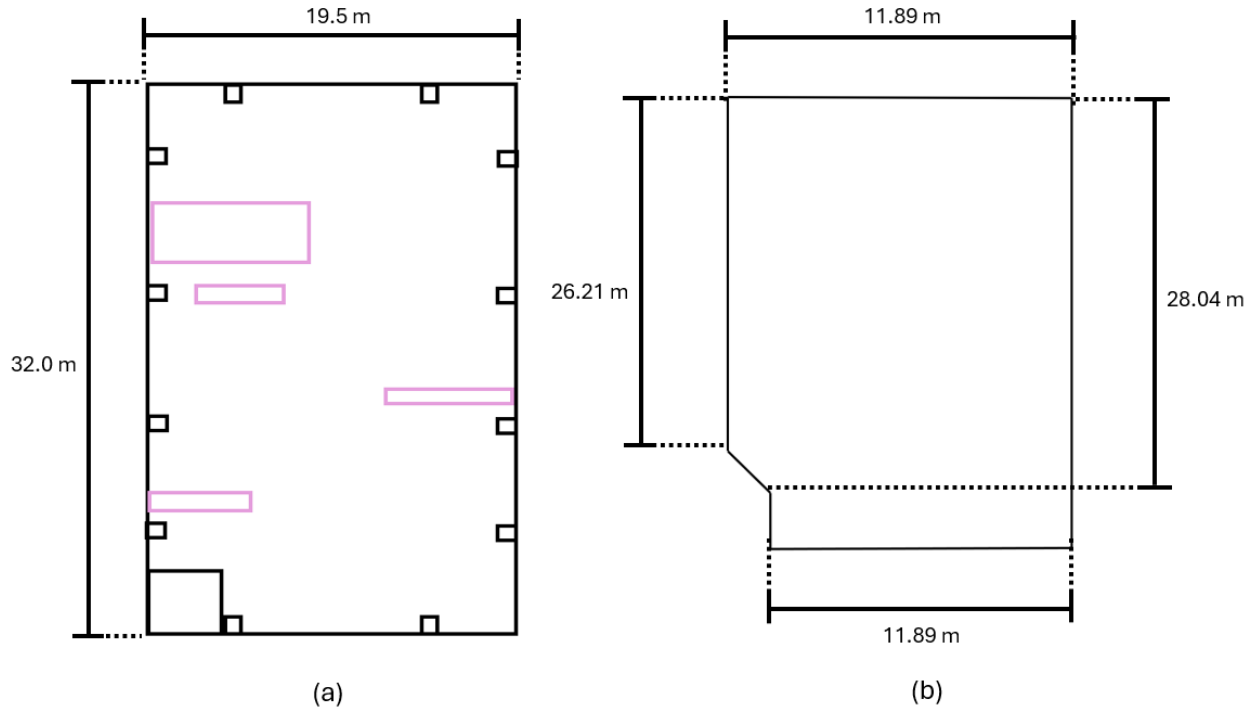


Figure 3.2: (a) Room 47 Top View - Pink and black boxes represent objects possibly introducing wireless noise: miscellaneous equipment and metal beams (b) Bin 3906 Top View

### 3.3.1. Experiment 1: Obstacle-Free Small Volume Environment in Lab

Experiment 1 served as an initial validation of the RTLS setup, aiming to confirm that the system could achieve localization accuracy comparable to that reported in similar studies. It took place within a limited space in Room 47 as described in Figure 3.3. A 6 x 5 m coordinate system was mapped onto the floor to facilitate structured positioning and data collection. Anchor placement objects were selected based on three criteria: stability (to avoid transmitter damage), unobstructed LOS for optimal signal reception, and varied height positioning to maximize Z-axis diversity. Actual tag locations are defined by Eq. 3.1.

$$\text{Actual Location (m)} = (X, Y, Z); X \in \{1,2,3,4,5\}, Y \in \{1,2,3,4\}, Z \in \{0.51,0.77,1.07\} \quad (3.1)$$

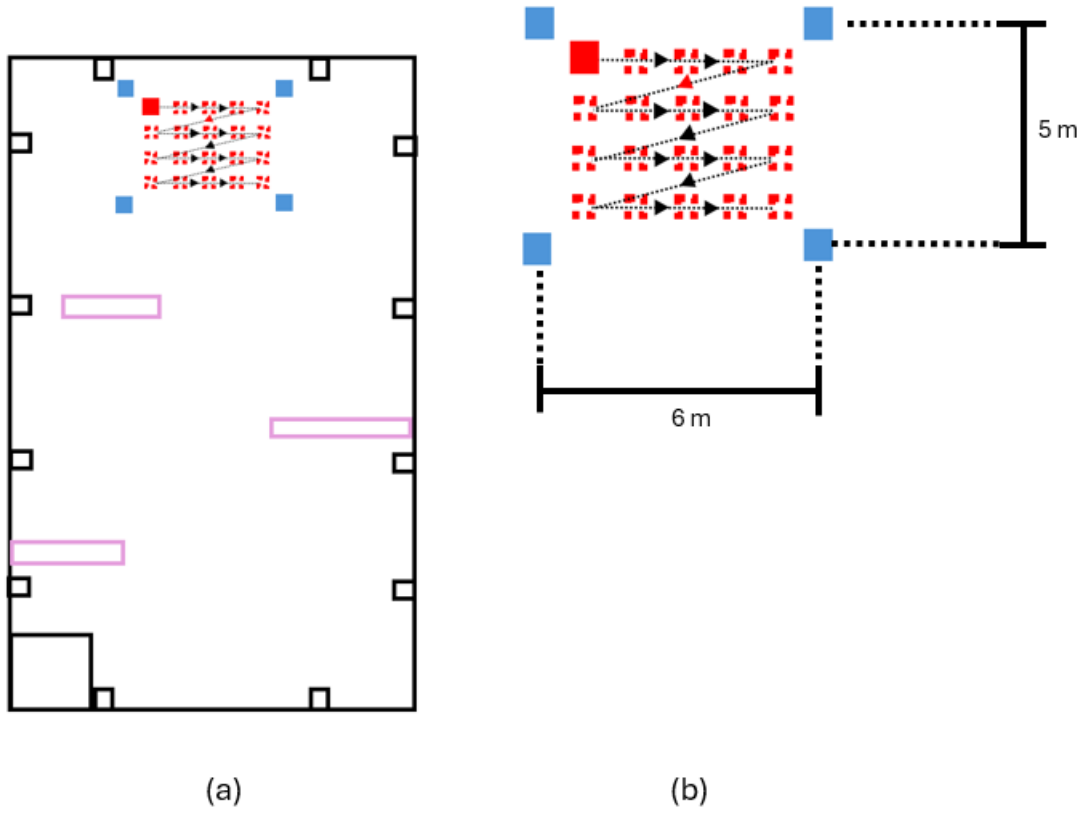


Figure 3.3: Experiment 1 Layout - (a) Top view of lab space (b) obstacle-free area within the room where anchors (blue) surround a volume through which an tag (red) is systematically moved through discrete locations for measurement.



Figure 3.4: Experiment 1 Setup - Picture of obstacle-free area in lab. The tag was mounted on a tripod, aligned with each designated (X, Y) coordinate on the grid to ensure accurate determination of its actual position.

**3.3.2. Experiment 2: Uniform Anchor Height Large Volume Environment at Lab**

Experiment 2 was designed to test the feasibility of positioning all anchors at the same height, the advantage of which being unobstructed deployments above the expanding potato pile. All anchors were mounted on steel support beams at a height equivalent to those of anchors 1 and 3 from the Experiment setup. This arrangement aimed to replicate farm-like conditions to allow for extrapolation of the results. The tag was placed in locations according to Eq. 3.2 and illustrated in Figure 3.5.

$$\text{Actual Locations (m)} = (X, Y, Z); X \in \{2, 4, 6, 8, 10\}, Y \in \{-4.97, 0, 4.97\}, Z \in \{1, 2.5, 4\} \quad (3.2)$$

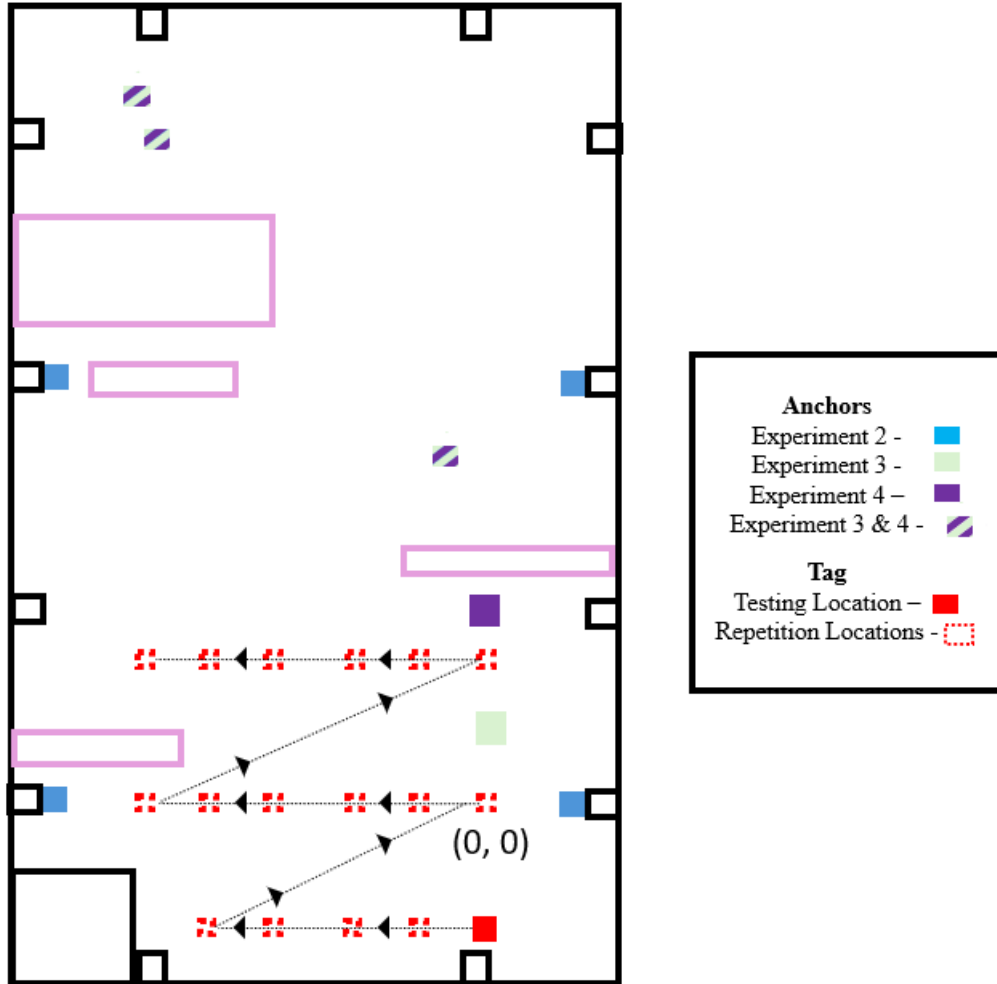


Figure 3.5: Experiments 2-4 Layouts - Top view of Room 47

### 3.3.3. Experiments 3 and 4: Small and Large Pile Anchor Locations in Lab

Experiments 3 and 4 were designed to replicate the conditions of in-field testing by mimicking the distribution of anchor placements observed in operational environments. Controlled simulation experiments were conducted in Room 47 at Dalhousie University, Bible Hill, Nova Scotia, where anchor placements were arranged to emulate the spatial configurations found in real-world applications. Adjustments were made to accommodate immovable obstacles in the warehouse, ensuring the experimental setup aligned as closely as possible with the intended design (Figure 3.5). For consistency, the same tag positions were used throughout these experiments, as defined

by Eq. 3.2, allowing for a structured evaluation of localization accuracy under laboratory conditions.

### 3.3.4. Experiment 5: Bin-piler Large Volume Environment in Field

Experiment 5 aimed to validate the RTLS system's performance in a large, open agricultural storage environment, specifically within Bin 3906 (Figure 3.6 and 3.7). The choice of this inactive bin allowed for a controlled setup that mimicked real-world conditions without the interference of ongoing operations. This setup promoted Z-axis diversity, enhancing the system's ability to localize in three dimensions, which is particularly important for agricultural applications where vertical position tracking can impact logistical planning. While assumptions were made regarding the ideal flatness of the floor and perpendicularity of the walls, these simplifications were necessary for straightforward data interpretation. However, these assumptions might have introduced minor inaccuracies.

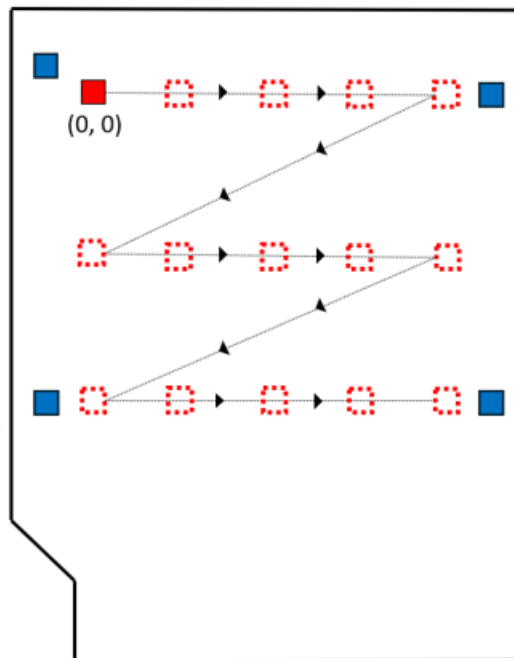


Figure 3.6: Experiment 5 Setup – Top view sketch of Bin 3906. The tag (red) was mounted on a bin-piler, aligned with each designated (X,Y) coordinate on the grid to ensure accurate

determination of its actual position. Anchors (blue) surround the experimental volume at two discrete heights.

The bin was measured at 12 m in width, 26 m in length, and 4.26 m in height. To provide thorough spatial coverage, the four anchor points were strategically chosen as shown in Figure 3.6 and 3.7. A 2D grid was drawn on the bin floor to standardize location measurements. For optimal LOS and stability, Anchors 1 and 3 were mounted on the sheet metal walls, while Anchors 2 and 4 were placed on chairs. To map positions within the bin, the bin-piler (Cobra, AVR, Rotterdam, Netherlands) (Figure 3.7) was maneuvered such that the crest (end of the bin-piler's arm) aligned with predetermined X and Y floor coordinates. A weighted string was attached to the crest to ensure control over the Z-axis, allowing precise vertical measurements. The tag was secured near the crest of the bin-piler (Figure 3.8). The small offset between the tag and the crest center was assumed negligible, with any residual error addressed by the SVR algorithm in post-processing.

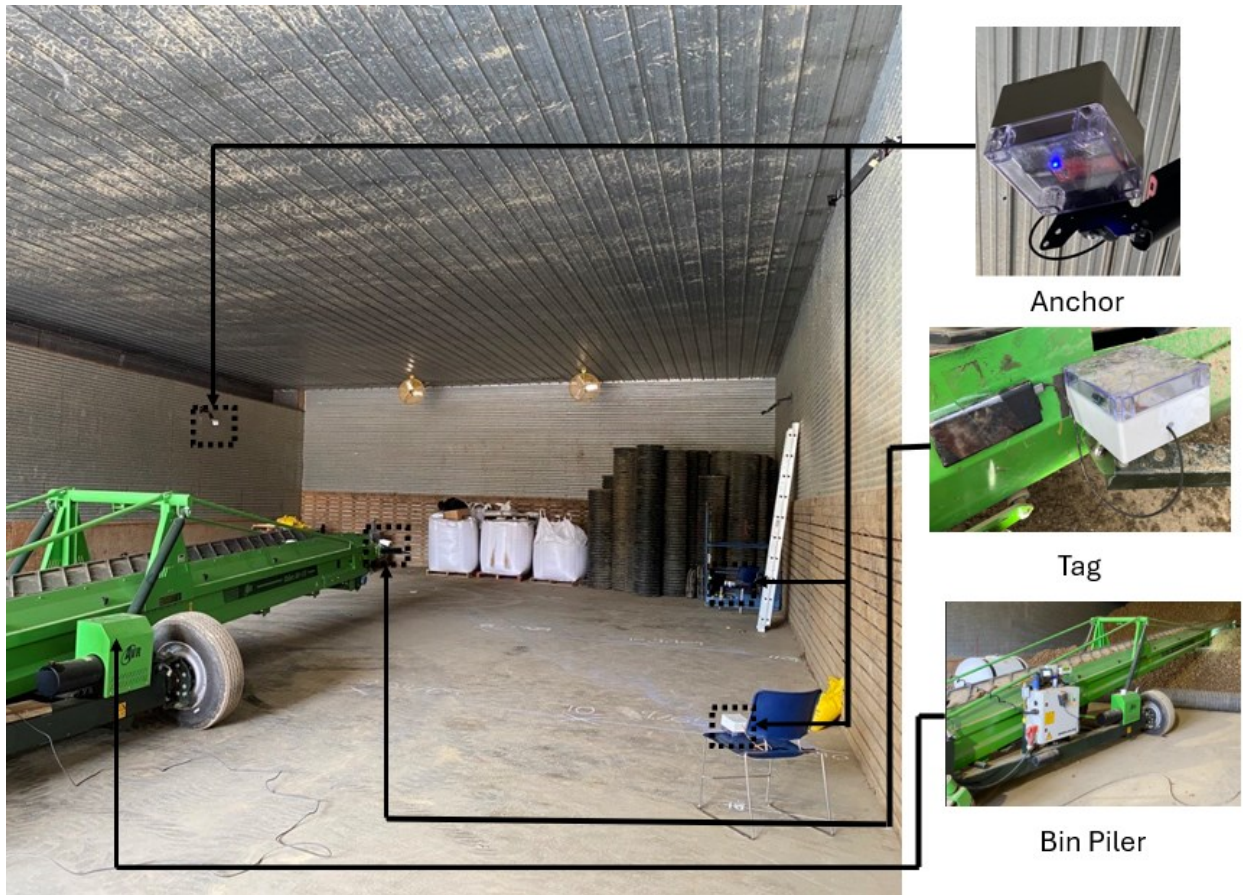


Figure 3.7: Bin 3906 Experiment 5 Setup - tag mounted along the side of the bin-piler crest and four anchors placed at different heights as determined in Table 3.1.

The tag was placed in locations according to (Eq. 3.4).

$$\text{Actual Locations (m)} = (X, Y, Z); X \in \{2,4,6,8,10\}, Y \in \{0, 4.91, 9.82\}, Z \in \{1,2.5,4\} \quad (3.4)$$

### 3.3.5. Experiments 6 and 7: Harvest Operations Small and Large Pile in Field

These experiments were conducted during active harvest operations. Building on the off-season testing conducted in the main storage, these trials aimed to assess RTLS performance under dynamic conditions as the storage area filled with a potato pile. Initial anchor placements were positioned with respect to the storage building's layout and dimensions, and according to the potato pile. To accommodate the growth of the pile, the anchors were set and adjusted, small and large pile, according to Table 3.1.

Contrary to Experiment 5, two major adjustments were necessary to prevent anchor obstruction by the potato pile. Anchors 1 and 3, originally mounted on the sheet metal wall, were relocated to the outer edge of the catwalk or observation deck (Figure 3.8). Anchors 2 and 4, initially placed on chairs, were moved closer to the bay door, away from the maximum range of the pile. The tag was mounted on the bin-piler, which maneuvered continuously over the growing pile rather than holding fixed positions. The RTLS recorded data at an average transmission interval of 19.8 seconds, capturing the bin-piler's real-time position as it operated.



Figure 3.8: Experiment 7 Anchor 1 (Blue LED) – Anchor seated atop catwalk hand railing overlooking storage Bin 3906, while bin-piler is in operation.

#### **3.4. System Design and Evaluation Methods**

The RTLS system operates by the tag, first, initiating communication with the anchor. The tag and anchor use Gaussian pulse transmission employing either third or seventh-derivative pulses, which

through PPM, conducts ranging via the TWR algorithm, using a matched filter. The TWR is conducted through the use of the DW1000 Arduino library (Open-source community - with significant contributions from Thomas Trojer, thotro repository, Github). Later, the tag continues broadcasting its signal until connection is established, and TWR is performed with all four anchors. Once the tag has determined the distance between itself and all four anchors, these distances are inputted into the Kalman Filter, using the SimpleKalmanFilter Arduino library (Luis Rodenas, denyssene repository, Github). The Kalman filter is configured using 1, 1 and 0.01 for initial estimation error, measurement error and process noise, respectively. This Kalman Filter was used for Experiments 1-4, while it was not used for Experiments 5-7. These distances are then fed into LS to generate the predicted 3D location of the tag (Figure 3.9).

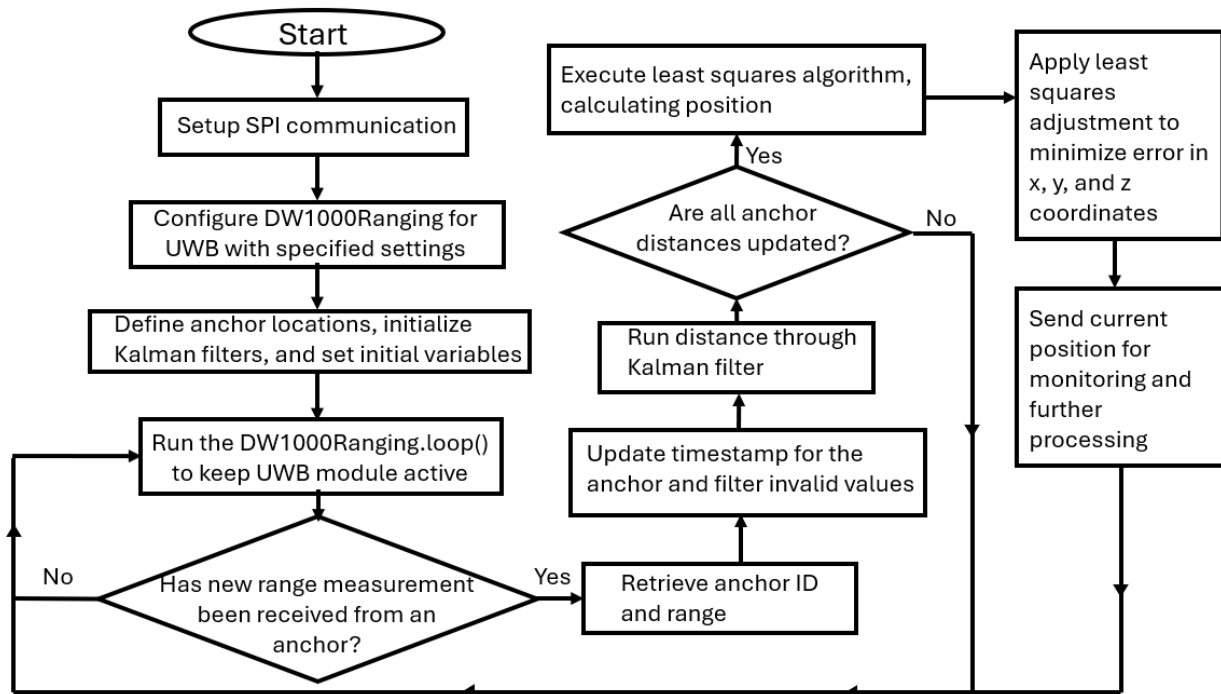


Figure 3.9: Tag Software Flowchart

At the computer, the predicted tag location is augmented by the actual measured tag locations, organized, and saved in an Excel file. First, outliers were removed using the interquartile range

method, and implemented with Python’s pandas library (McKinney, 2010). These predicted and actual locations served as the input for the SVR model, which was configured to use the linear kernel. To ensure robust evaluation, the dataset was split into two subsets: 80% of the data was used for training the SVR model, while the remaining 20% was reserved for testing the model’s performance on unseen data. In this implementation, the SVR model was designed to predict corrections to the predicted 3D locations. The predicted X, Y, and Z locations served as the model’s input features. The corresponding actual X, Y, and Z locations acted as the target variables, serving as the ground truth for the model.

After the model was trained, and tested, the test results were used to determine the total Root Mean Square Error ( $RMSE_{total}$ ) Eq. 3.8.  $RMSE_{total}$  is the average Euclidean distance, or displacement, between actual and predicted locations of the tag:  $(X_a, Y_a, Z_a)$  and  $(X_p, Y_p, Z_p)$ . RMSE is a commonly used metric for evaluating RTLS, as it represents and quantifies system accuracy (Alarifi et al., 2016). The subscript “total” will be used to differentiate the 3-dimensional RMSE, from RMSE for X, Y and Z predictions separately, which will also be calculated (Eq. 3.9-3.11). Variables  $\Delta X_n$ ,  $\Delta Y_n$  and  $\Delta Z_n$  represent the absolute difference predicted X, Y and Z coordinates from actual measured values (Eq. 3.5-3.7).

$$\Delta X_n = | X_a - X_p | \quad (3.5)$$

$$\Delta Y_n = | Y_a - Y_p | \quad (3.6)$$

$$\Delta Z_n = | Z_a - Z_p | \quad (3.7)$$

$$RMSE_{total} = \frac{\sum_{n=1}^{100} \text{sqrt}(\Delta X_n^2 + \Delta Y_n^2 + \Delta Z_n^2)}{100} \quad (3.8)$$

$$\text{RMSE}_X = \frac{\sum_{n=1}^{100} \text{sqrt}(\Delta X_n^2)}{100} \quad (3.9)$$

$$\text{RMSE}_Y = \frac{\sum_{n=1}^{100} \text{sqrt}(\Delta Y_n^2)}{100} \quad (3.10)$$

$$\text{RMSE}_Z = \frac{\sum_{n=1}^{100} \text{sqrt}(\Delta Z_n^2)}{100} \quad (3.11)$$

### 3.5. Results and Discussion

Controlled Grid experiments, conducted in systematically measured and gridded environments (Experiments 1–5), were designed to evaluate the RTLS system’s accuracy against recorded ground truth locations in stable, controlled settings without dynamic factors like equipment movement or potato pile growth. Figures 3.10–3.19 present the raw data from these experiments, including actual tag locations, LS predictions, and SVM-corrected predictions. Generalized LS results for all localization experiments, apart from during harvest operations, can be seen in Table 3.2. For the results after post processing using SVR (Table 3.3).

#### 3.5.1. Controlled Grid LS Experimental Generalized Results and Discussion

In Experiment 1, looking at the results in the XZ planes (Figure 3.10), predictions in the negative X direction tended to underestimate the height of the tag, while predictions in the positive X direction exhibited the opposite trend. However, the overestimation errors in the positive X direction were of smaller magnitude compared to the underestimations. Horizontally, predictions were distinguishable by distinct clusters of similarly colored markers, indicating clear separation of predicted location distributions in the X direction. Vertically, however, predictions for different tag heights were more closely grouped, showing no discernible relationship between actual tag height and predicted height. The predicted heights span a total range of approximately 5.5 m, which contrasted sharply with the actual tag heights, which range from 0.52 m to 1.07 m. This significant

disparity highlighted considerable error in the Z direction. Additionally, the deviation of predictions appeared larger in Figure 3.10 (a), as evidenced by the broader clustering of points in this plot compared to other Y values. This suggested increased variability in predictions for this specific Y position. Finally, SVM corrected predictions generally appeared closer to the actual tag locations than with LS Algorithm alone.

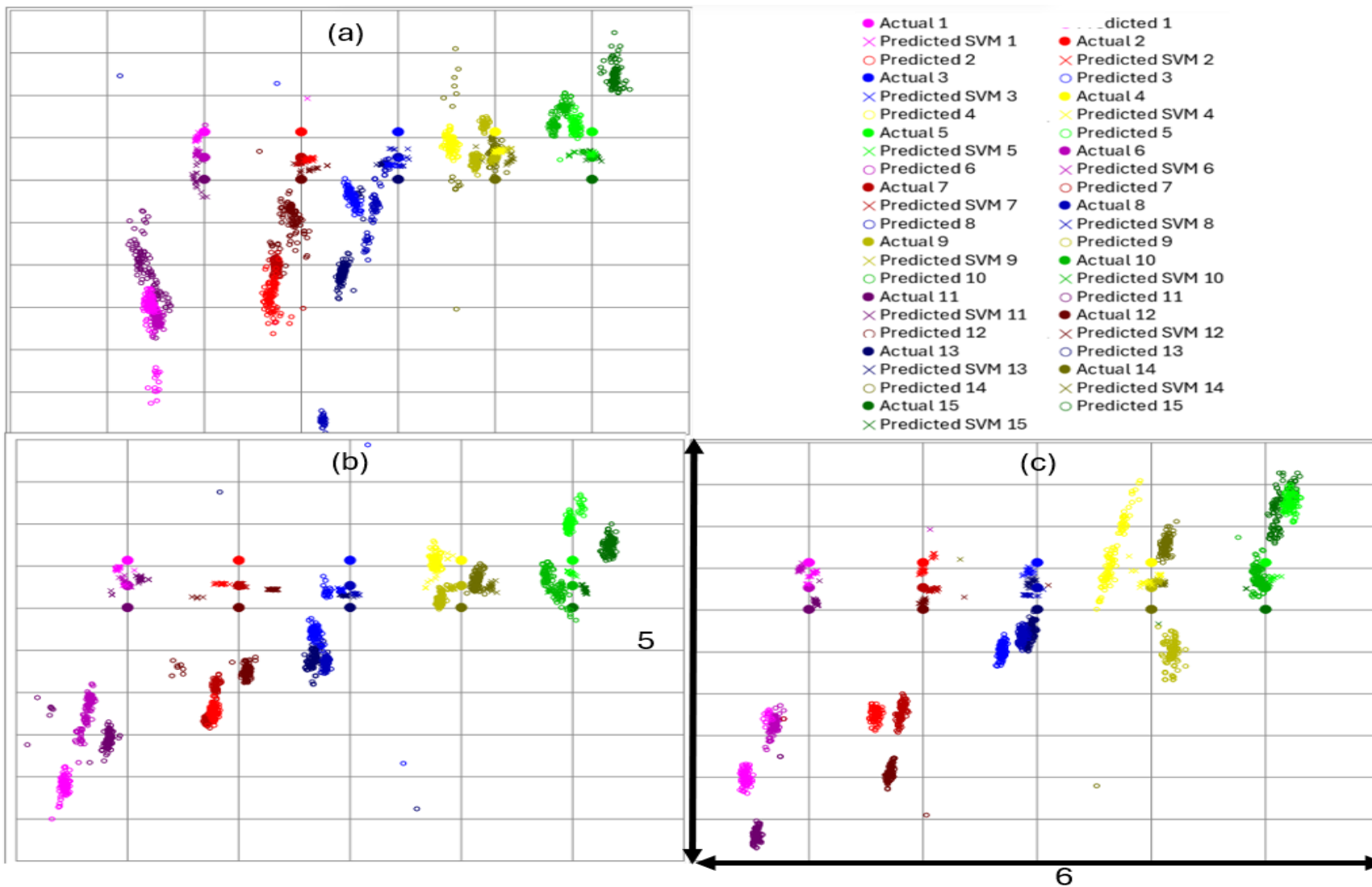


Figure 3.10: Experiment 1 XZ Plane Scatter Plots where (a)  $Y = 2$ , (b)  $Y = 3$ , (c)  $Y = 4$   
 – Three scatter plots representing a 2D plane of the experimental volume, separated by Y value

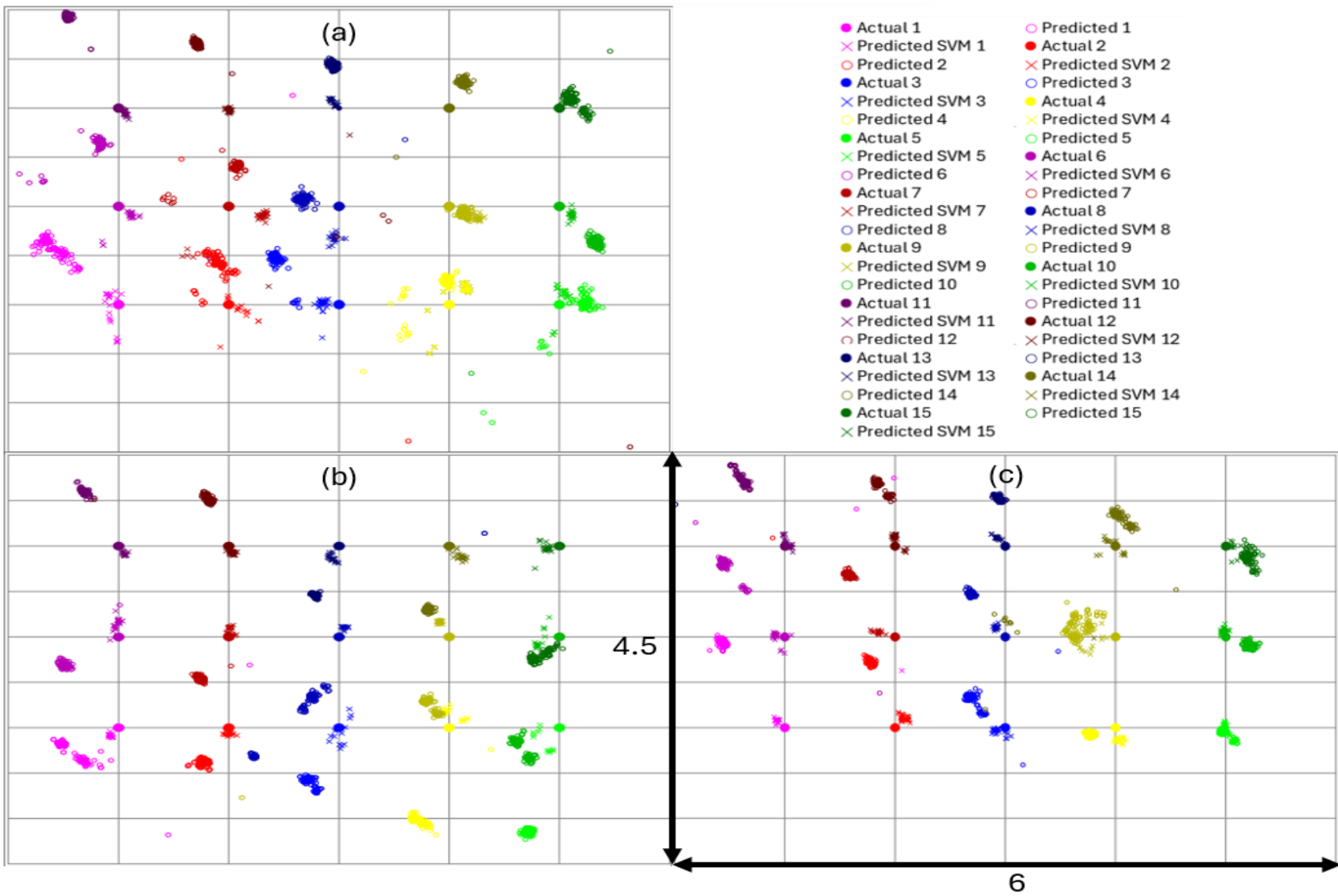


Figure 3.11: Experiment 1 XY Plane Scatter Plots where (a)  $Z = 0.51$ , (b)  $Z = 0.77$ , (c)  $Z = 1.07$

In the XY plane of Experiment 1 (Figure 3.11), a clear pattern emerged between predictions and the Y direction. Clusters of predictions were distinguishable in both the horizontal and vertical directions, indicating a stronger correlation between actual and predicted locations in both the X and Y direction, as opposed to the Z direction. However, predictions in the more positive Y regions, represented by darker shades, tend to overestimate the Y location of the tag, particularly for lower X-coordinate positions. Accuracy did not appear to vary greatly with height, as all three plots show a similar difference between actual tag locations and predictions. This was likely a product of the relatively small range of tag heights during the experiment: ranging only from 0.52 – 1.07 m. Overall, predictions were more tightly clustered, suggesting lower deviation in predicted locations and improved consistency in the XY plane.

In the XZ plane of Experiment 2 (Figure 3.12), predictions formed vertically elongated clusters that horizontally aligned with their corresponding actual locations, indicating relatively minimal error in the X dimension. However, zoomed-in planes reveal a total range of Z predictions spanning approximately 15 meters, which significantly exceeded the actual tag height range of 1 to 4.22 meters, highlighting considerable variability in Z predictions. LS predictions often formed these vertically stretched patterns, appearing as lines across the plots. This behavior could be attributed to the slow-acting Kalman Filter, which used a feedback mechanism to iteratively minimize prediction error. Notably, these lines tended to "point" towards the actual tag locations, with predictions closer to the actual locations occurring later in the observation plane, reflecting the Kalman Filter's calibration process. The observed 'slowness' of the Kalman Filter was indicative of high variance in its input – specifically, the LS predictions—which makes it challenging to curtail error over time. This variance complicated the evaluation of prediction

accuracy, requiring multiple iterations for the filter to converge effectively to the actual tag locations.

Two clear outliers are visible in the zoomed-out planes. In Figure 3.12 (c), one set of predictions deviates significantly in the Z direction. In Figure 3.12 (b), predictions stand out as outliers in both the X and Z dimensions. The difference in Z-axis range between the zoomed-in and zoomed-out planes reflected the considerable localization error of some predictions, particularly in the z direction.

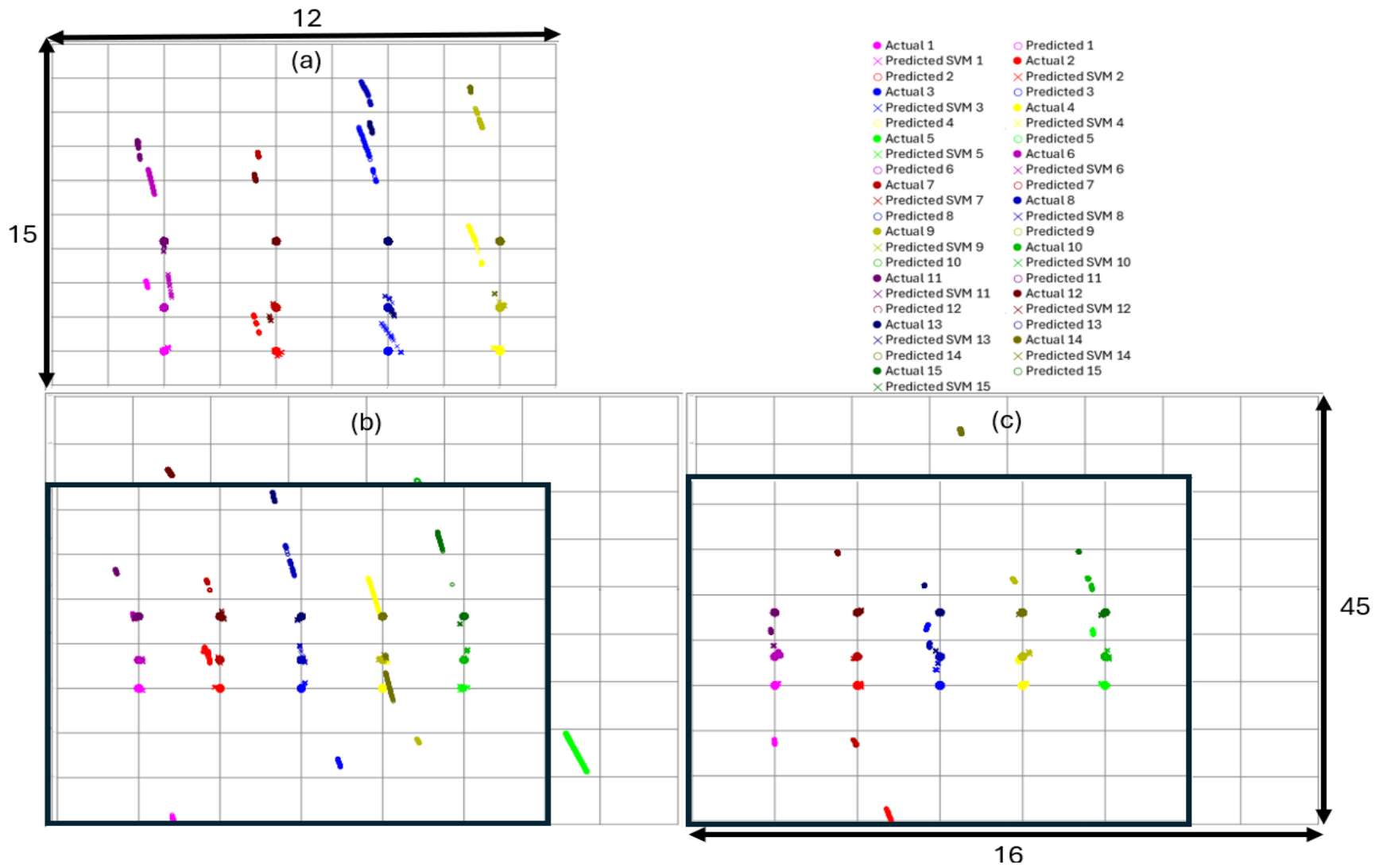


Figure 3.12: Experiment 2 XZ Plane Scatter Plots where (a)  $Y = -4.909$ , (b)  $Y = 0$ , (c)  $Y = 4.909$  – Embedded subplots represent zoomed-in planes of actual tag locations, and nearby predictions. Zoom-in planes have equivalent dimensions, as do zoomed-out

The XY plane of Experiment 2 (Figure 3.12) demonstrated relatively accurate localization in both the X and Y dimensions, with LS predictions and, particularly, SVM-corrected positions aligning closely with the actual tag locations. The results exhibit extremely low variability, reflecting the consistency of predictions entering the Kalman Filter and the overall stability of the system. This accuracy and low variability was relatively consistent across all plots. Although there is one set of outliers of Location 5 in Figure 3.13 (a), their sheer number in comparison to the rest of data was relatively small, highlighting strong prediction accuracy and minimal variability across the XY plane in this experiment.

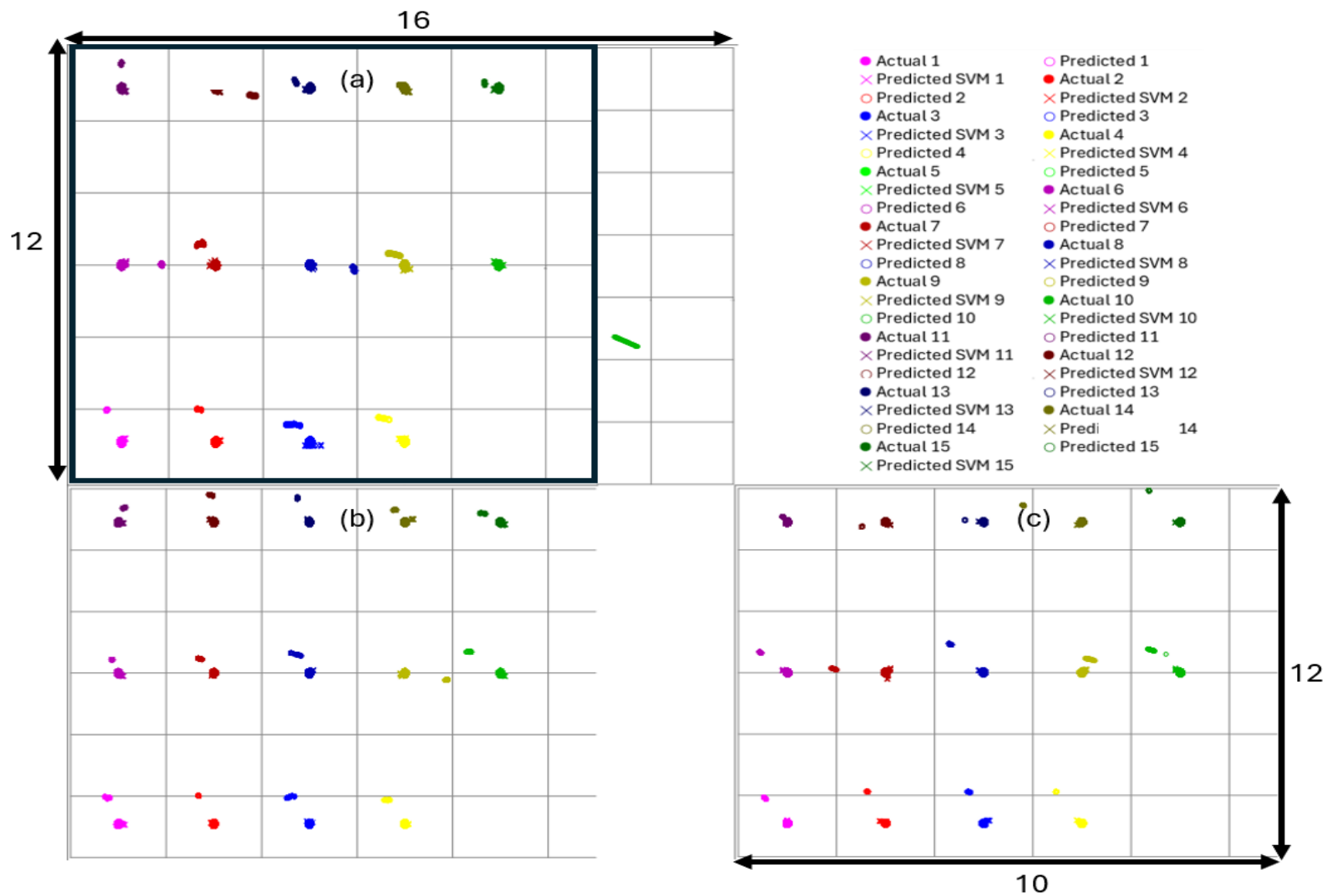


Figure 3.13: Experiment 2 XY Plane Scatter Plots where a)  $Z = 1$ , b)  $Z = 2.27$ , and c)  $Z = 4.22$

In the XZ plane of Experiment 3 (Figure 3.14), significant vertical, and horizontal elongation in the clusters highlighted substantial variability in predictions for both the X and Z directions. This is evident in the relative range of zoomed out planes, both X and Z axes being approximately two times their zoomed-in counterparts. This contrasted starkly with other positions, which achieved relatively consistent, and accurate localization. The zoomed-in planes reveal tighter clustering of SVM-corrected predictions, which are more closely aligned with the actual tag positions, demonstrating the effectiveness of SVM in improving prediction accuracy. Similar system behavior can be observed in the XY plane (Figure 3.15), showcasing relatively consistently, erratic performance across all three dimensions. In Experiment 3, Figure 3.15 (b) demonstrated the most reliable accuracy, as no predictions sit outside the zoomed-in plane.

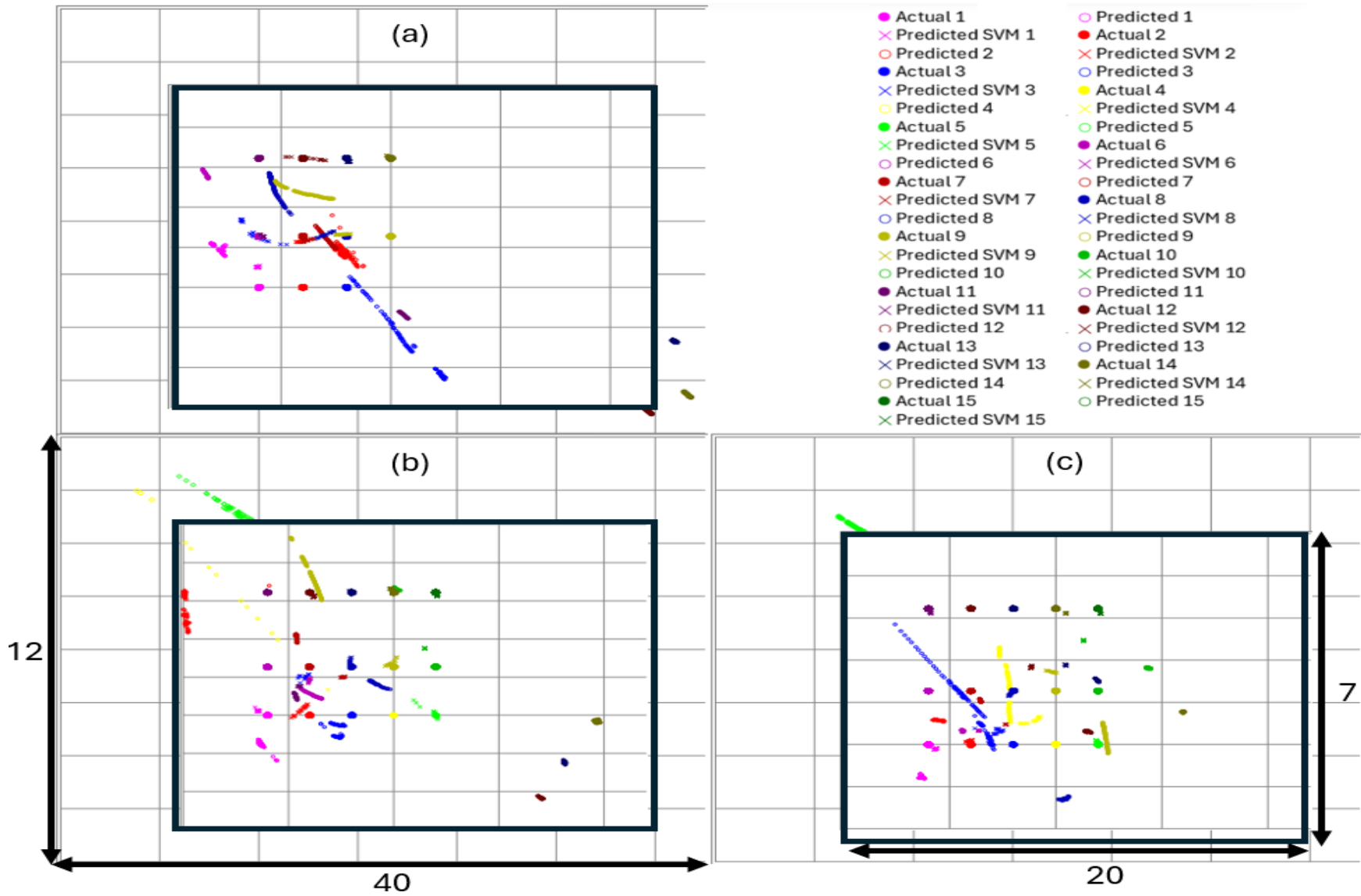


Figure 3.14: Experiment 3 XZ Plane Scatter Plot where (a)  $Y = -4.909$ , (b)  $Y = 0$ , (c)  $Y = 4.909$

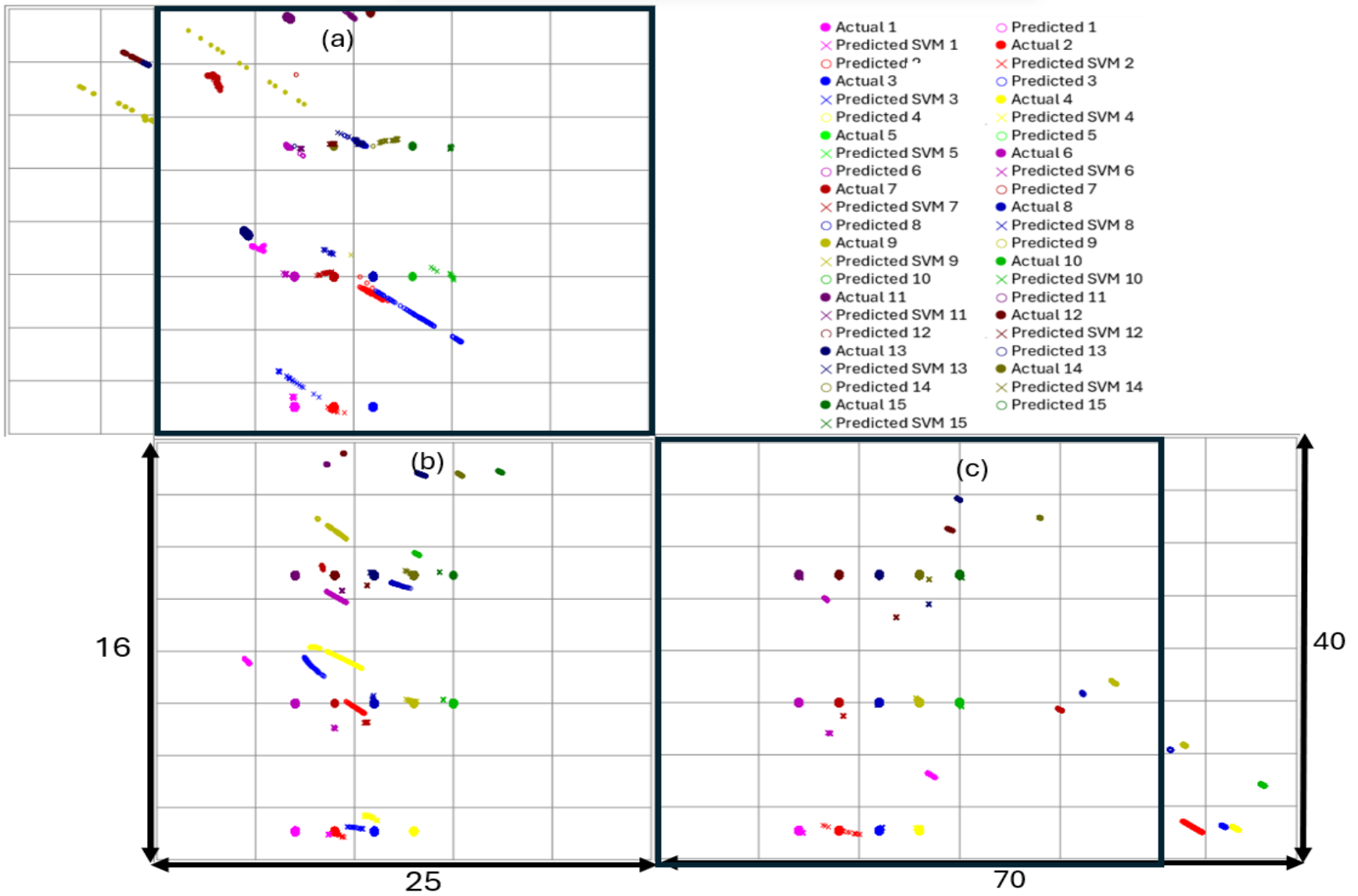


Figure 3.15: Experiment 3 XY Plane Scatter Plots where (a)  $Z = 1$  (b)  $Z = 2.27$  (c)  $Z = 4.22$

The XZ plane results from Experiment 4 (Figure 3.16) reveal a notable absence of data points within the zoomed-in planes, indicating that many predictions deviated significantly from the actual tag locations. The largest errors are observed in the outliers present in Figure 3.16 (b) and (c). This observation was corroborated by the scale of the zoomed-out plane axes, particularly the 70-meter range in the Z direction, which underscores the magnitude of the error.

Unlike the linear patterns of successive predictions observed in previous experiments, the predicted locations in this experiment formed curved lines, suggesting more erratic behavior in the Kalman Filter output. This behavior could be attributed to challenges in the filter's performance when processing highly variable input data. Kalman Filters rely on iterative adjustments and feedback mechanisms to minimize error; however, when inputs exhibit significant variance or inherent noise, the filters can struggle to converge accurately, resulting in such irregular patterns. Interestingly, the curved lines formed by these predicted locations, when considered in combination with other locations, appeared to exhibit a consistent pattern across multiple plots. This could be linked to the identical testing sequence, where the tag was systematically rotated through the testing grid.

Another observation involves horizontal lines of successive predictions present across multiple plots. While these lines are not directed toward the actual tag locations, they suggest that the Kalman Filtered system was converging toward erroneous, perceived locations.

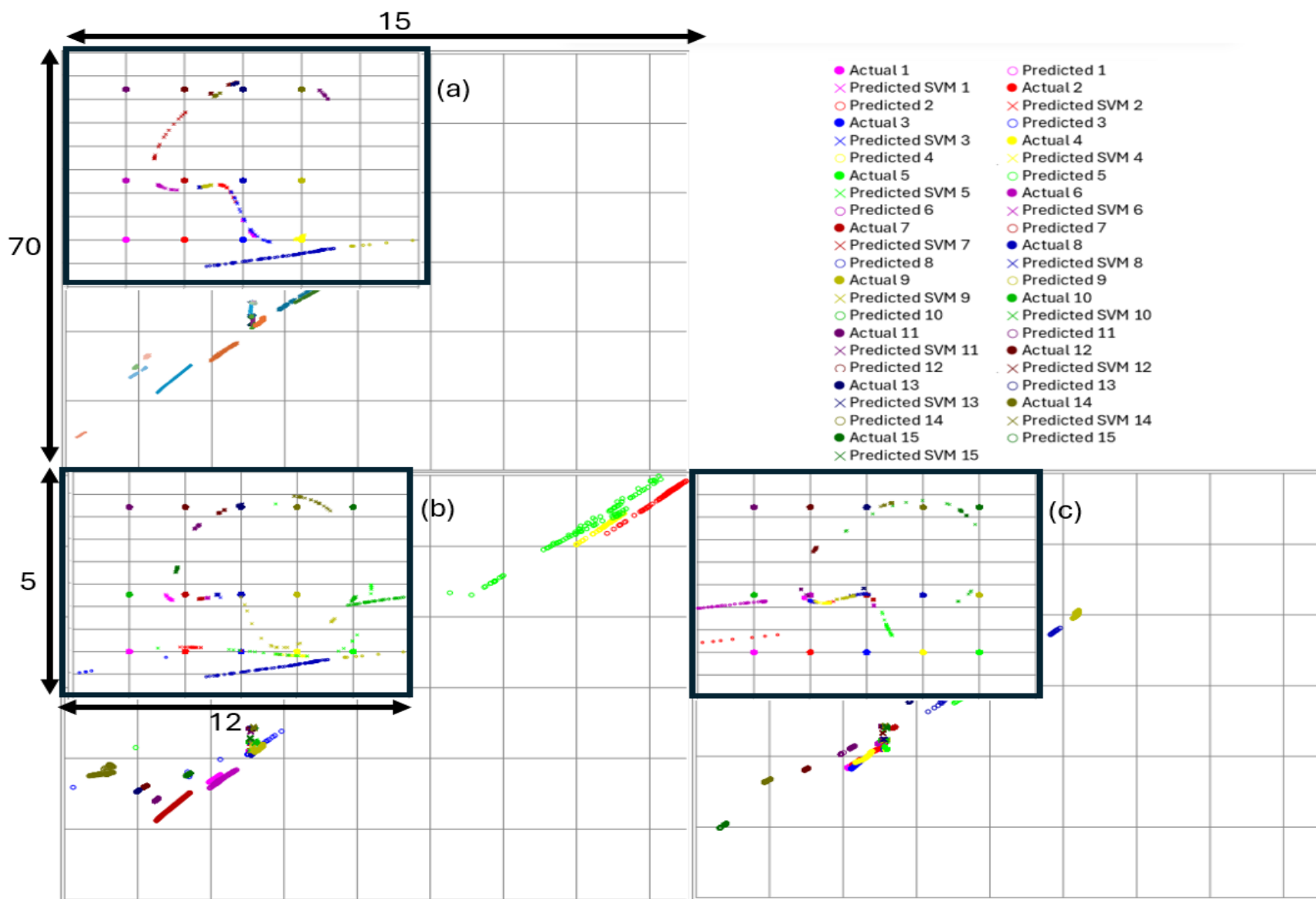


Figure 3.16: Experiment 4 XZ Plane Scatter Plots (a)  $Y = -4.909$  (b)  $Y = 0$  (c)  $Y = 4.909$

The XY plane of Experiment 4 (Figure 3.17) demonstrated the poorest localization performance among all controlled grid experiments. All three plots contain both zoomed-in and zoomed-out planes, revealing a vast range of location predictions across all tag heights. The scale of the zoomed-out plane axes—spanning 600 x 850 m—is orders of magnitude greater than in other experiments. This extreme range indicates a high prevalence of noise that has severely impacted localization accuracy, which is likely related to the existence of obstacles in the LOS between the tag and all anchors in this experiment.

A prominent feature in these plots is a long diagonal line of predictions in both X and Y directions appearing in all plots of Figure 3.17. The uniformity of these predictions along the same line may be attributed to the scale of the axes. The extreme zoomed-out scale reduced resolution between individual strands of predictions, corresponding to different actual locations, effectively merging them into a single, continuous line. Additionally, since the actual tag locations occupied the center of this line and the perspective is distant, all predictions appeared to "point" in the same general direction. Besides the issues with obstacles within the LOS, this poor performance may be related to the limitations of the Kalman Filter's ability to correct for extreme input variance in scenarios where signal degradation is severe.

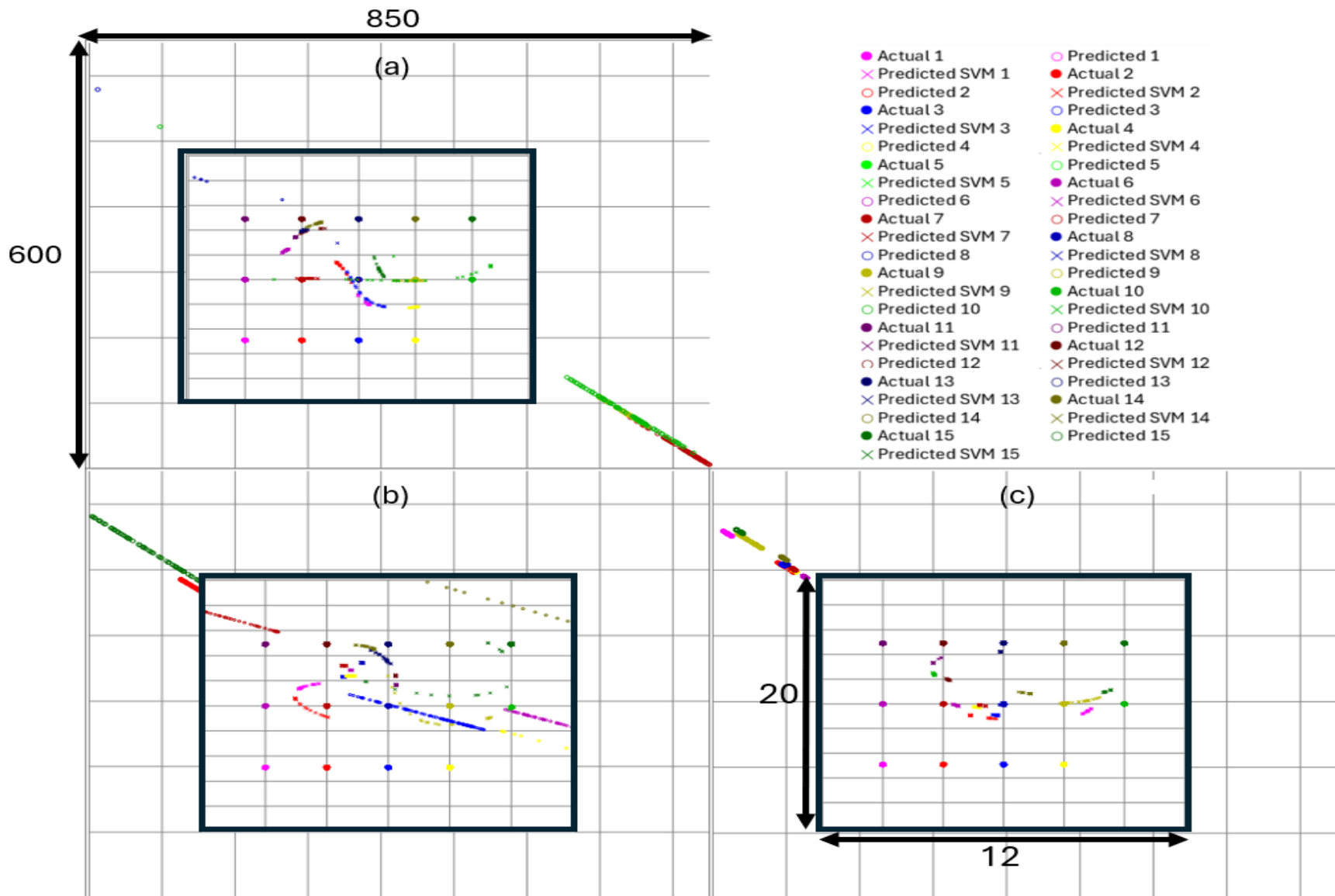


Figure 3.17: Experiment 4 XY Plane Scatter Plots (a)  $Z = 1$  (b)  $Z = 2.27$  (c)  $Z = 4.22$

In the XZ plane of Experiment 5 (Figure 3.18), near-vertical strands of successive predictions, similar to those observed in previous experiments, approached the actual tag locations. The verticality of these lines suggested relatively minimal error along the horizontal axis and some greater error in the vertical axis. This effect was most pronounced in Figure 3.18 (a) where the distance extended by just 2 meters. The near-vertical lines become less distinct in Figure 3.18 (b) and (c), where predictions appeared more tightly grouped and linear. This observation suggested that central Y values may provide a more stable environment for localization. Furthermore, the most accurate results are observed at the highest heights, in Figure 3.18 (c), as the tag was closer to all anchor locations (as illustrated in Figure 3.5), resulting in improved prediction accuracy due to stronger and more consistent signal quality.

In terms of spatial correlation, predictions from different locations aligned well with their actual X positions. However, the tag height predictions did not necessarily follow a discernible pattern, reflecting ongoing challenges in height localization. Overall, the results highlight the RTLS's consistent strengths in the horizontal plane while underscoring the influence of anchor proximity and Y position on localization performance. The absence of a clear pattern in height predictions pointed to areas for improvement in the system's ability to resolve Z-axis errors.

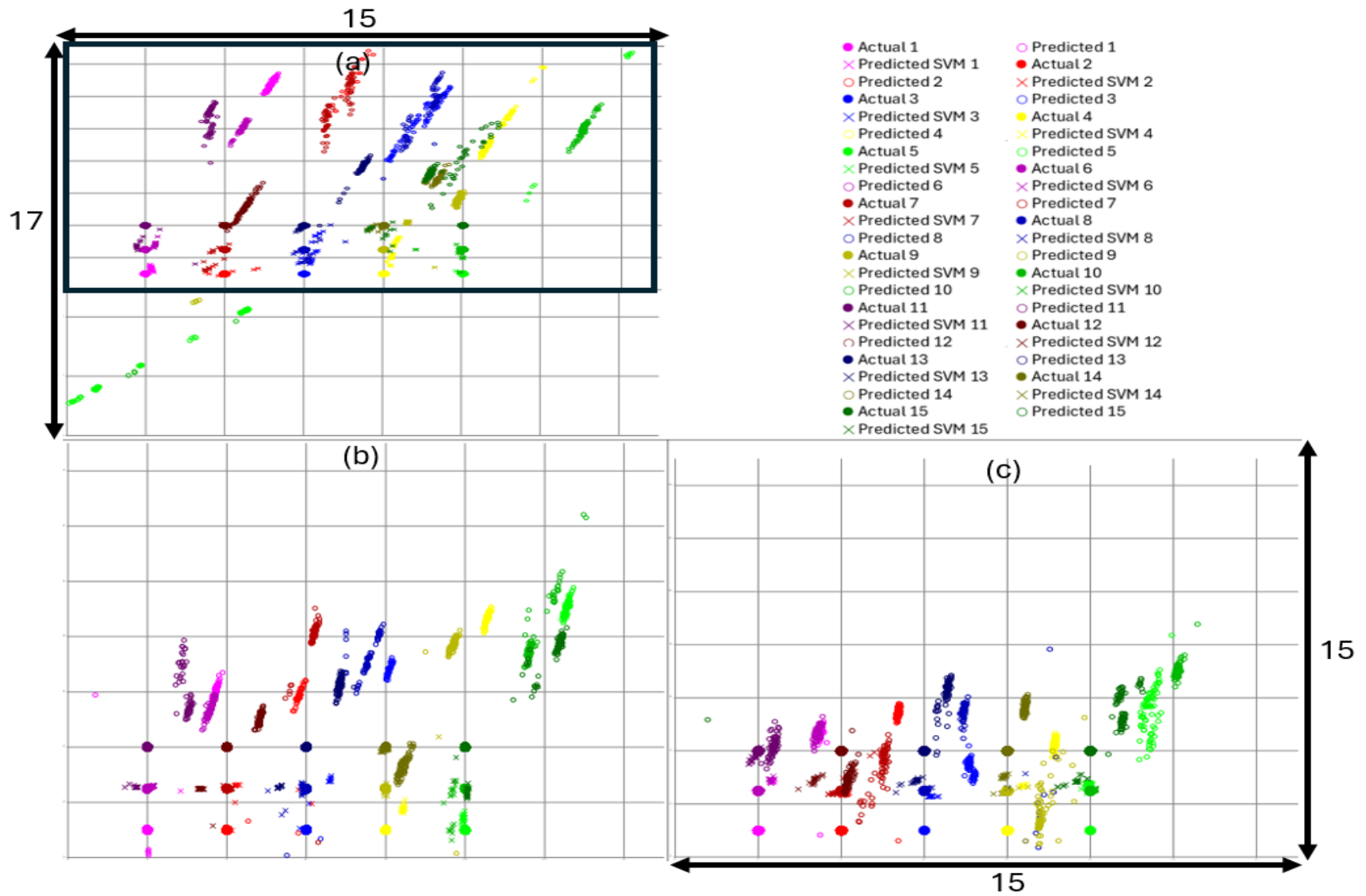


Figure 3.18: Experiment 5 XZ Plane Scatter Plots where (a)  $Y = 0$  (b)  $Y = 4.909$  (c)  $Y = 9.765$

The XY plane for Experiment 5 (Figure 3.19) demonstrated generally higher consistency and accuracy in predictions compared to the XZ plane, which aligns with the observation from previous experiments. Also, the concentrated nature of most clusters in the XY plane further underscores the system's relatively strong performance in these dimensions. While most predictions are tightly grouped, some notable exceptions exist. For example, predictions in the negative Y region for Figure 3.19 (a) showed increased variability, indicating reduced accuracy in this specific region before introducing SVM which improved precision and accuracy of the prediction..

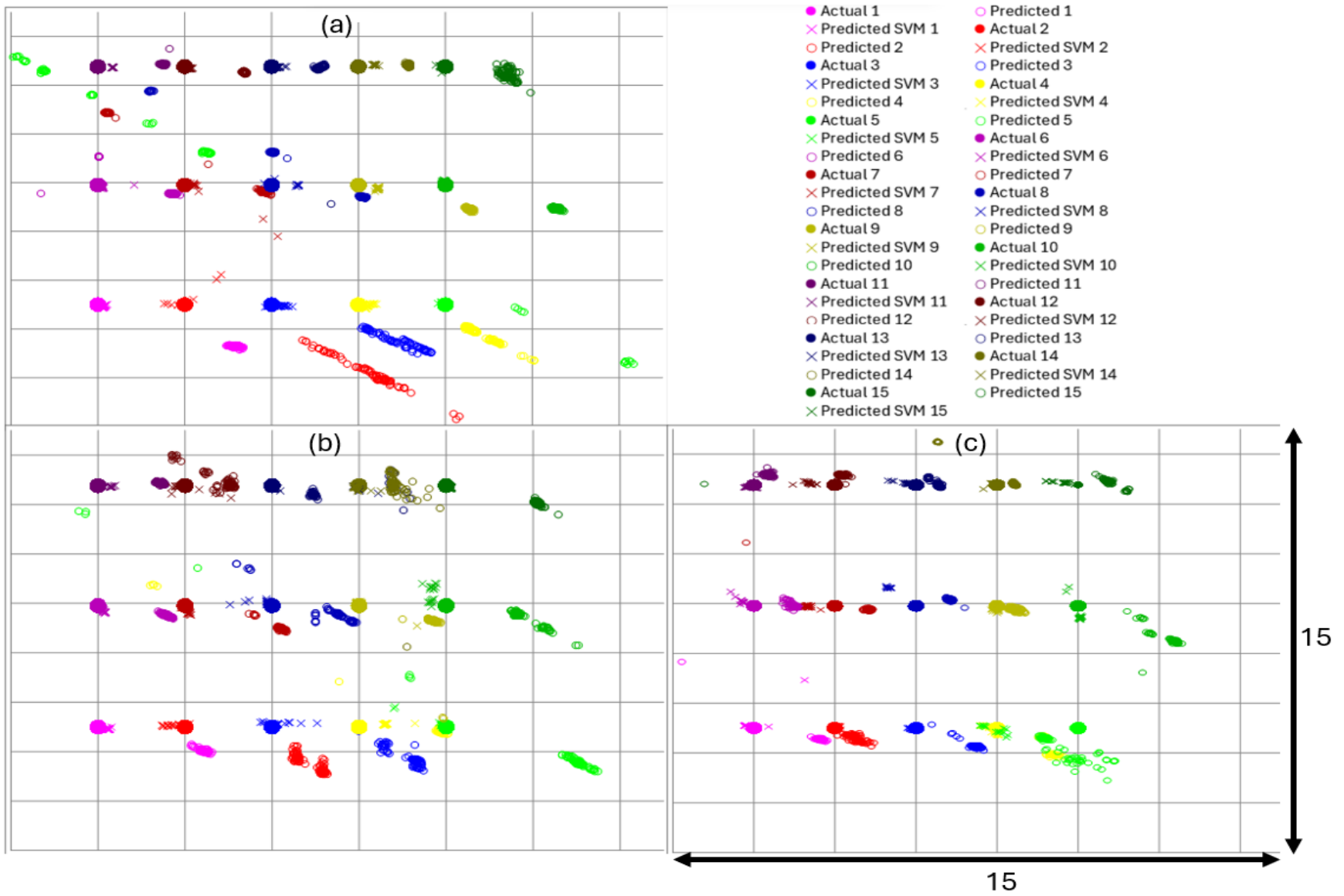


Figure 3.19: Experiment 5 XY Plane Scatter Plot where (a)  $Z = 1$  (b)  $Z = 2.27$  (c)  $Z = 4.22$

Table 3.2: Controlled Grid LS Algorithm Localization Experimental Results

Controlled Grid LS Algorithm Localization Experimental Results								
Experiment	Experiment Number	R2			RMS Error (m)			
		X	Y	Z	X	Y	Z	Total
<b>Obstacle-free small volume environment</b>	1	0.946	0.883	0.005	0.336	0.411	1.061	1.187
<b>Uniform anchor height large volume environment</b>	2	0.940	0.987	0.295	0.330	0.302	2.280	2.324
<b>Small pile anchor locations</b>	3	0.007	0.566	0.110	5.529	3.758	3.601	7.593
<b>Large pile anchor locations</b>	4	0.042	0.001	0.260	6.985	5.358	3.484	9.467
<b>Bin-piler large volume environment</b>	5	0.690	0.881	0.005	1.746	0.847	5.080	5.438

For Experiment 1, the RMSE across the X, Y, and Z axes was low, particularly for X and Y, which reflects accurate localization performance in these dimensions. In contrast, the  $RMSE_{total}$  was slightly higher, influenced by the contribution of the Z-dimension error. The high values of  $R^2$  for X and Y indicated a strong fit of the localization system’s predictions to the actual locations in these dimensions. The Z-dimension, with a near-zero  $R^2$ , exhibited significantly reduced predictive power compared to the X and Y dimensions. The disparity in performance across dimensions may be attributed to the relatively compact spatial configuration of anchors in the Z-dimension within the obstacle-free environment. While the horizontal anchor diversity supported strong predictions in the X and Y axes, the limited height variation in anchor positions likely constrained the accuracy in the Z-dimension. This result was mirrored in the  $RMSE_Z$  value, which was approximately 2.5 times greater than the  $RMSE_X$  and  $RMSE_Y$ . Overall, the results confirmed that the obstacle-free small volume environment facilitated the system’s strong localization accuracy in 2D (X and Y dimensions), achieving sub-meter accuracy. Experiment 2 demonstrated

low  $RMSE_x$  and  $RMSE_y$ , while  $RMSE_z$  was substantially higher at 2.280 m. Placing all anchors at a uniform height impaired the system's ability to localize accurately in the Z-dimension. Despite these challenges, the  $R^2$  values for the X and Y dimensions remained high at 0.940 and 0.987, respectively. The Z-dimension, however, yielded an  $R^2$  of 0.295, which, while indicative of limited predictive power, represents an improvement over Experiment 1's Z-dimension performance ( $R^2 = 0.005$ ). One explanation for this improvement may be the larger experimental volume, which increased the spatial diversity of anchors in the x and y dimensions (19.58 m and 13.94 m, respectively). Additionally, software-based pseudo-diversity in the Z-dimension, achieved by assigning artificial height variability to the anchors during computation, likely contributed to the improved  $R^2$  in the Z-dimension. This pseudo-diversity introduced height variation in the range of 2 to 5 m, enhancing the system's capacity to localize in 3D compared to Experiment 1, where the anchors exhibited a smaller total Z-range of 2.09 m. In summary, Experiment 2 underscored the importance of physical anchor height diversity for achieving optimal 3D positioning accuracy. Although software-based pseudo-diversity in the Z-dimension can partially mitigate the limitations of uniform anchor height, the elevated  $RMSE_x$  and reduced  $R^2$  values highlight its constraints. The results further validate the need for complementary techniques, such as SVR or Kalman filtering, to compensate for the lack of physical diversity in anchor configurations.

For Experiment 3, the high  $RMSE_{total}$  and low  $R^2$  across all dimensions highlighted the system's limited ability to predict accurately in this environment. The performance challenges observed in this experiment likely stem from the placement of anchors, which introduced multiple obstructions and inconsistencies in the LOS signals. Interestingly, despite the relatively high errors across all dimensions, the  $RMSE_z$  was not disproportionately large compared to  $RMSE_x$  and  $RMSE_y$ . This

may be attributed to the spatial diversity of anchors in the Z-dimension, with an anchor height range of 3.85 m. This reinforces the idea that sufficient anchor diversity in the Z-dimension can mitigate vertical localization errors, even in the presence of other challenges. Overall, the experiment underscored the impact of obstructed anchor configurations on system performance, particularly in the x and y dimensions, where LOS signal interruptions are most critical.

Results from Experiment 5 indicated relatively low  $RMSE_x$  and  $RMSE_y$ , while  $RMSE_z$  was significantly higher, resulting in a  $RMSE_{total}$  of 5.438 m. When compared to Experiment 2, which also featured a large volume environment, the experiments have comparable  $RMSE_{total}$  values. This similarity was likely due to the comparable anchor configurations in the x and y directions, with similar geometry and distances from anchors to the tags. However, Experiment 5 exhibited a notably higher  $RMSE_z$ , despite having an anchor height diversity of 2.95 m, in contrast to the uniform anchor height in Experiment 2, which may be explained by several factors. First, Bin 3906 of Experiment 5 was lined with sheet metal along its walls and ceiling, unlike the primarily concrete and insulated walls of Room 47 in Experiment 2. This environmental difference likely introduced greater multipath effects in Bin 3906, leading to increased localization errors, particularly in the Z-dimension. Second, the tag was mounted atop the bin-piler during Experiment 5. As the bin-piler is a large metallic structure, it may have obstructed LOS signals and generated additional multipath effects, further impacting accuracy. Additionally, while Experiment 2 lacked anchor height diversity, pseudo-diversity was introduced in its LS via the anchor location matrix, which likely reduced  $RMSE_z$ , whereas no similar software-based correction was applied in Experiment 5. Finally, the 100-location prediction approach used in Experiment 5 proved valuable in evaluating the RTLS's accuracy and consistency under challenging conditions. The results

highlight the RTLS's potential for use in open agricultural settings but also emphasize areas for improvement, particularly in Z-axis accuracy for large, vertically complex environments.

### **3.5.2. Controlled Grid LS Algorithm and SVR Localization Experimental Results and Discussion**

First, a variety of Regularization Parameter (C) and Epsilon values ranging from 1-100 for C and 0.1-1 for epsilon were tested in relation to RMSE. Across all experiments, the configuration of C = 100 and epsilon = 0.1 yielded the lowest RMSE, making it the most effective setting for accurate localization. This combination provided the most consistent results in terms of minimizing RMSE across X, Y, and Z dimensions. For example, in Experiment 2, this configuration achieved a total RMSE of 0.183 m (Table 3.3), significantly outperforming other combinations. The uniformity of this optimal combination suggested that, for RTLS applications in environments with similar constraints, setting C to a high value and epsilon to a low value can produce reliable and accurate localization. The success of this configuration in multiple environments also suggested a potential baseline for SVR hyperparameter settings in similar experimental setups.

For Experiment 1, the RMSE across the X, Y, and Z axes after SVR modeling was significantly lower than the results from LS alone (Table 3.2). The reduction in  $RMSE_X$  and  $RMSE_Y$  indicated the SVR model's ability to improve localization accuracy in these axes. Similarly, the  $RMSE_{total}$  was reduced from 1.187 m to just 0.183 m in Table 3.3, indicating that the SVR model provided a substantial refinement to the system's performance. However, despite the  $RMSE_Z$  reduction in the Z-dimension, the  $R^2$  value for the Z-dimension in Table 3.3 changed to -0.476, compared to 0.005 in Table 3.2. This negative  $R^2$  suggested that the SVR model introduced some predictive inaccuracies relative to the baseline LS. This discrepancy may reflect overfitting or an inability of the SVR model to effectively generalize the Z-axis predictions due to insufficient anchor height

diversity as the anchor configuration in the Z-dimension was limited to a total height range of 2.09 m, compared to the 6 m range in the X and Y dimensions.

In Experiment 2, while the Least Square algorithm struggled to achieve precise 3D localization, post-processing with the SVR algorithm (Table 3.3) significantly improved accuracy across all dimensions, bringing the overall  $RMSE_{total}$  down to approximately 0.183 m. These reductions in error demonstrate the SVR model's ability to recalibrate the Z-dimension data and enhance localization performance in environments with uniform anchor heights. Interestingly, the  $R^2$  value for the Z-dimension was 0.969, a significant improvement over the 0.295 observed in Table 3.2. One explanation for this improvement lies in the pseudo-diversity introduced in the Z-dimension during computation. By artificially assigning Z-values ranging from 2 to 5 m to the anchors, the algorithm effectively mimicked height diversity, which likely contributed to better 3D localization compared to Experiment 1.

For Experiment 3, while the  $RMSE_{total}$  using LS was poor due to the possible interference of obstacles across LOS, Post-processing with the SVR algorithm yielded significant improvements across all metrics (Table 3.3). Consequently, the  $RMSE_{total}$  improved dramatically from 7.593 m to 0.431 m. The anchor placement in Experiment 3 featured a height diversity of 3.85 m, the largest among all experiments, which likely contributed to the improved Z-dimension performance after applying SVR. The availability of one close anchor with clear LOS may also have played a role in reducing errors, as suggested by the results in Tables 3.2 and 3.3. While Experiment 4 exhibited the poorest  $RMSE_{total}$  and  $R^2$  values among all experiments using LS, likely due to anchor placement adjustments causing increased LOS signal obstructions, applying the SVR algorithm there was a substantial improvement (Table 3.3) overall. The contrasting results between Experiments 3 and 4, despite similar Anchor 2 and 3 placements, may be attributed to the

relocation of Anchor 1, which was moved in Experiment 4 farther away from the tag locations: from (0.00,3.70,4.00) to (0.00,11.44,3.92), likely degrading signal quality.

Both experiments featured similar anchor height diversity (3.85 m), which contributed to relatively low  $RMSE_Z$  in both Tables 4 and 5. However, the large pile environment in Experiment 4 introduced more significant LOS obstructions, leading to higher errors in the x and y dimensions. While SVR improved performance across all dimensions, in both experiments, the relative effectiveness was greater in Experiment 3 due to its less obstructed environment. These results reinforce the importance of having at least one close anchor with clear LOS to mitigate accuracy losses associated with obstructed or distant anchors.

Comparing Experiments 2 and 5, both experiments yielded comparable  $RMSE_{total}$  values in Table 3.2, likely owing to similar anchor configurations in the x and y directions, with similar geometry and distances between anchors and tags. However, Experiment 5 showed a higher  $RMSE_Z$  despite having a height diversity of 2.95 m, compared to the uniform anchor height in Experiment 2, suggesting additional environmental factors may have influenced Z-dimension accuracy. One possible explanation for this discrepancy – in addition to the material of the building – may be the location of the tag in Experiment 5 which was mounted atop the bin-piler, a large metallic structure that likely obstructed LOS signals and contributed further to multipath effects. Another contributing factor would have been the absence of a Kalman Filter during Experiment 5. Moreover, while pseudo-diversity was introduced in the LS of Experiment 2, no such software-based correction was applied in Experiment 5. The lack of these compensatory measures likely contributed to the higher  $RMSE_Z$  in Experiment 5.

Overall, Experiment 5 underscored the RTLS's potential for use in open agricultural settings while highlighting the importance of mitigating multipath effects, enhancing LOS conditions, and

employing advanced filtering techniques to achieve more accurate Z-dimension localization in large, vertical spaces. The application of SVR consistently improved localization accuracy across all experiments, particularly in the X and Y dimensions.  $RMSE_X$  and  $RMSE_Y$  saw substantial reductions, achieving sub-quarter-meter accuracy in most cases, and nearly perfect  $R^2$  values were observed in these dimensions for Experiments 1, 2, and 5. In the Z-dimension, SVR mitigated errors to varying extents, with the effectiveness largely dependent on anchor height diversity and environmental factors.

Table 3.3: Controlled Grid General Localization Experimental Results

Controlled Grid General Localization Experimental Results								
Experiment	Experiment Number	R2			RMS Error (m)			
		x	y	z	x	y	z	Total
<b>Obstacle-free small volume environment</b>	1	0.988	0.985	-0.476	0.083	0.083	0.139	0.183
<b>Uniform anchor height large volume environment</b>	2	0.999	1.000	0.969	0.067	0.067	0.156	0.183
<b>Small pile anchor locations</b>	3	0.931	0.996	0.878	0.334	0.154	0.226	0.431
<b>Large pile anchor locations</b>	4	0.503	0.898	0.873	1.303	0.794	0.308	1.557
<b>Bin piler large volume environment</b>	5	0.978	0.998	0.549	0.193	0.077	0.533	0.572

### 3.5.3. Harvest Operations Small and Large Pile in Field Results and Discussion

Results are presented in four 3D plots, for Experiments 6 and 7 (Figures 3.20-3.23). The axes ranges are automatically generated based on the data, with Experiment 6 spanning  $X = 0-14$  m,  $Y$

= 0–16 m, and Z = 0–20 m, and Experiment 7 extending to X = 0–20 m, Y = 0–16 m, and Z = 0–20 m (Figure 3.20 & 3.21). Notably, these ranges exceeded the actual dimensions of the storage bin (X = 12 m, Y = 26 m, Z = 5 m), suggesting that many predictions placed the tag and bin-piler outside the actual confines of the bin, which was inaccurate. This inaccuracy was further compounded by the operational reality that the bin-piler did not cover the entire storage area (particularly in the y-dimension); instead, it filled specific sections of the bin based on the existing potato pile height and shape per the respective day. The high magnitude of these inaccuracies was largely due to the absence of SVR post-processing, due to a lack of measured actual tag locations (which were impractical during operations), as well as the lack of a Kalman Filter. Also, localization errors are likely further compounded by the unique unpredictability, and inconsistency of operations.

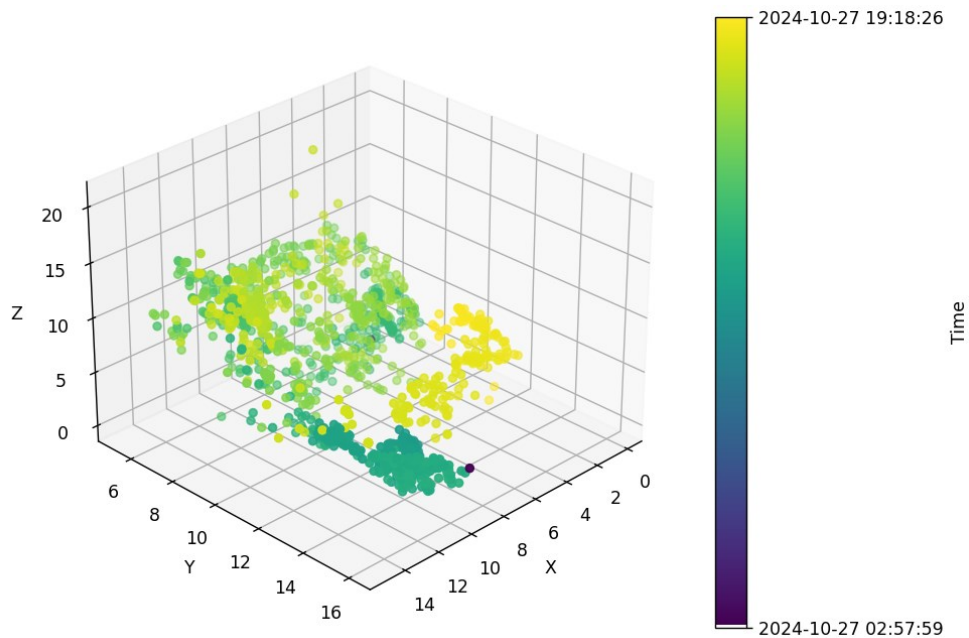


Figure 3.20: Experiment 6 3D Plot Isometric View

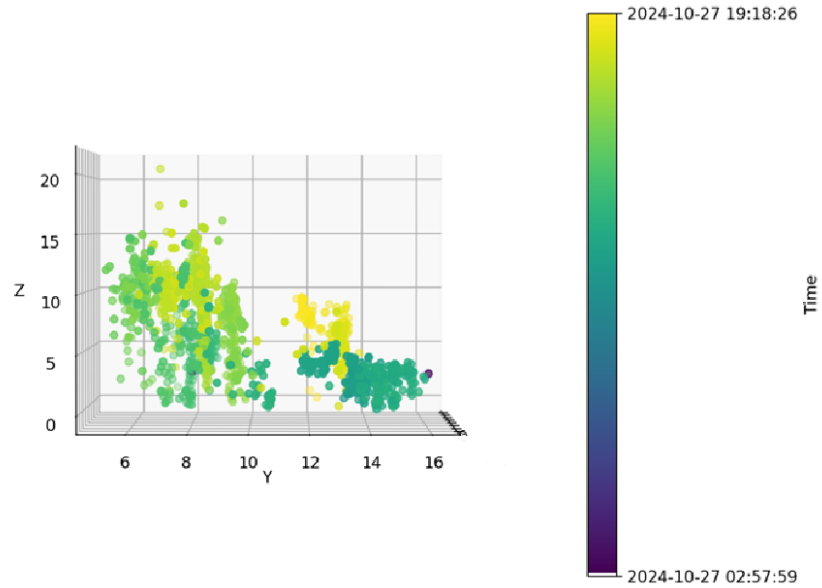


Figure 3.21: Experiment 6 3D Plot YZ Plane – This YZ Plane corresponds to viewing the pile from the catwalk-side of Bin 3906, normal to the bin-piler’s arm.

Despite inaccuracies in the absolute coordinates, there was evidence of relative accuracy in the localization predictions, particularly in how the predicted positions track the typical movement patterns of the bin-piler. During Experiment 6, the predictions initially cluster around (11, 15, 5), corresponding to periods when the bin-piler was manually operated and held stationary by the operator to address low sections of the potato pile or attend to other tasks. Subsequently, the predictions move in a negative Y direction and positive Z direction, indicating that the bin-piler arm extended further into the storage, reaching over the pile - away from the bin-piler base and storage entrance. This upward trend in Z aligns with the physical characteristic of the potato pile, as the back of the pile tended to be higher than the front. The spread of predictions in this volume, concentrated near the face of the pile rather than the floor, evenly distributed, suggested that the bin-piler was in autonomous mode, maneuvering around the pile’s face under laser guidance.

Further analysis of the YZ plane (side-view) plot for Experiment 6 reveals a distinct distribution pattern. Predicted tag locations primarily cluster into two zones: one between  $Y = 6-10$  m and  $Z$

= 0–15 m, and another between Y = 12–16 m and Z = 0–10 m. These clusters align with operational practices in potato storage, where “stairs” or “layers” are intentionally formed along the pile’s surface to limit tuber rolling, thereby minimizing mechanical damage, bruising, and potential rot. As the bin-piler forms these layers, the tag, attached to the bin-piler, naturally occupies discrete positions along the Y-axis. Additionally, predictions further into the storage facility (negative Y direction) tend to exhibit higher Z values, consistent with the pile’s physical structure, where the back was taller than the front. On Experiment 7, similar patterns are observed, though they are less distinct than Experiment 6 (Figure 3.22 & 3.23). This reduction in clarity was likely due to the increased distance between the anchors and the tag, which may have led to weaker signal strength and thus reduced localization accuracy. These findings highlight the RTLS system's capacity to capture general movement patterns and behaviors of the bin-piler, though with limitations in precision under real-world conditions, especially when faced with increased anchor-to-tag distances and signal interference from the pile.

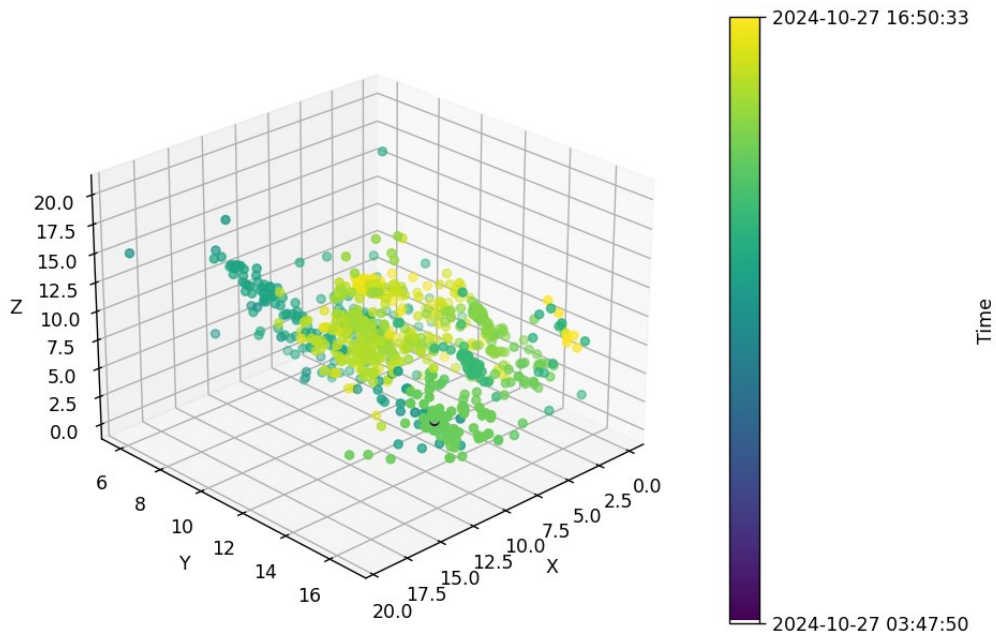


Figure 3.22: Experiment 7 3D Plot Isometric View

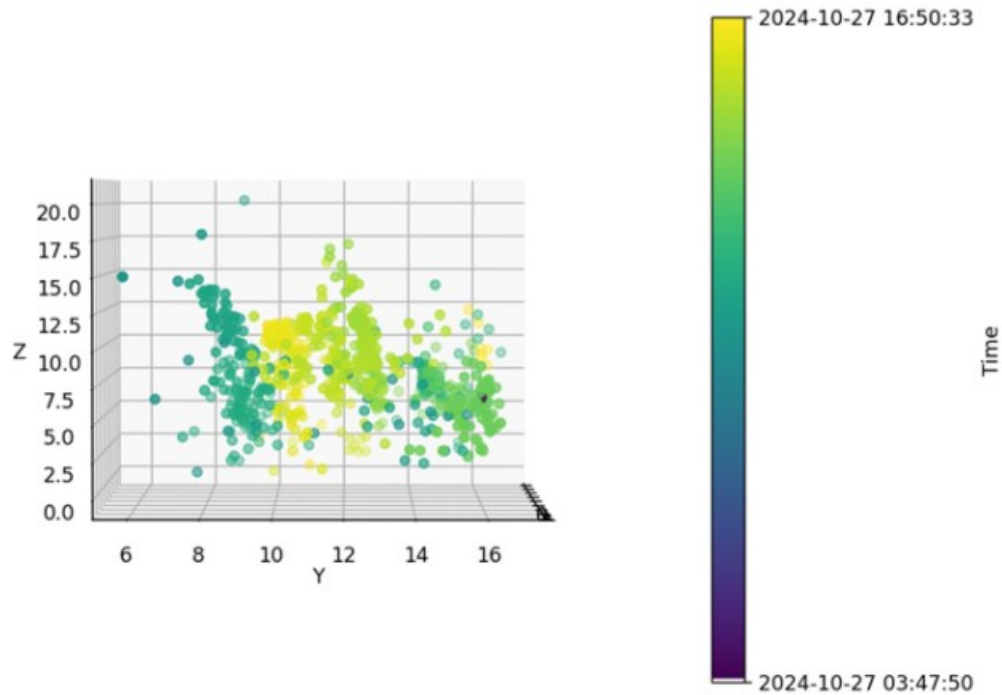


Figure 3.23: Experiment 7 3D Plot YZ Plane

### 3.6. Summary

Chapter 3 focused on the development and evaluation of a potato bin-piler localization system using UWB RTLS for both lab and field environments. The primary objective of this chapter was to determine the precise location of the bin-piler tip during the storage process, enabling the creation of a synchronized quality map for stored potato tubers.

Key findings reveal the importance of anchor placement, spatial diversity, and Z-axis variation in achieving precise localization. Algorithms like LS, Kalman Filter, and SVR are employed to mitigate inaccuracies caused by environmental factors such as signal interference and multipath effects. The experiments highlight sub-meter accuracy in controlled environments and identify challenges, such as reduced accuracy in Z-dimensions in larger or real-world scenarios.

Additionally, SVR hyperparameter tuning demonstrates the impact of regularization and error tolerance parameters on localization accuracy, offering insights into optimizing system

performance. Overall, this chapter establishes a foundational framework for precise and reliable localization in agricultural storage, providing a pathway for enhanced traceability and management in potato storage facilities.

## **4. Mapping of Potato Quality Data by Synchronizing with Localization Information**

### **4.1. Overview**

The objective of Chapter 4 is to develop a system to synchronize quality data collected by a grading system located at a conveyor out of the storage unit with RTLS, as the potato gets transported from the harvest trucks to the bin-piler. This grading and localizing synchronization system (GLSS) leverages magnetic sensors and UWB boards to monitor key factors influencing tuber placement, including conveyor belt speed and the extension and retraction of the bin-piler arm. The specific objectives of this chapter are to:

1. Evaluate the performance of magnetic sensors and UWB boards and in capturing conveyor dynamics and bin-piler movements,
2. Apply a multi-feature linear regression model to numerically capture the speed and displacement data of the different conveyor speeds and arm extensions with high precision,
3. Implement LoRa technology for efficient long-range, low-power data transmission.

This chapter also outlines experimental methods for validating the system's accuracy, capturing real-time measurements to confirm data synchronization. Through these methods, the system aims to improve traceability by linking grading data with precise storage placement, contributing to enhanced agricultural storage management and operational efficiency

### **4.2. Materials**

#### **4.2.1. Belt Speed Monitoring**

A magnetic sensor (Reed 59060, Littelfuse, Chicago, Illinois, United States) is used to monitor the rotational speed of a conveyor shaft, enabling synchronized tracking between tuber imaging and storage placement. The sensor's output is monitored using an Arduino Uno using digital GPIO,

which calculates the conveyor speed and transmits this data to the grading station via LoRa (RYLR896, REYAX, Taipei, Taiwan) (Figure 4.1).

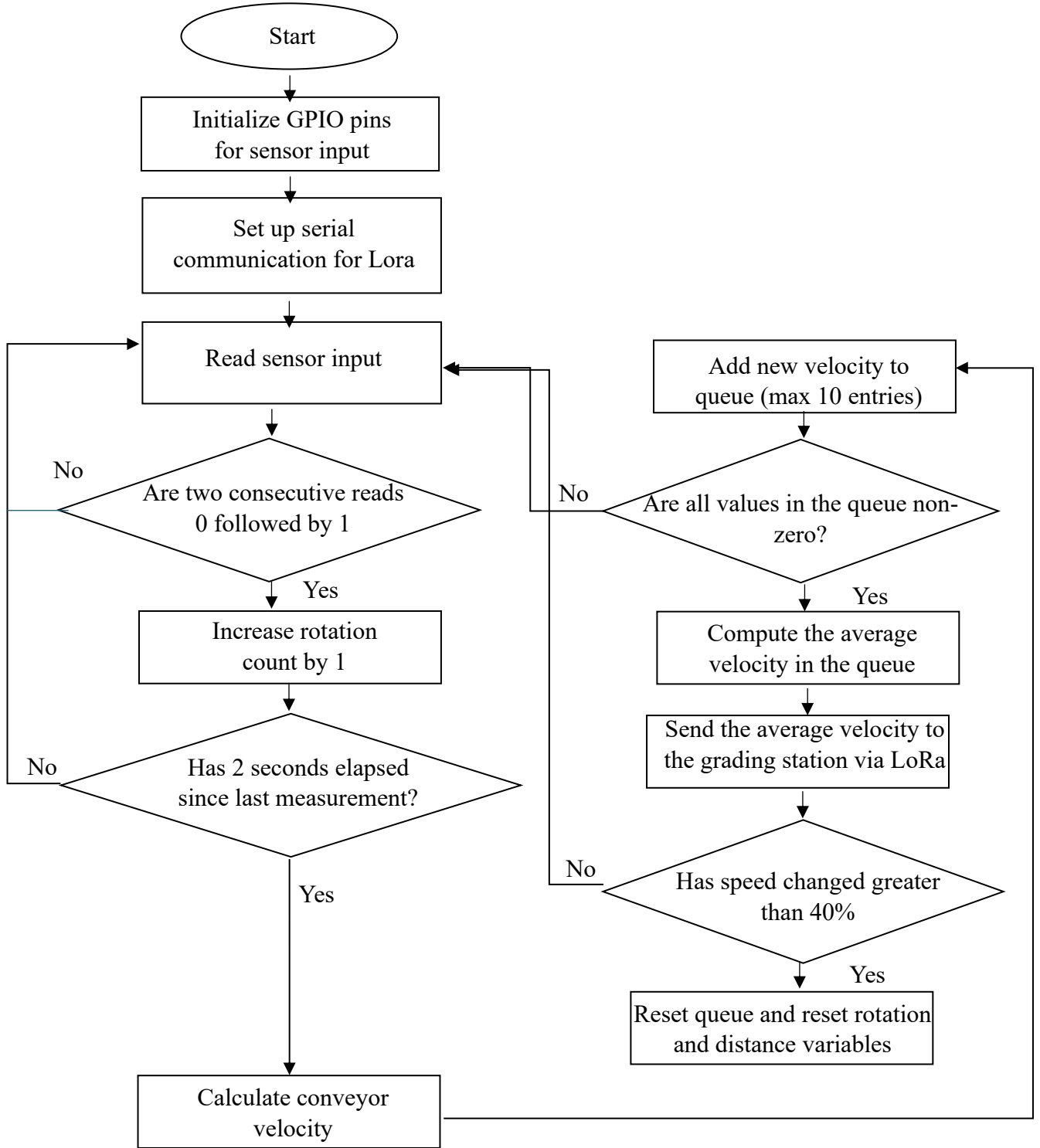


Figure 4.1: Belt Speed Monitoring Software Flowchart

#### **4.2.2. Conveyor Extension and Retraction Monitoring**

In the GLSS, the conveyor extension and retraction monitoring setup utilized a pair of one UWB anchor and one tag, similar to the one used in RTLS, to measure the extension and retraction of a bin-piler arm operating at Bin 3906. This distance data was then transmitted to the grading station computer via LoRa antenna of the tag, allowing the system to continuously adjust for variations in tuber travel time based on arm extension.

### **4.3. System Design, Experimental Design and Setup**

#### **4.3.1. GLSS Experiment**

This experiment was conducted in Bin 3906 using the bin-piler to evaluate the accuracy of the GLSS in predicting tuber travel time. The experiment proceeded in parallel measurements of bin-piler extension/retraction and belt speed to calculate tuber path length and travel time (Figure 4.2). The bin-piler length was monitored continuously, measuring the amount of hydraulic extension and retraction ( $UWB_n$ ). This setup allowed for active measuring of the hydraulic movement of the bin-piler arm, directly impacting the path length that tubers travel from the grading station to the bin-piler crest. In GLSS, The pair of anchor and tag used IR-UWB Gaussian pulse transmission, employing either third or seventh-derivative pulses, and implementing the TWR protocol to get the TOF measurements which led to calculating the displacement of the bin-piler's arm as it extended or retracted. The baseline distance of the bin-piler (BD), corresponding to the fully retracted position, was added to each UWB measurement to determine the actual path length change. On the other hand, belt speed ( $M_n$ ) was recorded using a magnetic sensor attached to the bin-piler shaft. This sensor operates with a normally open (NO) configuration, closing its relay upon exposure to a magnetic field, allowing RPM measurement. In this case the Arduino board on which the sensor was mounted transmitted the data to the Grading Station using LoRa. All data,

including the UWB measurements and belt speed, were used for travel time predictions using Eq. 4.1.

A camera (DSC-RX0M2, Sony, Tokyo, Japan) was mounted above the crest of the bin-piler, capturing images approximately every second using OpenCV libraries. These images were timestamped and saved to the laptop to provide visual verification of tuber positioning and timing. During each trial, tubers were loaded onto the bin-piler belt and allowed to travel from the bin entry to the bin-piler's crest, where they would drop off (Figure 4.3). The travel time was then measured manually from initial loading to crest drop-off, providing a reference time for each tuber (Eq. 4.2). To ensure sufficient data for analysis, the process of capturing images and recording time was repeated 30 times. This experiment was also repeated at different combination of distance (12, 13.5, and 15 meters) and belt speed (0.805, 0.895, and 1.013 m/s). Eventually, a two-feature linear regression model was implemented, incorporating both bin-piler extension and belt speed as the parameters, and actual drop time as the target. The data set was split, 80% for training and 20% for testing. After the model was trained and tested, the average difference between predictions, and actual drop times were calculated (Eq. 4.3).

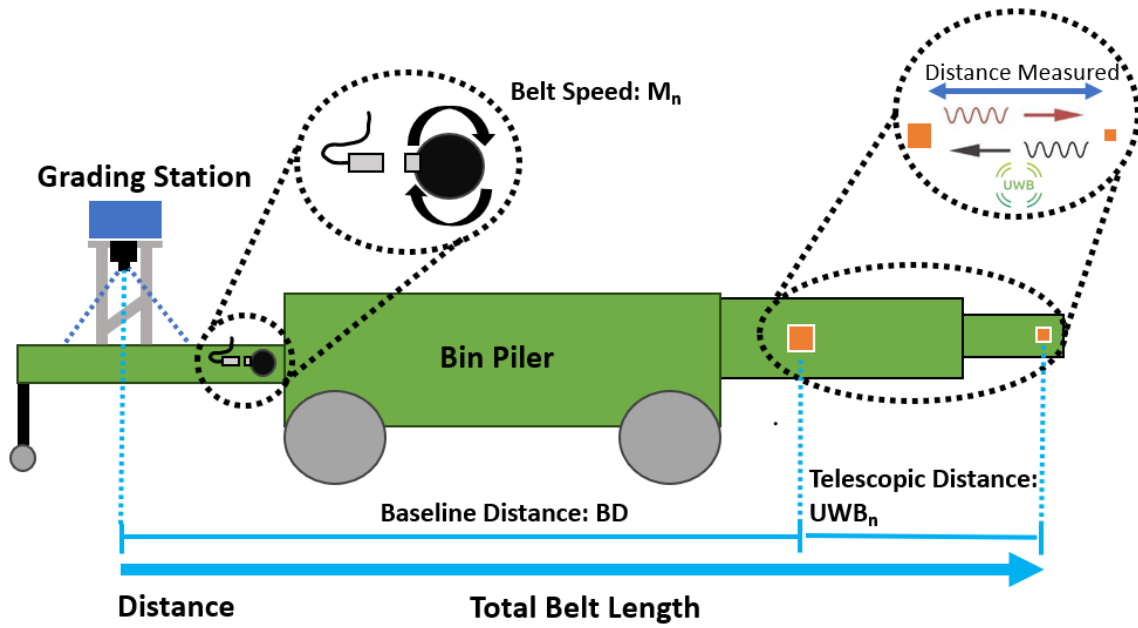


Figure 4.2: Location of Synchronization Sensors on Bin-piler

$$\frac{BD + UW_{B_n}}{M_n} = (\text{Predicted Drop Time})_n \quad (4.1)$$

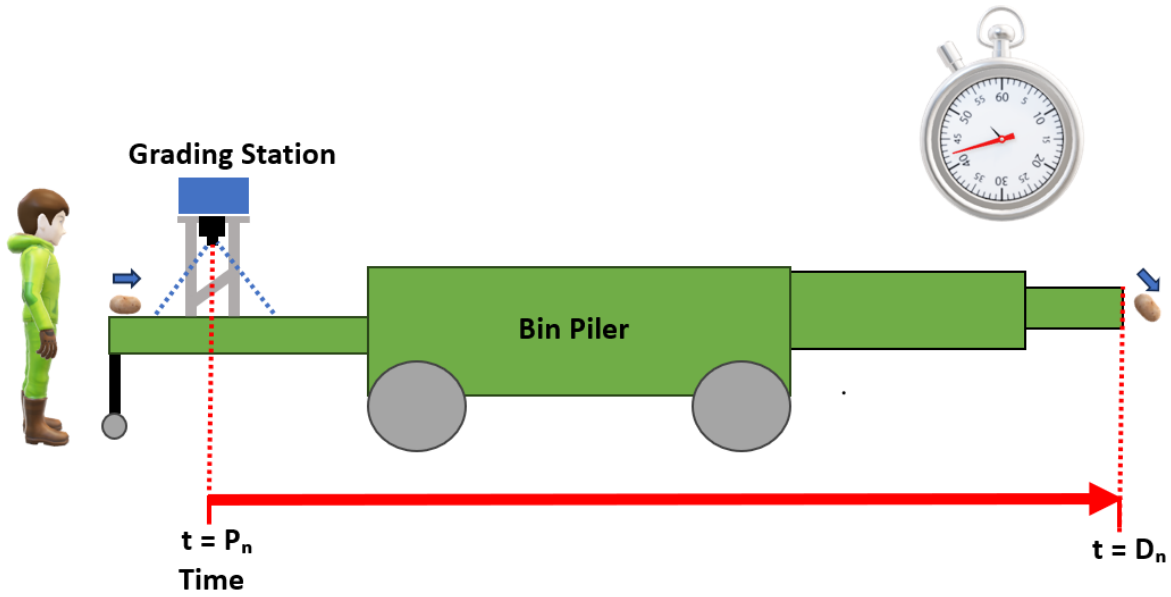


Figure 4.3: Synchronization Experiment Actual Travel Time Diagram

$$D_n - P_n = (\text{Actual Drop Time})_n \quad (4.2)$$

$$\frac{\sum_{n=1}^{30} |(\text{Actual Drop Time})_n - (\text{Predicted Drop Time})_n|}{30} \quad (4.3)$$

#### 4.3.2. Quality Map Generation and Server Upload

Following data generation at the grading station (Figure 4.4), the quality map was created through post-processing, rather than autonomously or in real-time. A Python script was executed to merge the outputs from the grading station.

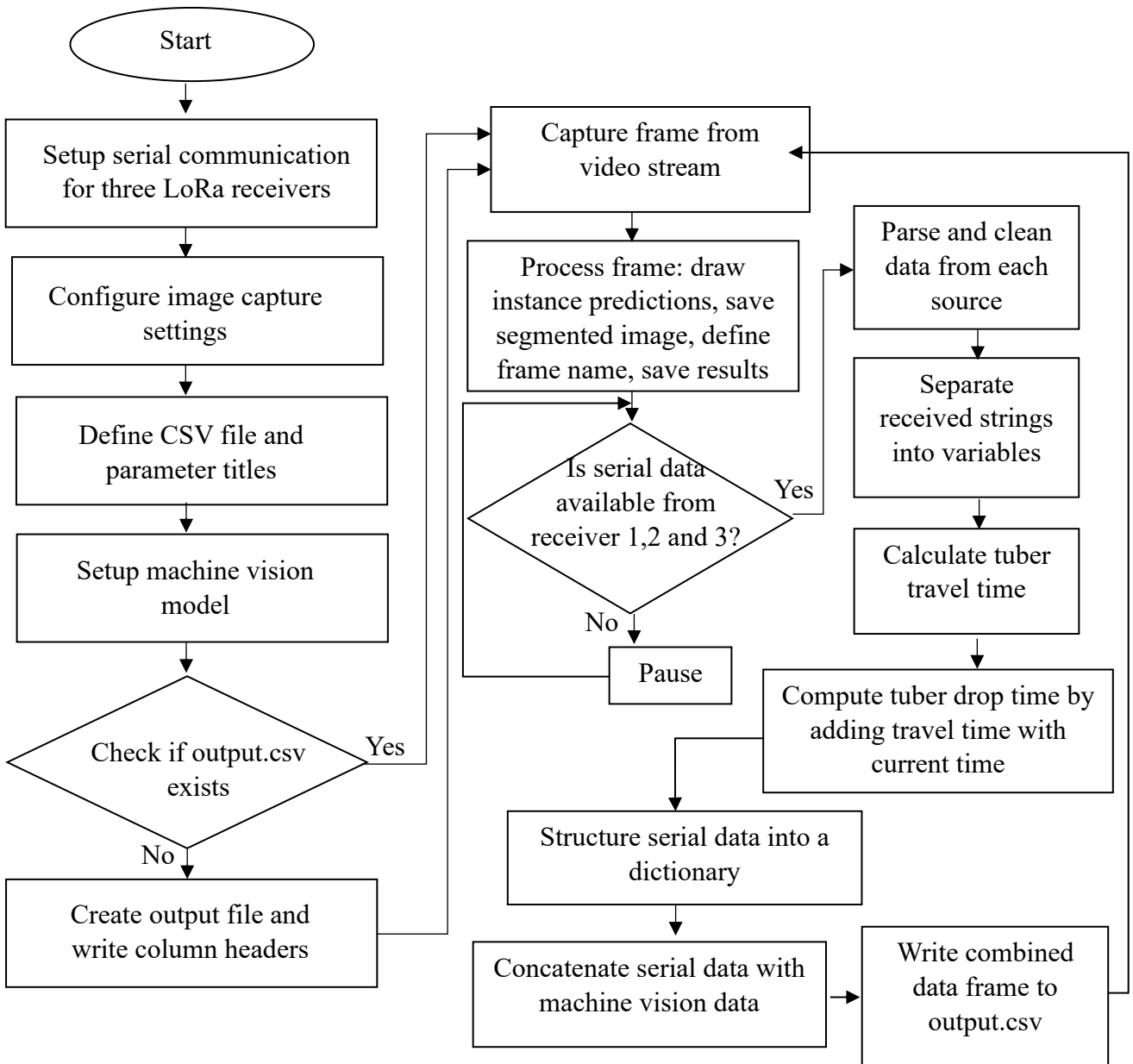


Figure 4.4: Grading Station Software Flowchart

#### 4.4. Results and Discussion

Figure 4.5 illustrates the raw data analysis using the box and whisker plots, showcasing the comparison of actual, predicted and corrected travel times. The actual times demonstrated relatively consistent ranges across all plots, serving as the baseline for assessing prediction

accuracy. Predicted times without the linear regression model exhibited a consistent tendency to overestimate travel times, as their median and upper whiskers were generally positioned above those of the actual times. The corrected times produced by the linear regression model align more closely with the actual times, with medians that fall nearer to the actual values, in 7 of the 9 plots. Interquartile ranges appeared relatively consistent between predicted times, with and without the Linear Regression model. The most pronounced errors can be observed at bin-piler extension distances of 13.5 m. Since belt speed measurement is independent of bin-piler extension – there is no reason for belt shaft rotation measurement could be affected by this – there therefore must be a tendency for the ranging to overestimate bin-piler extension at this orientation.

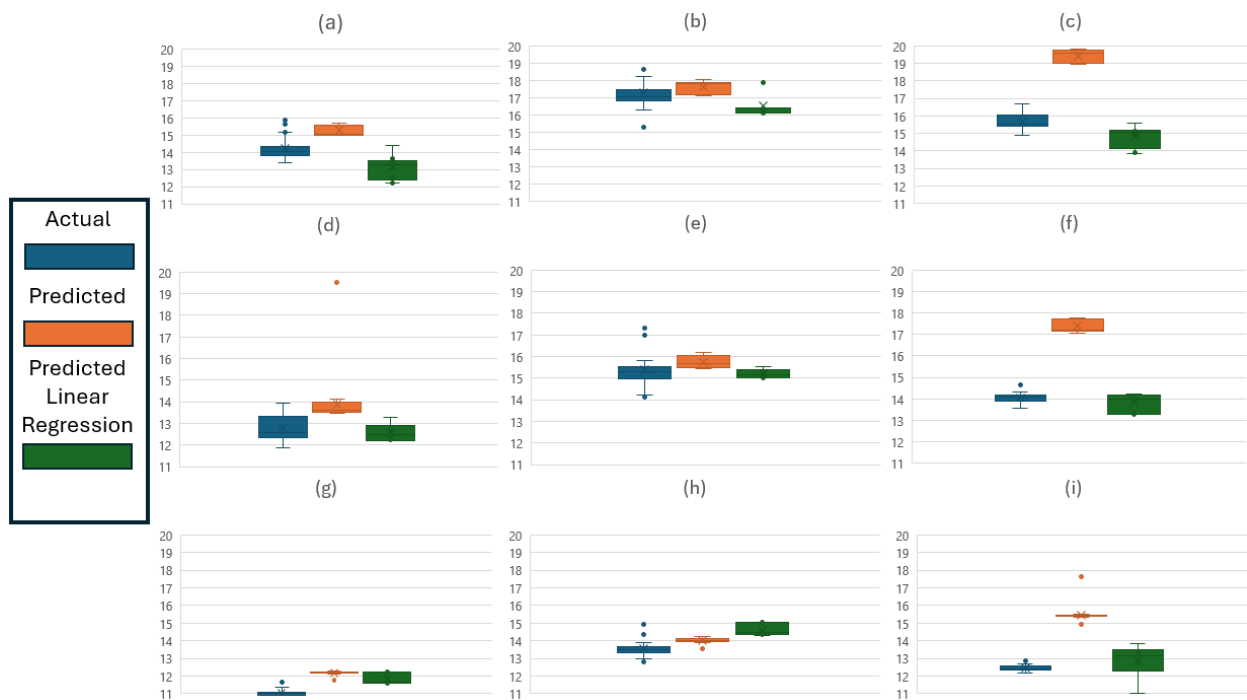


Figure 4.5: GLSS Box and Whisker Plots where (a) 12 m, 0.805 m/s, (b) 13.5 m, 0.805 m/s, (c) 15 m, 0.805 m/s, (d) 12 m, 0.895 m/s, (e) 13.5 m, 0.895 m/s, (f) 15 m, 0.895 m/s, (g) 12 m, 1.013 m/s, (h) 13.5 m, 1.013 m/s, (i) 15 m, 1.013 m/s

Table 4.1: GLSS Experimental Results - Outside of brackets represent RMSE with Linear Regression model. Inside brackets are RMSE without the Linear Regression model.

<b>Synchronization Error (s)</b>			
<b>Total Belt Length (m)</b>	<b>Belt Speed (m/s)</b>		
	0.805	0.895	1.013
12	1.353 (1.127)	0.692 (1.175)	0.971 (1.148)
13.5	0.912 (0.739)	0.589 (0.732)	1.104 (0.585)
15	0.806 (3.716)	0.356 (3.349)	0.899 (2.977)

The initial analysis of raw data yielded an average error of 1.727 s (Table 4.1) with a standard deviation of 0.514 seconds. This baseline error was primarily due to inherent limitations in using only raw sensor data, which did not account for variability in belt speed or the dynamic extension and retraction of the bin-piler. Given this, applying linear regression was anticipated to improve accuracy by modeling the relationship between these factors and tuber travel time more effectively. Applying a linear regression model with one feature—predicted travel time alone—reduced the average error to 1.127 seconds but increased the standard deviation to 0.891 seconds. While the single-feature regression improved the overall accuracy, the increase in standard deviation indicated that significant variance remained unaccounted for in the prediction. The high variance suggested that tuber travel time was influenced by additional dynamic factors beyond what can be explained by predicted time alone. On the other hand, the two-feature model showed a marked improvement, yielding an average error of 0.875 seconds with a standard deviation of 0.618 seconds. By accounting for variability in both belt speed and bin-piler extension, the two-feature model better reflected the operational dynamics affecting tuber travel time, offering a more reliable estimation due to its capacity to capture the interdependent effects of belt speed and bin-piler length on tuber movement. As tubers travel across the bin-piler, both features constitute independent parameters: belt speed directly influences the travel rate, while the bin-piler’s extension impacts the total distance traveled.

Once data is concatenated, it is time to produce the quality map (Figure 4.6). This is done, similarly, by way of a Python script using Plotly library to generate an interactive map, where the user can drag to change the point of view and hover above 3D points to see the corresponding quality information for each mapped point (Figure 4.7). Sequential alignment of the grading station data was found to be practical for creating the quality map (Figure 4.8). Given the nature of tuber handling, harvesting, and transportation, operations do not occur in strict synchrony with the grading process, therefore time-matching files cannot work as a strategy for traceability. Instead, tubers are harvested and loaded in a continuous manner, often filling truckloads that follow a logical sequence from harvest to storage. The sequential order is preserved throughout the supply chain. Tubers harvested first typically settle at the bottom of field carts, while those harvested later rest on top. When offloaded at an intermediary in-field sorting station, tubers retain this order before being loaded into transport trucks via conveyor systems. At storage, these tubers are once again offloaded in sequence, with those at the bottom of the truck bed entering the storage facility first. Consequently, tubers at the bottom of each truckload correspond to those harvested first.

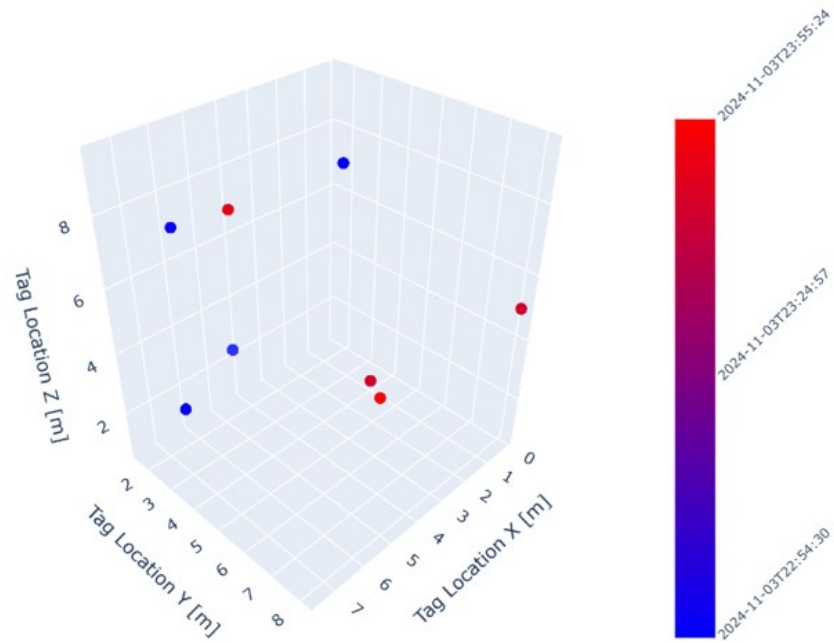


Figure 4.6: Quality Map Interactive 3D Plot – Each dot represents 1 data point: a frame taken at the grading station, tuber instance, predicted drop-off time and location. Position within the grid corresponds to bin-piler crest location.

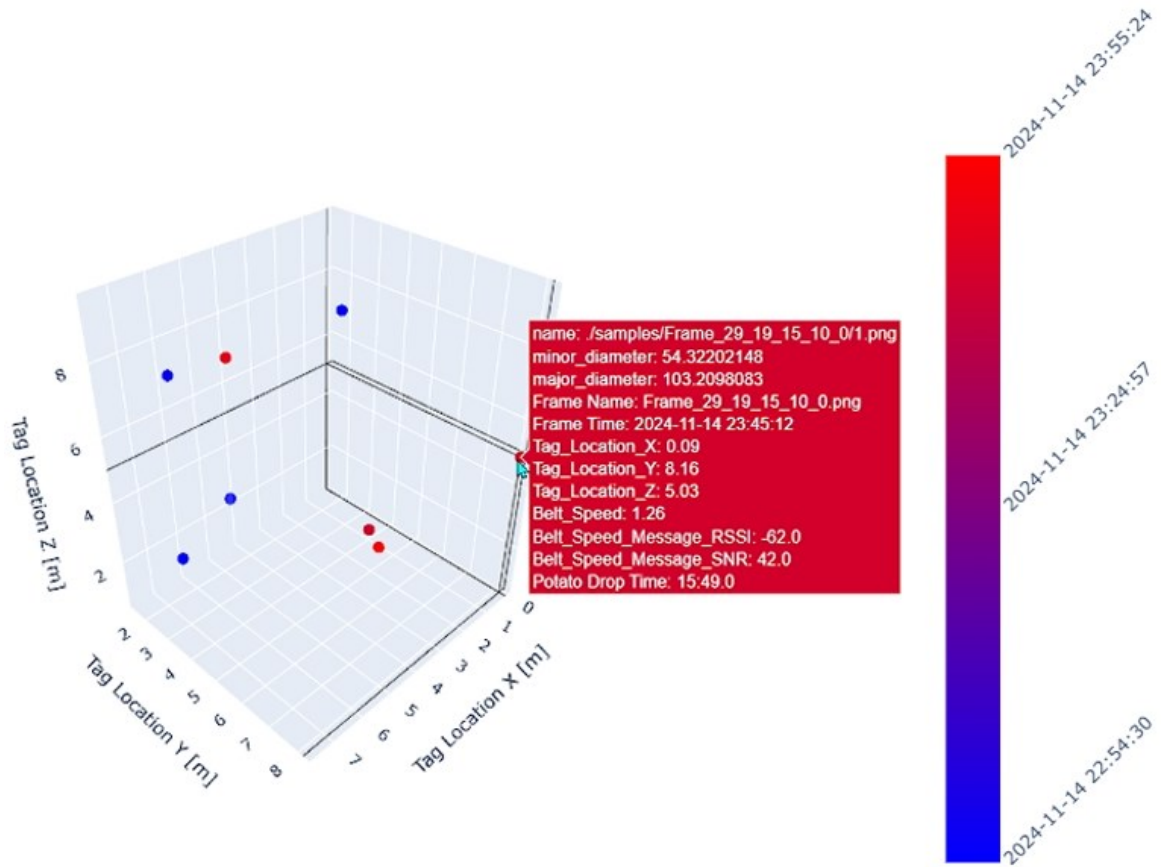


Figure 4.7: Quality Map Interactive 3D Plot with Features

## Grading Results

## Localization and Synchronization Results

name	minor_diameter	major_diameter	Frame Name	Frame Time	Tag_Location_X	Tag_Location_Y	Tag_Location_Z	Belt_Speed	Belt_Speed_Message_RSSI	Belt_Speed_Message_SNR	Potato Drop Time
./samples	54.71828842	124.9198303	Frame_29_19_10_33_0.png	22:54.5	3.89	5.49	9.44	1.26	-61	43	23:02.4
./samples	42.63311005	91.89266205	Frame_29_19_10_33_0.png	22:54.5	3.89	5.49	9.44	1.26	-61	43	23:02.4
./samples	48.33908081	90.64620972	Frame_29_19_10_33_0.png	22:54.5	3.89	5.49	9.44	1.26	-61	43	23:02.4
./samples	53.98912811	102.7260513	Frame_29_19_10_33_0.png	22:54.5	3.89	5.49	9.44	1.26	-61	43	23:02.4
./samples	50.93417358	113.7386856	Frame_29_19_10_33_0.png	22:54.5	3.89	5.49	9.44	1.26	-61	43	23:02.4
./samples	51.37008286	113.0536728	Frame_29_19_10_33_0.png	23:45.2	0.9	3.91	0.66	1.26	-62	39	23:48.1
./samples	50.36060333	106.4811935	Frame_29_19_10_33_0.png	23:45.2	0.9	3.91	0.66	1.26	-62	39	23:48.1
./samples	35.2248497	86.32444	Frame_29_19_10_33_0.png	23:45.2	0.9	3.91	0.66	1.26	-62	39	23:48.1
./samples	48.34386826	85.32029724	Frame_29_19_10_33_0.png	23:45.2	0.9	3.91	0.66	1.26	-62	39	23:48.1
./samples	43.78012466	95.77140806	Frame_29_19_10_33_0.png	23:45.2	0.9	3.91	0.66	1.26	-62	39	23:48.1
./samples	52.91262436	114.5981903	Frame_29_19_10_33_0.png	23:50.4	4.01	1.49	6.81	1.26	-62	44	23:58.6
./samples	50.36060333	106.4811935	Frame_29_19_10_33_0.png	23:50.4	4.01	1.49	6.81	1.26	-62	44	23:58.6
./samples	34.286026	74.42015076	Frame_29_19_10_33_0.png	23:50.4	4.01	1.49	6.81	1.26	-62	44	23:58.6

Figure 4.8: Grading and Quality Results Output File - Localization and Synchronization results (blue square) aligned with Grading results (red square)

#### **4.5. Summary**

Chapter 4 focused on the development of the GLSS aimed at achieving real-time synchronization between potato grading and storage processes. This system integrates magnetic and UWB boards to monitor critical factors such as conveyor belt speed and bin-piler arm movements, ensuring precise tracking of tuber placement from the grading station to storage. The system leverages LoRa technology for efficient long-range, low-power data transmission and applies multi-feature linear regression to enhance prediction accuracy. The chapter also details the creation of a quality map through post-processing. Sequential alignment of data ensures accurate integration of grading and localization information, enabling the generation of a detailed, interactive 3D quality map using Python and Plotly. This map allows stakeholders to analyze spatial and temporal variations in tuber quality, providing valuable insights for storage management and traceability. Despite challenges, such as manual data transfer and the need for basic technical proficiency to utilize visualization tools, the system demonstrates potential for optimizing agricultural operations. By linking grading and storage data, the system enhances traceability, improves quality management, and supports better decision-making in post-harvest processes. Future improvements may focus on automating data synchronization and exploring advanced machine learning techniques for greater accuracy and efficiency.

## **5. Conclusion**

This thesis has presented a novel approach to post-harvest potato tuber traceability through the development of an integrated system leveraging real-time localization, wireless communication, and remote sensing. By establishing a quality mapping framework within a bulk storage facility, this study has demonstrated the feasibility of tracking and assessing tuber quality spatially and temporally, an advancement that holds significant promise for reducing post-harvest losses and improving quality control. The methodological innovations discussed herein illustrate how precise localization, combined with real-time data acquisition, can provide a more granular understanding of quality variations within a storage environment.

The results of this research highlight the practical benefits and limitations of implementing RTLS in agricultural contexts. The system was shown to perform reliably under various conditions, from controlled warehouse environments to dynamic, large-scale storage facilities. Despite challenges associated with signal interference, NLOS conditions, and z-axis accuracy, the RTLS maintained sub-meter precision under ideal configurations, supporting its applicability to bulk storage management. Moreover, by validating the system's effectiveness in differentiating quality attributes spatially, this study offers a foundation for enhancing current practices in storage monitoring and management.

### **5.1. Steps Forward**

- Future research should focus on refining the system's accuracy in larger, less controlled environments by optimizing anchor configurations and exploring alternative algorithms to mitigate Z-axis variability. Additionally, expanding the system's synchronization capabilities, particularly through wireless data transfer to central farm databases, would further streamline post-harvest monitoring and enable real-time decision-making.

- An important next step is to integrate the Python script for generating the quality map into a user-friendly application. Embedding this functionality within an application would enhance usability, allowing stakeholders to visualize and interact with the quality map more intuitively. This application could include customizable options for users to adjust the appearance of the map, such as modifying the color bar to reflect different parameters within storage (e.g., tuber size, field source, or harvest day). This flexibility would enable users to tailor the map display to emphasize specific quality attributes or traceability markers, further enhancing its practical utility. Autonomous integration of other traceability system data could be another key area for improvement. This could involve exploring alternative systems, such as HarvestEye by Root Crop Technology, to assess their compatibility and integration prospects for a seamless flow of data. This automation would reduce labor demands and minimize errors in data handling, enhancing the overall efficiency of the system.
- In terms of hardware improvements, increasing the number and range of tags could provide a significant boost in localization accuracy and reliability. New UWB boards with output amplifiers, such as those offered by Makerfab, have an extended maximum range of up to 120 m—a 400% increase over the current boards. Adopting these enhanced UWB modules could enable the system to cover larger storage areas with greater positional accuracy, especially in complex environments with obstacles or extended range requirements. Furthermore, replacing the current belt speed sensors with models capable of measuring fractional rotations would enhance the precision of conveyor tracking. The existing system captures only full rotations and relies on a rolling average through approximating intermediate speeds. By adopting sensors with finer resolution – not limited to complete shaft rotations - the system could achieve more accurate real-time tracking of conveyor speed, thereby improving the quality and reliability of positional data for each tuber frame.

- One promising direction is to experiment with different non-linear kernels for SVR models. While the current implementation uses a linear kernel, non-linear kernels such as RBF or polynomial kernels could capture complex relationships between the predicted and actual 3D locations. This approach may help account for non-linearities in the spatial positioning data, under challenging conditions where the tag's signal experiences interference or multipath propagation. A systematic comparison of these kernels, paired with hyperparameter tuning, could identify configurations that yield lower error rates and greater consistency across varied experimental setups.
- The Kalman Filter configuration is another area ripe for exploration. The current settings—1 for initial estimation error, 1 for measurement error, and 0.01 for process noise—were effective in initial experiments but may not represent the optimal configuration for all scenarios. Future work could involve varying these parameters to evaluate their impact on the system's performance under different environmental conditions, such as varying levels of noise or dynamic changes in the experimental setup. Additionally, advanced Kalman Filter variants, such as the Extended Kalman Filter or Unscented Kalman Filter, could be explored to better handle non-linearities in the system and improve positioning accuracy in more complex environments. Ultimately, the methods and technologies explored in this thesis represent a step forward in post-harvest traceability and quality assurance, contributing to more sustainable and efficient potato storage practices and setting the groundwork for broader applications across agricultural supply chains.

## References

- Abreu, P.H., Xavier, J., Silva, D.C., Reis, L., & Petry, M.R. (2014). Using Kalman Filters to Reduce Noise from RFID Location System. *The Scientific World Journal*. <http://dx.doi.org/10.1155/2014/796279>
- Agriculture and Agri-Food Canada (AAFC) (2022). *Potato Market Information Review*. Government of Canada. Retrieved from <https://agriculture.canada.ca/en/agriculture-and-agri-food-canada/canadas-agriculture-sectors/horticulture/horticulture-sector-reports/potato-market-information-review-2020-2021>
- Akello, R., Turinawe, A., Wauters, P., & Naziri, D. (2022). Factors Influencing the Choice of Storage Technologies by Smallholder Potato Farmers in Eastern and Southwestern Uganda. *Agriculture*, 12(2), 240. <https://doi.org/10.3390/agriculture12020240>
- Alarifi, A., Al-Salman, A., Alsaleh, M., Alnafessah, A., Al-Hadhrami, S., Al-Ammar, M. A., & Al-Khalifa, H. S. (2016). Ultra wideband indoor positioning technologies: Analysis and recent advances. *Sensors*, 16(5), 707. <https://doi.org/10.3390/s16050707>
- Al-Mallahi, A. (2024). Precision crop production engineering – increasing productivity using digital technology. In R. Y. Yada, R. Van Acker, M. Scanlon, & D. Gray (Eds.), *Future food systems*, 65-76. Academic Press. <https://doi.org/10.1016/B978-0-443-15690-8.00014-X>
- Badhai, S., Gupta, A. K., & Koiri, B. (2022). Precision Farming Components and Importance of Precision Farming: A Review. In N. D. Totewad, T. R. Parashurama, K. S. Vinayaka & B. K. Das (Eds.), *Advances in Microbiology*, 3. Retrieved from [https://www.researchgate.net/publication/360035290\\_Precision\\_Farming\\_Components\\_and\\_Importance\\_of\\_Precision\\_Farming\\_A\\_Review](https://www.researchgate.net/publication/360035290_Precision_Farming_Components_and_Importance_of_Precision_Farming_A_Review)
- Barrett, T. W. (2000). History of Ultrawideband (UWB) Radar & Communications: Pioneers and Innovators. *Progress In Electromagnetics Symposium 2000*. Retrieved from [https://www.researchgate.net/publication/305681751\\_History\\_of\\_Ultrawideband\\_UWB\\_Communications\\_Radar\\_Part\\_1\\_UWB\\_Communications](https://www.researchgate.net/publication/305681751_History_of_Ultrawideband_UWB_Communications_Radar_Part_1_UWB_Communications)
- Basir, M. S., Buckmaster, D., Raturi, A., & Zhang, Y. (2024). From pen and paper to digital precision: A comprehensive review of on-farm recordkeeping. *Precision Agriculture*, 25, 2643-2682. <https://doi.org/10.1007/s11119-024-10172-7>
- Bongiovanni, R., & Lowenberg-Deboer, J. (2004). Precision Agriculture and Sustainability. *Precision Agriculture*, 5, 359-387. <https://doi.org/10.1023/B.0000040806.39604.aa>
- Booth, R. H., & Shaw, R. L. (1981). *Principles of potato storage*. International Potato Center. Retrieved from <https://www.semanticscholar.org/paper/Principles-of-potato-storage.-Booth-Shaw/b4c17783d3047640fbf2816c0f450710beeb234a>

Caliskhan, M. E., Yousaf, M. F., Yavuz, C., Zia, M. A. B., & Calikhan, S. (2023). History, production, current trends, and future prospects. In M. E. Caliskhan, A. Bakhsh, & K. Jabran (Eds.), *Potato Production Worldwide*, 1-18. Academic Press. <https://doi.org/10.1016/B978-0-12-822925-5.00016-5>

Choi, H., Son, S., Kim, J., & Baek, Y. (2010). RF-Based Indoor Locating System for NLOS Environment. *24th IEEE International Conference on Advanced Information Networking and Applications*, 628-633. <https://doi.org/10.1109/AINA.2010.90>

Contigiani, M., Pietrini, R., Mancini, A., & Zingaretti, P. (2016). Implementation of a tracking system based on UWB technology in a retail environment. *2016 12th IEEE/ASME International Conference on Mechatronic and Embedded Systems and Applications (MESA)*, 1-6. <https://doi.org/10.1109/MESA.2016.7587123>

D'Altroy, T. N. (1987). Huánuco Pampa: An Inca city and its hinterland by Craig Morris and Donald E. Thompson [Review of the book Huánuco Pampa: An Inca city and its hinterland, by C. Morris & D. E. Thompson]. *American Antiquity*, 52(2), 426. <https://doi.org/10.2307/281811>

Delamare, M., Bouteau, R., Savatier, X., & Iriart, N. (2020). Static and dynamic evaluation of an UWB localization system for industrial applications. *Sci*, 2(2), 23. <https://doi.org/10.3390/sci2020023>

Demestichas, K., Peppes, N., Alexakis, T., & Adamopoulou, E. (2020). Blockchain in agriculture traceability systems: A review. *Applied Sciences*, 10(12), 4113. <https://doi.org/10.3390/app10124113>

Dewhirst, O. P., Evans, H. K., Roskilly, K., Harvey, R. J., Hubel, T. Y., & Wilson, A. M. (2016). Improving the accuracy of estimates of animal path and travel distance using GPS drift-corrected dead reckoning. *Ecology and Evolution*, 6(17), 6210-6222. <https://doi.org/10.1002/ece3.2359>

Elbes, M., Al-Fuqaha, A., & Raye, A. (2012). Gyroscope Drift Correction based on TDOA technology in support of Pedestrian Dead Reckoning. *2012 IEEE Globecom Workshops*, 314-319. <https://doi.org/10.1109/glocomw.2012.6477589>

Food and Agriculture Organization of the United Nations. (2024). FAOSTAT: Crops and livestock products. *FAOSTAT*. Retrieved from <https://www.fao.org/faostat/en/#data/QCL>

Gezici, S. (2008). A Survey on Wireless Position Estimation. *Wireless Personal Communication*, 44, 263-282. <https://doi.org/10.1007/s11277-007-9375-z>

Gezici, S., Poor, H. V., Kobayashi, H., Buehrer, R. M., & Sahinoglu, Z. (2005). Localization via ultra-wideband radios: A look at positioning aspects for future sensor networks. *IEEE Signal Processing Magazine*, 22(4), 70-84. <https://doi.org/10.1109/MSP.2005.1458289>

- Gokhale, P., Bhat, O., Bhat, S. (2018). Introduction to IOT. *International Advanced Research Journal in Science, Engineering and Technology*, 5(1). Retrieved from [https://www.researchgate.net/publication/330114646\\_Introduction\\_to\\_IOT](https://www.researchgate.net/publication/330114646_Introduction_to_IOT)
- González-Amarillo, C.A., Corrales-Munoz, J.C., Mendoza-Moreno, M. A., González-Amarillo, A.M., Hussein, A.F., & Arunkumar, N. (2018). An IoT-Based Traceability System for Greenhouse Seedling Crops, *IEEE Access*, 6, 67528-67535, 2018, doi: 10.1109/ACCESS.2018.2877293
- Grambozov, A., Atanasovski, V., & Gavrilovska, L. (2015). Practical evaluation of TDOA, AOA and hybrid methods for geolocation of wireless transmitters. *IEEE International Symposium on Broadband Multimedia Systems and Broadcasting*. <https://doi.org/10.1109/bmsb.2015.7177280>
- Greentronics. (2021). Ritetrace – Fully Automated Track & Trace System. Retrieved from <https://greentronics.com/products/ritetrace/>
- Guenthner, J. F. (1995). Economics of potato storage. *American Potato Journal*, 72, 493-502. <https://doi.org/10.1007/BF02851682>
- Hafner, G., Barabosz, J., Leverenz, D., Maurer, C., Kranert, M., Göbel, C., Friedrich, S., Ritter, G., Teitscheid, P., & Wetter, C. (2013). Analysis evaluation and optimization of food management systems. *Garbage and Waste*, 11. <https://doi.org/10.37307/j.1863-9763.2013.11.08>
- Halawa, F., Dauod, H., Lee, I. G., Li, Y., Yoon, S. W., & Chung, S. (2020). Introduction of a real-time location system to enhance the warehouse safety and operational efficiency. *International Journal of Production Economics*, 224. <https://doi.org/10.1016/j.ijpe.2019.107541>
- Haverkort, A. J., & Kempenaar, C. (2016). Recent advances in biotechnology and information technology in the potato industry. *The Dundee Conference: Proceedings Crop Protection in Northern Britain 2016*, 183-190. Retrieved from <https://edepot.wur.nl/410605>
- Huang, S., Guo, Y., Zha, S., Wang, F., & Fang, W. (2017). A real-time location system based on RFID and UWB for Digital Manufacturing Workshop. *Procedia CIRP*, 63, 132-137. <https://doi.org/10.1016/j.procir.2017.03.085>
- Jiang, Y., & Leung, V. C. M. (2007). An asymmetric double-sided two-way ranging for crystal offset. *International Symposium on Signals, Systems and Electronics*, 525-528. <https://doi.org/10.1109/issse.2007.4294528>
- Jiménez Ruiz, A. R., & Granja, F. S. (2017). Comparing Ubisense, BeSpoon, and DecaWave UWB Location Systems: Indoor Performance Analysis. *IEEE Transactions on Instrumentation and Measurement*, 66(8), 2106-2117. <https://doi.org/10.1109/TIM.2017.2681398>
- Keiser, A., Häberli, M., Schnyder, E., & Berchier, P. (2007). Influence of the farming system and specific cultivation methods on the slug damage level in Swiss potato production. Proceedings of the IOBC/WPRS Working Group on Insect Pathogens and Entomoparasitic Nematodes, 26-29. Retrieved from <https://www.cabidigitallibrary.org/doi/full/10.5555/20063197387>

- Kufakunesu, R., Hancke, G. P., & Abu-Mahfouz, A. (2020). A survey on adaptive data rate optimization in LoRaWAN: Recent solutions and major challenges. *Sensors*, 20(18), 5044. <https://doi.org/10.3390/s20185044>
- Kumar, D., & Kalita, P. (2017). Reducing postharvest losses during storage of grain crops to strengthen food security in developing countries. *Foods*, 6(1), 8. <https://doi.org/10.3390/foods6010008>
- Laird, J. (2012). Clock Synchronization Terminology. *UNH InterOperability Laboratory*. Retrieved from [https://www.iol.unh.edu/sites/default/files/knowledgebase/1588/clock\\_synchronization\\_terminology.pdf](https://www.iol.unh.edu/sites/default/files/knowledgebase/1588/clock_synchronization_terminology.pdf)
- Li, H., Miura, R., Nishikawa, H., Kagawa, T., & Kojima, F. (2016). Tracking of Warehouse Forklifts Using an Indoor Positioning System Based on IR-UWB. *International Conference on Indoor Positioning and Indoor Navigation*. Retrieved from <https://www.semanticscholar.org/paper/Tracking-of-Warehouse-Forklifts-Using-an-Indoor-on-Li-Miura/27977b023abce26f4977a149a18c73978b42e858>
- Li, Z., Li, X., Mou, G., Jiang, D., Bao, X., & Wang, Y. (2019). Design of Localization System Based on Ultra-Wideband and Long-Range Wireless. *2019 IEEE 11th International Conference on Advanced Infocomm Technology (ICAIT)*, 142-146. <https://doi.org/10.1109/ICAIT.2019.8935892>
- Liu, H., Darabi, H., Banerjee, P., & Liu, J. (2007). Survey of wireless indoor positioning techniques and systems. *IEEE Transactions on Systems, Man, and Cybernetics - Part C: Applications and Reviews*, 37(6), 1067–1080. <https://doi.org/10.1109/TSMCC.2007.905750>
- Liu, B., Wu, X., Reddy, V., Kang, D. M., & Liu, W. (2010). A RTLS/DR based localization system architecture for indoor mobile robots. *2010 IEEE International Symposium on "A World of Wireless, Mobile and Multimedia Networks"*, 1-6. <https://doi.org/10.1109/WOWMOM.2010.5534949>
- McKinney, W. (2010). *Data Structures for Statistical Computing in Python*. Proceedings of the 9<sup>th</sup> Python in Science Conference, 51-56. Retrieved from <https://api.semanticscholar.org/CorpusID:13156234>
- Marano, S., Gifford, W. M., Wymeersch, H., & Win, M. Z. (2010). NLOS identification and mitigation for localization based on UWB experimental data. *IEEE Journal on Selected Areas in Communications*, 28(7), 1026–1035. <https://doi.org/10.1109/JSAC.2010.100907>
- Mendoza-Silva, G. M., Torres-Sospedra, J., & Huerta, J. (2019). A meta-review of indoor positioning systems. *Sensors*, 19(20), 4507. <https://doi.org/10.3390/s19204507>

- Meunier, B., Pradel, P., Sloth, K. H., Cirie, C., Delval, E., Mialon, M. M., & Veissier, I. (2018). Image analysis to refine measurements of dairy cow behavior from a real-time location system. *Biosystems Engineering*, *173*, 32-44. <https://doi.org/10.1016/j.biosystemseng.2017.08.019>
- Miah, M. A. (2009). *Post harvest losses and technical efficiency of potato storage systems in Bangladesh*. Bangladesh Agricultural Research Institute. Retrieved from [https://www.researchgate.net/publication/315885911\\_Post\\_Harvest\\_Losses\\_and\\_Technical\\_Efficiency\\_of\\_Potato\\_Storage\\_Systems\\_in\\_Bangladesh](https://www.researchgate.net/publication/315885911_Post_Harvest_Losses_and_Technical_Efficiency_of_Potato_Storage_Systems_in_Bangladesh)
- Mikoda, M., Kalinowski, K., Ćwikła, G., Grabowik, C., & Foit, K. (2020). Accuracy of real-time location system (RTLS) for manufacturing systems. *International Journal of Modern Manufacturing Technologies*, *12*. Retrieved from [https://www.semanticscholar.org/paper/ACCURACY-OF-REAL-TIME-LOCATION-SYSTEM-\(RTLS\)-FOR-Mikoda-Kalinowski/3e7642c8ed3b823cf0286a174e1ec7bb4dae4179](https://www.semanticscholar.org/paper/ACCURACY-OF-REAL-TIME-LOCATION-SYSTEM-(RTLS)-FOR-Mikoda-Kalinowski/3e7642c8ed3b823cf0286a174e1ec7bb4dae4179)
- Molisch, A. F. (2009). Ultra-wideband communications: An overview. *URSI Radio Science Bulletin*, *329*, 31-42. doi: 10.23919/URSIRSB.2009.7909730
- Monta, S., Promwong, S., & Kingsakda, V. (2016). Evaluation of ultra-wideband indoor localization with trilateration and min-max techniques. *2016 13th International Conference on Electrical Engineering/Electronics, Computer, Telecommunications and Information Technology (ECTI-CON)*, 1-4. <https://doi.org/10.1109/ECTICon.2016.7561496>
- Naumann, M., Koch, M., Thiel, H., Gransee, A., & Pawelzik, E. (2020). The importance of nutrient management for potato production part II: Plant nutrition and tuber quality. *Potato Research*, *63*, 121-137. <https://doi.org/10.1007/s11540-019-09430-3>
- Niu, Z., Yang, H., Zhou, L., Taha, M. F., He, Y., & Qiu, Z. (2023). Deep learning-based ranging error mitigation method for UWB localization system in greenhouse. *Computers and Electronics in Agriculture*, *205*. <https://doi.org/10.1016/j.compag.2022.107573>
- Nikookar, H., & Prasad, R. (2009). Chapter 2: UWB for wireless communications. In *Introduction to Ultra Wideband for Wireless Communications*, 11-27. Springer. <https://doi.org/10.1007/978-1-4020-6633-7>
- Olsen, N. (2014). Potato Storage Management: A global perspective. *Potato Research*, *57*(3-4), 331-333. <https://doi.org/10.1007/s11540-015-9283-7>
- Paul, V., & Ezekiel, R. (2004). Evaluation of heap and pit methods of potato storage in the central Indo-Gangetic Plains. *Indian Journal of Agricultural Sciences*, *74*(12), 665-668. Retrieved from [https://www.researchgate.net/publication/259151918\\_Evaluation\\_of\\_heap\\_and\\_pit\\_methods\\_of\\_potato\\_storage\\_in\\_the\\_central\\_Indo-Gangetic\\_Plains](https://www.researchgate.net/publication/259151918_Evaluation_of_heap_and_pit_methods_of_potato_storage_in_the_central_Indo-Gangetic_Plains)
- Paustian, M., & Theuvsen, L. (2017). Adoption of precision agriculture technologies by German crop farmers. *Precision Agriculture*, *18*, 701-716. <https://doi.org/10.1007/s11119-016-9482-5>

- Pelka, M. (2015). Position Calculation with Least Squares Based on Distance Measurements. *Lübeck University of Applied Sciences*. Retrieved from [https://www.th-luebeck.de/fileadmin/media\\_cosa/Dateien/Veroeffentlichungen/Sammlung/TR-2-2015-least-squares-with-ToA.pdf](https://www.th-luebeck.de/fileadmin/media_cosa/Dateien/Veroeffentlichungen/Sammlung/TR-2-2015-least-squares-with-ToA.pdf)
- Phan, T. A., Krizhanovskii, V., Han, S.-K., Lee, S.-G., Oh, H.-S., & Kim, N.-S. (2007). 4.7pJ/pulse 7th derivative Gaussian pulse generator for impulse radio UWB. *2007 IEEE International Symposium on Circuits and Systems (ISCAS)*, 3043–3046. <https://doi.org/10.1109/ISCAS.2007.377988>
- Phillips, W. R. (1957). *Potato storage*. Canada Department of Agriculture. <https://archive.org/details/potatostorage00phil>
- Pinhero, R. G., Coffin, R., & Yada, R. Y. (2009). Post-harvest storage of potatoes. In J. Singh & L. Kaur (Eds.), *Advances in potato chemistry and technology*, 339-370. Academic Press. <https://doi.org/10.1016/B978-0-12-374349-7.00012-X>
- Pirch, H., & Leong, F. (2020). Introduction to impulse radio UWB seamless access systems. *FIRA Consortium*. Retrieved from <https://www.firaconsortium.org/sites/default/files/2020-04/fira-introduction-impulse-radio-uwb-wp-en.pdf>
- Porto, S. M. C., Arcidiacono, C., Giummarra, A., Anguzza, U., & Cascone, G. (2014). Localization and identification performances of a real-time location system based on ultra-wide band technology for monitoring and tracking dairy cow behavior in a semi-open free-stall barn. *Computers and Electronics in Agriculture*, 108, 221–229. <https://doi.org/10.1016/j.compag.2014.08.001>
- Rácz-Szabó, Á., Molnár, Z., Süle, Z., & Pfeiffer, A. (2020). Real-time locating system in production management: A comprehensive review. *Sensors*, 20(23), 6766. <https://doi.org/10.3390/s20236766>
- Rastovski, A., & Van Es, A. J. H. (1981). *Storage of potatoes: Post-harvest behavior store design storage practice handling*. International Book Distributors. Retrieved from [https://books.google.ca/books/about/Storage\\_of\\_Potatoes.html?id=kntZEUwO8V8C&redir\\_esc=y](https://books.google.ca/books/about/Storage_of_Potatoes.html?id=kntZEUwO8V8C&redir_esc=y)
- Rathje, P., & Landsiedel, O. (2024). Precise Ranging: Modeling bias and variance of double-sided two-way ranging with TDoA extraction under multipath and NLOS effects. *arXiv preprint*. <https://doi.org/10.48550/arXiv.2410.12826>
- Reynders, B., & Pollin, S. (2016). Chirp spread spectrum as a modulation technique for long-range communication. *Symposium on Communications and Vehicular Technologies (SCVT)*, 1-5. <https://doi.org/10.1109/SCVT.2016.7797659>

- Rohmah, M., F., Putra, K., G., D., Hartati, R., S., & Ardiantoro, L. (2021). Comparison Four Kernels of SVR to Predict Consumer Price Index. *Journal of Physics: Conference Series*, 1737(1). doi:10.1088/1742-6596/1737/1/012018
- Ruiz-Gracia, L., & Lunadei, L. (2011). The role of RFID in agriculture: Applications, limitations, and challenges. *Computers and Electronics in Agriculture*, 79, 42-50. <https://doi.org/10.1016/j.compag.2011.08.010>
- Sahinoglu, Z., Gezici, S., & Guvenc, I. (2008). *Ultra-wideband Positioning Systems: Theoretical Limits Ranging Algorithms and Protocols*. Cambridge University Press. <https://doi.org/10.1017/CBO9780511541056>
- Schantz, H. G. (2007). A real-time location system using near-field electromagnetic ranging. *IEEE Antennas and Propagation Society International Symposium*, 3792-3795. <https://doi.org/10.1109/APS.2007.4396365>
- Schorling, E. (2001). Methods and technologies in potato storage. *Landtechnik*, 56(5), 328-329. Retrieved from <https://eurekamag.com/research/003/890/003890645.php>
- Scholtz, R. A., & Win, M. Z. (1997). Impulse radio. *IEEE International Symposium on Personal, Indoor and Mobile Radio Communications*. Retrieved from <http://ultra.usc.edu/assets/002/35801.pdf>
- Shamaas, M. (2022). Introduction to LoRa technology. *ResearchGate.net*. Retrieved from [https://www.researchgate.net/publication/360872918\\_Introduction\\_to\\_LoRa\\_Technology](https://www.researchgate.net/publication/360872918_Introduction_to_LoRa_Technology)
- Singh, R. K., Aernouts, M., De Meyer, M. D., Weyn, M., & Berkvens, R. (2020). Leveraging LoRaWAN technology for precision agriculture in greenhouses. *Sensors*, 20(7), 1827. <https://doi.org/10.3390/s20071827>
- Sodeyama, K., Ishibashi, K., & Kohno, R. (2010). An analysis of interference mitigation capability of low duty-cycle UWB communications in the presence of wideband OFDM system. *Wireless Personal Communications*, 54(1), 39-52. <https://doi.org/10.1007/s11277-009-9713-4>
- Sung, S., Kim, H., & Jung, J. I. (2023). Accurate indoor positioning for UWB-based personal devices using deep learning. *IEEE Access*, 11, 20095-20113. <https://doi.org/10.1109/ACCESS.2023.3250180>
- Swain, M., Zimon, D., Singh, R., Hashmi, M. F., Rashid, M., & Hakak, S. (2021). LoRa-LBO: An Experimental Analysis of LoRa Link Budget Optimization in Custom Build IoT Test Bed for Agriculture 4.0. *Agronomy*, 11(5), 820. <https://doi.org/10.3390/agronomy11050820>
- Trautman, D., Goddard, E., & Nilsson, T. (2008). Traceability: A literature review (Project Report No. 08-02). *Department of Rural Economy, Faculty of Agricultural, Life and Environmental Sciences, University of Alberta*. Retrieved from <https://ideas.repec.org/p/ags/ualbpr/52090.html>

- Tsai, C. C. (1998). A localization system of a mobile robot by fusing dead-reckoning and ultrasonic measurements. *IEEE Transactions on Instrumentation and Measurement*, 47(5), 1399-1404. <https://doi.org/10.1109/19.746618>
- Vaduva, I. (2021). Pros and Cons of Bulk or Boxed Storage. *Potato Business*, 3, 22-23. Retrieved from <https://www.potatobusiness.com/pb-special-feature/pros-and-cons-of-bulk-or-boxed-potato-storage/>
- Velasquez, N., Medina, C., Castro, D., Acosta, J. C., & Mendez, D. (2017). Design and development of an IoT system prototype for outdoor tracking. *Proceedings of the International Conference on Future Networks and Distributed Systems* (Article 3105575). Association for Computing Machinery. <https://doi.org/10.1145/3102304.3105575>
- Welch, G., & Bishop, G. (2001). An Introduction to the Kalman Filter. Chapel Hill, NC: University of North Carolina at Chapel Hill, Department of Computer Science. Retrieved from <http://info.acm.org/pubs/toc/CRnotice.html>
- Will, M. K., Buttner, K., Kaufholz, T., Muller-Graf, C., Selhorst, T., & Krieter, J. (2017). Accuracy of a real-time location system in static positions under practical conditions: Prospects to track group-housed sows. *Computers and Electronics in Agriculture*, 142, 473-484. <https://doi.org/10.1016/j.compag.2017.09.020>
- Willersinn, C., Mack, G., Mouron, P., Keiser, A., & Siegrist, M. (2015). Quantity and quality of food losses along the Swiss Potato Supply Chain: Stepwise investigation and the influence of quality standards on losses. *Waste Management*, 46, 120-132. <https://doi.org/10.1016/j.wasman.2015.08.033>
- Win, M. Z., Dardari, D., Molisch, A. F., Wiesbeck, W., & Zhang, J. (2009). History and Applications of UWB. *Proceedings of the IEEE*, 97, 198-204. <https://doi.org/10.1109/JPROC.2008.2008762>
- World Wildlife Federation (WWF). (2014). Food losses in meat, vegetables, and bread. *World Wildlife Federation Schweiz, Zürich*. Retrieved from <https://www.worldwildlife.org/>
- Xue, H., & Yang, Z. (2021). Potato Dry Rot Caused by *Fusarium* spp. and Mycotoxins Accumulation and Management. In S. M. Mirmajlessi (Ed.), *Fusarium – An Overview of the Genus*, 1-22. <https://doi.org/10.5772/intechopen.100651>
- Zhang, C., Bao, X., Wei, Q., Ma, Q., Yang, Y., & Wang, Q. (2016). A Kalman filter for UWB positioning in LOS/NLOS scenarios. In *Proceedings of the 2016 Fourth International Conference on Ubiquitous Positioning, Indoor Navigation and Location Based Services (UPINLBS)*, 73-78. <https://doi.org/10.1109/UPINLBS.2016.7809953>
- Zhang, F., Yang, L., Liu, Y., Ding, Y., Yang, S., & Hao, L. (2022). Design and Implementation of Real-Time Localization System (RTLs) Based on UWB and TDoA Algorithm. *Sensors*, 22, 4353. <https://doi.org/10.3390/s22124353>

Zhao, K., Zhao, T., Zheng, Z., Yu, C., Ma, D., Rabie, K., & Kharel, R. (2020). Optimization of time synchronization and algorithms with TDOA-based indoor positioning technique for Internet of Things. *Sensors*, 20(22), 6513. <https://doi.org/10.3390/s20226513>

Zhou, Y., Law, C. L., & Xia, J. (2012). Ultra low-power UWB-RFID system for precise location-aware applications. *IEEE Wireless Communications and Networking Conference Workshops (WCNCW)*, 154-158. <https://doi.org/10.1109/WCNCW.2012.6215480>